THE STUDY OF MANY-ELECTRON SYSTEMS

by

Yu Zhou

Dissertation submitted to the Faculty of the
Virginia Polytechnic Institute and State University
in partial fulfillment of the requirements for the degree of
DOCTOR OF PHILOSOPHY
in
Physics

APPROVED:

Samuel P. Bowen
Samuel P. Bowen, Chairman

Clayton D. Williams
Clayton D. Williams, Co-Chairman

Ting-Kuo Lee
Ting-Kuo Lee

Jay D. Mancini
Jay D. Mancini

L. David Roper
L. David Roper

R.K.P. Zia
Royce K. P. Zia

December, 1991
Blacksburg, Virginia

THE STUDY OF MANY-ELECTRON SYSTEMS

by

Yu Zhou

Samuel P. Bowen and Clayton D. Williams, Chairmen
Physics

(ABSTRACT)

Various methods and approximation schemes are used to study many-electron interacting systems. Two important many-particle models, the Anderson model and the Hubbard model, and their electromagnetic properties have been investigated in many parameter regimes, and applied to physical systems.

An Anderson single-impurity model Hamiltonian based calculation of the magnetic susceptibility is performed for YbN in the presence of crystal fields using an alteration of the Non-Crossing Approximation proposed by Zwicknagl et.al., incorporating parameters obtained from ab initio band structure calculations. It yields good agreement with experimental data. For the Anderson lattice model, a variational scheme which uses specific many-electron wavefunctions as basis is applied to both one- and two-dimensional systems represented by symmetric Anderson lattice Hamiltonians. Without much computational effort, the ground state energy is well approximated, especially in strong-coupling limit. Some electronic properties are examined using the variational ground state wavefunction.

The one-dimensional Hubbard model has been solved exactly for small-size clusters by diagonalizing the Hamiltonian in the basis of many-electron Bloch states. The results for the energy spectrum and eigenfunctions of the ground state and low-lying excited states are presented. Also, mean field calculations of the two-dimensional single-band Hubbard model and Cu-O lattice model (three-band Hubbard model) are carried out for various physical quantities including the energy, occupation probability, staggered magnetization, momentum distribution Fermi surface and density of states, by using a projection operator formalism.

To develop a systematic approach to solving many-electron problems, the many-particle partition function for the free electron gas system is explored using a cumulant expansion scheme. Starting from the ground state, the partition function can be approximated to any order in terms of excitation energy. Its application to interacting systems such as the Anderson model and the Hubbard model is briefly discussed.

Acknowledgements

I am very fortunate to have Dr. Sam Bowen as my advisor, and especially grateful for his guidance, inspiration and support throughout my graduate study. I learned from not only his wide knowledge of physics, but also his philosophy, attitude and way of thinking which I will benefit in my life. And the discussions during those long trips and at the Taco Bell are always enjoyable.

My sincere gratitude to Dr. Dale Koelling for his wise advice, friendly encouragement and invaluable contributions during my three years of working at Argonne. I owe much of my busy and happy learning and research experience in that period to him. His help and scholarly influence on my professional career extends far beyond this PhD dissertation.

This dissertation would not have been possible without the financial support given by the Materials Science Division and the Division of Educational Programs at Argonne National Laboratory, and by Department of Physics at Virginia Tech.

I wish to express my appreciation to Dr. Jay Mancini at Fordham University for his friendship and stimulating discussions. He not only made great contributions to many of the research projects, but also served on my graduate committee, patiently went through the first draft of my dissertation. I wish I had learned more from him on the basketball court.

I would like to thank Dr. Art Fedro at Argonne for his help and direction in the mean-field calculations of the Hubbard model and Cu-O lattice model, Dr. Rene Monnier at ETH, Switzerland, for his encouragement, contribution and supplying references and experimental data during the calculation of the magnetic susceptibility of YbN, Dr. T. C. Leung at Iowa State University for helping with computer program used to solve Green functions from self-consistent coupling equations.

I would like to thank Dr. T. K. Lee, Dr. David Roper and Dr. Royce Zia for serving on my graduate committee, Dr. Clayton Williams for taking the responsibility of being co-chairman.

I wish to thank Mrs. Chris Thomas for her help and keeping me in touch with the campus while I am at Argonne National Laboratory.

Finally, I wish to express great appreciation to my parents, to my brothers, and to JZ, for their support and encouragement which made this dissertation possible.

Table of Contents

1 Introduction 1

2 Magnetic Susceptibility of YbN 3

2.1 Ytterbium monopnictides and the Anderson model 4

2.2 The ZZF formalism for YbN 7

2.3 The magnetic susceptibility of YbN 11

2.3.1 The validity of the ZZF approximation for low-degeneracy systems . 12

2.3.2 Application of the ZZF approximation to YbN 15

2.4 Summary 18

3 Variational Calculations of the Anderson Lattice 20

3.1 The Anderson lattice Hamiltonian 21

3.2 Variational formalism 22

3.2.1 The variational basis vectors 23

3.2.2 The Hamiltonian matrix elements 26

3.3 Ground state of the one-dimensional Anderson lattice 32

3.4 Ground state of the two-dimensional Anderson lattice 39

3.5 Summary 45

4 One Dimensional Hubbard Model: Exact Diagonalization 47

4.1 The Hubbard model 48

4.2 The many-electron Bloch states of Hubbard rings 50
4.3 The exact solutions of small Hubbard rings 53
    4.3.1 Four sites with three electrons 54
    4.3.2 Half-filled four-site system 56
    4.3.3 Four electrons in six- and eight-site rings 59
    4.3.4 Four electrons in five- and seven-site rings 59
    4.3.5 Half-filled six-site system 63
4.4 Summary 63

5 Two Dimensional Hubbard Model:
Projection Operator Mean-Field Calculation 65

5.1 The projection operator based mean field formalism 68
    5.1.1 The multi-band Hubbard Hamiltonian and the projection operator . . 68
    5.1.2 The equations of motion for the Green's functions 70
5.2 Calculations of the 2D single-band Hubbard model 77
5.3 Calculations of the CuO_2 lattice model 86
    5.3.1 The 3-orbital Hubbard model of the CuO_2 lattice 87
    5.3.2 Static properties and comparison with MC results 89
    5.3.3 Density of states of the CuO_2 lattice model 97
5.4 Summary 105

6 Many-Electron Partition Function 107

6.1 The cumulant expansion formula 108
6.2 Canonical partition function 116
6.3 The grand partition function 123
6.4 Summary 125

7 Conclusion 128

Bibliography 132

Appendix A Energy Sums in Partition Functions 140

Vita 144

List of Figures

2.1 Energy dependent coupling functions for YbN 8

2.2 Low temperature (T=1.5K) behavior of the imaginary part of the dynamical susceptibility divided by frequency 13

2.3 The static susceptibility $\chi(T)$ versus temperature T for $N_f = 6$ 14

2.4 Low temperature (T = 1.161K) behavior of $\sigma_f(\omega)/\omega$ versus ω for YbN 16

2.5 Magnetic susceptibility $\chi(T)$ for YbN 17

3.1a Diagrammatic representation of the first seven of thirteen basis states 27

3.1b Diagrammatic representation of the last six of thirteen basis states 28

3.2 Ground state energy per site of the 16-site lattice 34

3.3 Ground state energy per site of 8, 32 and 64-site lattices 37

3.4 The square of the f-orbital single site magnetization vs. U for one-dimensional 16-site lattice 38

3.5 Ground state energy as a function of U for different two-dimensional lattice sizes 41

3.6 Ground state energy as a function of U for 4x4 lattice 42

3.7 Ground state energy as a function of U for 8x8 lattice 43

3.8 Ground state energy as a function of U for 16x16 lattice 44

4.1 Eigenstate energy spectrum of the four-site, three-electron Hubbard ring. . . 57

4.2 Eigenstate energy spectrum of the four-site, four-electron Hubbard ring . . . 58

4.3 Eigenstate energy spectra of the six-site and eight-site Hubbard rings with four electrons 60

4.4 Eigenstate energy spectra of the five-site and seven-site Hubbard rings with four electrons 61

4.5 Eigenstate energy spectrum of the half-filled six-site Hubbard ring 62

5.1 Energy per site versus band filling <n> for U = 4 and $\beta = 6$ 79

5.2 Local magnetic moment $<m_z^2>$ vs. band filling <n> for U = 4 and $\beta = 6$ . . 80

5.3 Effective hopping energy vs. U for half-filled case 82

5.4 Effective hopping energy t_{eff}/t vs. <n> for U=4 and $\beta = 10$ 83

5.5 Momentum distribution function $<n_k>$ vs. k along (1,1) direction 84

5.6 Fermi surface for <n> = 0.87, U = 4 and $\beta = 6$ 85

5.7 Charge transfer regime: the hole occupation numbers on the Cu site $<n_{Cu}>$ and O site $<n_O>$ vs. band filling $<n> = <n_{Cu}> + 2<n_O>$ 91

5.8 Mott-Hubbard regime: the hole occupation numbers on the Cu site $<n_{Cu}>$ and O site $<n_O>$ vs. band filling $<n> = <n_{Cu}> + 2<n_O>$ 92

5.9 Effect of t_{pp} on the hole occupation at the Cu and O sites versus band filling in the charge transfer limit 93

5.10 Hole-occupation number on the Cu sites $<n_d>$ as a function of the charge transfer energy ε 94

5.11 The squared local moment on the Cu site $<m_z^2> = <(n_\uparrow - n_\downarrow)^2>$ 95

5.12 The staggered magnetic moment $<m_z> = |<n_\uparrow - n_\downarrow>|$ on the Cu site vs. band filling $<n>$ 96

5.13 The Cu, O and total density of states for the paramagnetic half-filled system 99

5.14 The density of states for the anti-ferromagnetic half-filled system 100

5.15 Density of states obtained from SBMF, POMF and the Hubbard I approximation for half-filling 101

5.16 The staggered magnetic moment $<m_z>$ on the Cu site vs. $<n>$ using the LDA parameters 102

5.17 The total density of states for band fillings $<n> = 1.0$, 1.2 and 1.4 103

5.18 The total density of states obtained from the POMF and the Hubbard I calculations for $<n> = 1.5$ 104

Chapter 1

Introduction

Various theories have been developed to study the electronic structures in condensed matter physics. Band structure calculations yield very accurate results for non-localized and weakly interacting electrons in solids. They are widely used to explain the electromagnetic properties of many materials. However, because those calculations are based on single-particle motions, there is great difficulty dealing with systems within which the electrons are strongly correlated or strongly localized. For instance, in the band structure calculations for transition metal oxide materials, the Fermi level coincides with the flat energy band of the localized f-electron states, indicating that these materials are conductors, which is qualitatively wrong. Also, some experimentally observed effects such as the Kondo resonance and the phase transition in surface magnetizations are due to the strong many-body interaction between valence electrons and conduction electrons, or between the localized electrons themselves, and these effects can not be easily derived from theories and calculations based on solving single-particle equations of motion.

An alternative to describing systems with single-particle wavefunctions is to solve the many-body Hamiltonian directly. Apparently this is a very complex and difficult task, but the effects of correlations between particles can be revealed relatively easily comparing with single-particle based calculations. The starting point of many-body calculations is to describe the interacting systems by a many-particle model Hamiltonian, such as the Heisenburg model, the Anderson impurity model and the Hubbard model Hamiltonians. Various theories and approximations schemes have been developed for solving these Hamiltonians, including variational approximations, large degeneracy expansion schemes, numerical solutions such as exact diagonalizations of small clusters and quantum Monte Carlo calculations, and many mean-field theories.

In this thesis, a few methods mentioned above have been applied to the Anderson single impurity model, Anderson lattice model, single-band Hubbard model and three-band Hubbard (the CuO_2 lattice) model in order to study various ground state and thermodynamic properties for different many-body interacting systems. The dissertation is organized as follows: Chapter 2 describes the calculations of low temperature magnetic susceptibility of YbN using an approximation to the $1/N_f$ (N_f being f-orbital degeneracy) expansion solution to the Anderson impurity Hamiltonian. A variational solution to the one- and two-dimensional Anderson lattice model using many-particle Bloch states as basis is presented in Chapter 3. In Chapter 4, the effort to find exact solutions for small clusters of the one-dimensional Hubbard model is made for various sizes and symmetries. In relation to the studies of high temperature superconductivity, a Mori-projection-operator based mean-field calculation is carried out in Chapter 5 for the two-dimensional single-band Hubbard model and CuO_2 lattice model; the results for many thermodynamic properties and the quasi-particle density of states are presented. The last research project is an attempt to find the many-body partition function using a cumulant expansion scheme, which is described in detail in Chapter 6. Chapter 7 includes final conclusions and comments.

Chapter 2

Magnetic Susceptibility of YbN

Much effort has been expended on understanding the properties of hybridizing rare earth systems such as the ytterbium monopnictides. These materials have some interesting low temperature features such as a broad bump observed in specifit heat measurements and a near-constant magnetic susceptibility indicating a non-magnetic Fermi liquid state [Stutius, 1969; Ott, 1982]. These properties are believed to be interacting many-electron effects which cannot be explained from one-particle band structure calculations because of the highly localized f-orbital in ytterbium. In this chapter, the low temperature magnetic susceptibility of YbN is calculated by applying the Zwicknagl, Zevin and Fulde (ZZF) approximation [Zwicknagl, 1990] for the spectral densities of the occupied and empty f-states, derived from a degenerate Anderson impurity model which incorporates crystal fields. The model, in which each crystal field level couples to the band states with its own hybridization function, has been successfully applied using the non-crossing approximation (NCA) to explain the specific heat structure at low temperatures [Monnier, 1990]. The ZZF approximation removes the spurious zero-temperature behavior of the parent Non-Crossing Approximation for the susceptibility by representing the low-energy empty-f density spectrum by a delta-function. Surprisingly, even at low crystal field degeneracy

(N=2) of YbN the Shiba relation (a Fermi-liquid relation for the magnetic susceptibility at zero temperature) is very nearly satisfied, in spite of the fact that ZZF approximation is based on the 1/N expansion. The appropriate experimental impurity susceptibility for comparison is extracted from the measurement by removing an empirical exchange interaction. The resultant Kondo temperature ($T_0 = 8.49$K) is consistent with previous specific heat estimates (10-11K), and the agreement with experiment is good.

2.1 Ytterbium monopnictides and the Anderson model

Experimentally, the magnetic susceptibility of Yb monopnictide materials changes from a Curie-like behavior (1/T) at high temperature to a constant value, indicative of a non-magnetic Fermi liquid state, below a characteristic (Kondo) temperature [Oyamada, 1988; Degiorgi, 1990]. The compact size of the Yb f-orbitals severely limits the range of their interactions and they are frequently approximated as an assembly of uncoupled impurities. Such rare earth impurities in metals are commonly described by the infinite-U degenerate Anderson Model [Anderson, 1961] which was explained in detail in [Monnier, 1986] and [Monnier, 1990]:

$$H^{U=\infty} = H_{band} + H_f^{U=\infty} + H_{mix}^{U=\infty} \tag{2.1a}$$

where the conduction band energy

$$H_{band} = \sum_k \varepsilon_k n_k \tag{2.1b}$$

the f-electron energy

$$H_f^{U=\infty} = \sum_i \varepsilon_i n_i \tag{2.1c}$$

with crystal field level index i, and

$$H_{mix}^{U=\infty} = \sum_{k,i} V(k)\,(\,c_k^\dagger f_i + f_i^\dagger c_k\,) \tag{2.1d}$$

is the hybridization between localized f-electrons f_i and conduction electrons c_k, with hybridization integral V(k). In the infinite U limit, no double occupancy is allowed in f-states.

For the severely restricted case that the f-orbital coupling to the band states is constant in energy and independent of orbital, the Bethe Ansatz formalism yields the exact ground state and thermodynamic properties [Tsvelick, 1982; Tsvelick, 1983; Andrei, 1983; Hewson, 1985; Rasul, 1989] of the model. A numerical approach not suffering from these restrictions is the so-called non-crossing approximation (NCA) [Bickers, 1985; Bickers, 1987; Zhang, 1984; Coleman, 1984; Monnier, 1990], in which the magnetic degeneracy N is used as a self-consistent expansion parameter. A diagrammatic 1/N expansion is used to solve two coupled integral equations for the self-energy of empty and occupied f-states, from which the spectral densities of these two f-states can be derived. Using this technique it is observed that the empty-f spectral density ρ_0 has a very sharp peak at an energy slightly below the f-orbital energy [Bickers, 1987] and a broad feature around the Fermi energy. The low energy peak corresponds to the ground state of the interacting many particle system, and therefore plays an important role in the low temperature properties of the system. The broad features near the Fermi energy represent long-lived excited states of the system and should be less important at low temperatures. The specific heat of Ytterbium-pnictides in the presence of crystal fields (CF) with a doublet ground state has been calculated using NCA with reasonable success [Monnier, 1990].

Attempts to reproduce the magnetic susceptibility behavior using the NCA for YbN, YbP and YbAs [Monnier, 1990] have failed because the NCA does not satisfy certain Fermi-liquid relations (e.g., the Shiba relation) in the zero-temperature limit [Bickers, 1987]. This non-Fermi-liquid behavior causes a singularity in the localized f-moment spectral density at zero-temperature, which leads to a divergent magnetic susceptibility at low temperatures.

Recently, Zwicknagl, Zevin and Fulde [Zwicknagl, 1990] (ZZF) have proposed a scheme in which the low-energy peak in the empty-f spectral function ρ_0 is approximated as a δ-function and other high energy features of ρ_0 are ignored. This approximation beneficially does not exhibit the low-temperature spurious features of the NCA. Additionally, the magnitude of the numerical calculation for practical physical properties is significantly reduced. ZZF applied this scheme to a CF split model in which the coupling between band states and impurity states was constant in energy. For this system with an f-ground state degeneracy of 6, their magnetic susceptibility at low temperature compared well to those obtained from the NCA. In this chapter, we assess the ZZF approximation scheme for the susceptibility of YbN by calculating the low-temperature magnetic susceptibility in the presence of CF splittings where the lowest f-level degeneracy is only 2, and compare the results with recent experimental data [Zhou, 1991a].

2.2 The ZZF formalism for YbN

In the presence of CF, the $4f^{13}$ $F_{7/2}$ multiplet of Yb is split into three levels [Monnier, 1990]: Γ_6 (ground state with energy ε_6, degeneracy $N_6 = 2$), Γ_8 ($N_8 = 4$) and Γ_7 ($N_7 = 2$). In the ZZF approximation, the spectral function $\rho_0(\omega)$ of the empty 4f state is:

$$\rho_0(\omega) = (1-n_f)\,\delta(\omega-\omega_0) \tag{2.2}$$

where

$$\omega_0 = \varepsilon_6 - T_0 \tag{2.3}$$

n_f is the f-valence at zero-temperature and T_0 the Kondo temperature. With Eq.(2.2), the spectral function $\rho_i(\omega)$ of the occupied 4f state can be obtained from an integral equation of the NCA [Zwicknagl, 1990; Zevin, 1988]:

$$\rho_i(\omega) = \frac{1}{\pi}\,\frac{(1-n_f)\,\gamma_i(\omega-\omega_0)\,f(\omega_0-\omega)}{(\omega-\varepsilon_i)^2 + \left[(1-n_f)\,\gamma_i(\omega-\omega_0)\,f(\omega_0-\omega)\right]^2} \tag{2.4}$$

where $f(\omega)$ is the Fermi function:

$$f(\omega) = \frac{1}{e^{\beta\omega}+1} \tag{2.5}$$

and $\gamma_i(\omega) = \pi V_i^2(\omega)$ is the coupling width between band states and each CF level Γ_i as a function of energy determined using a tight binding fit to an ab initio band structure

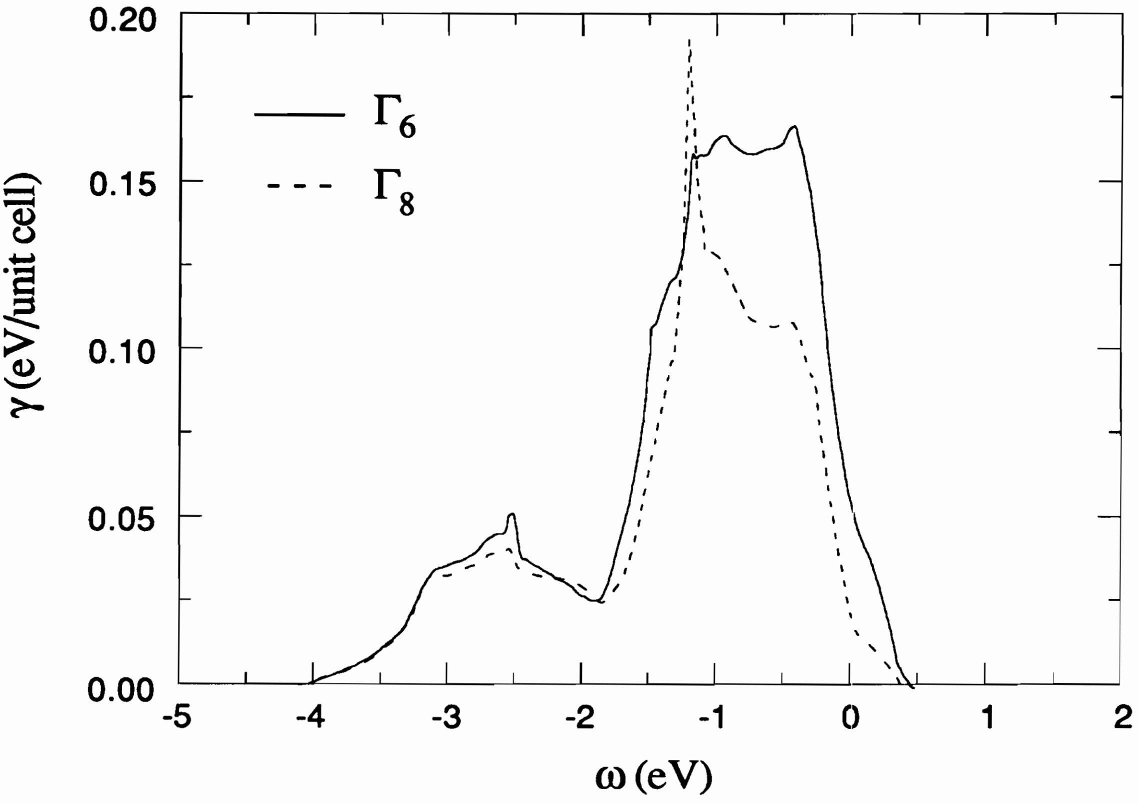

Fig. 2.1 **Energy dependent coupling functions for YbN.** $\gamma_i(\varepsilon)$ are plotted for the lowest two crystal field levels Γ_6 and Γ_8 of a 4f hole on the ytterbium ion, determined from a tight binding fit to an ab initio band structure calculation (Monnier, 1990). The zero of energy is at the Fermi level.

calculation [Monnier, 1990]. For YbN, $\gamma_6(\omega)$ and $\gamma_8(\omega)$ as functions of frequency are shown in Fig.2.1.

The relation between T_0 and the f-valence n_f can be obtained for zero temperature using:

$$n_f = \left[\frac{1}{Z_f} \sum_i N_i \int_{-\infty}^{+\infty} d\omega \; e^{-\beta\omega} \, \rho_i(\omega) \right]_{T=0} \tag{2.6}$$

where Z_f is the partition function of the 4f electron:

$$Z_f = (1 - n_f)\, e^{-\beta\omega_0} + \sum_i N_i \int_{-\infty}^{+\infty} d\omega \, e^{-\beta\omega} \, \rho_i(\omega) \tag{2.7}$$

in which Eq.(2.2) has been used. With a spectral function given by Eq.(2.4), and setting the energy zero at the Fermi energy, the relation between n_f and T_0 follows the simple expression:

$$n_f = \frac{C}{1 + C} \tag{2.8}$$

where

$$C \equiv \frac{1}{\pi} \sum_i N_i \int_{-\infty}^{0} \frac{\gamma_i(\omega)}{(\omega + \omega_0 - \varepsilon_i)^2} \, d\omega \tag{2.9}$$

This same result can be derived from a variational approach [Gunnarsson, 1983; Langreth, 1966]. Taking the hybridization width γ_i as a constant in energy, Eq.(2.8) can be further simplified:

$$n_f = (1 - n_f)\sum_i N_i \frac{\gamma_i}{\pi(T_0 + \varepsilon_i - \varepsilon_6)} \tag{2.10}$$

which is exactly the same as eq.(11a) in [Zwicknagl, 1990]. However, with the energy-dependent $\gamma_i(\omega)$ shown in Fig. (2.1), Eq.(2.8) is used throughout our calculations and discussions.

With CF levels Γ_6 and Γ_8, the imaginary part of the dynamic susceptibility is [Bickers, 1987; Zwicknagl, 1990]

$$\begin{aligned}\sigma_f(\omega,T) &= \frac{(1 - e^{-\beta\omega})}{3 Z_f}\sum_i N_i\, \mu_i^2 \int_{-\infty}^{+\infty} d\varepsilon\, e^{-\beta\varepsilon}\, \rho_i(\varepsilon)\, \rho_i(\varepsilon+\omega) \\ &+ \frac{(1 - e^{-\beta\omega})}{3 Z_f} N_{68}\, \mu_{68}^2 \int_{-\infty}^{+\infty} d\varepsilon\, e^{-\beta\varepsilon}\left[\rho_6(\varepsilon)\, \rho_8(\varepsilon+\omega) + \rho_8(\varepsilon)\, \rho_6(\varepsilon+\omega)\right]\end{aligned} \tag{2.11}$$

where μ_i is the effective high temperature moment for the level Γ_i. The appropriate theoretical magnetic moments for YbN are [Monnier, 1990]

$$\mu_6 = \sqrt{\frac{16}{3}}\,\mu_B\,, \quad \mu_8 = \sqrt{\frac{1040}{147}}\,\mu_B\,, \quad \mu_7 = \sqrt{\frac{432}{49}}\,\mu_B \qquad (2.12a)$$

where μ_B is the Bohr magneton. The van Vleck contribution is included in the second term of the summation in eq. (11), in which

$$N_{68} \equiv \sqrt{N_6 N_8} = \sqrt{8}$$

$$\mu_{68} = g_{7/2}^2 \, \frac{70}{9} \, \frac{3}{N_{68}} \, \mu_B^2 \qquad (2.12b)$$

and $g_{7/2}$ is the Lande factor (8/7).

The temperature dependence of the static susceptibility is given by the principle value of an integral:

$$\chi(T) = P \int_{-\infty}^{+\infty} d\varepsilon \, \frac{\sigma(\varepsilon,T)}{\varepsilon} \qquad (2.13)$$

2.3 The magnetic susceptibility of YbN

In the calculation, the integrals in Eq. (2.11) were performed numerically using an FFT convolution algorithm. Consistent with the specific heat calculation of [Monnier, 1990], the difference between the Fermi energy ε_F and the lowest CF level energy ε_6 is taken as $(\varepsilon_6 - \varepsilon_F) = -0.5$eV. The value of the CF splitting $(\varepsilon_8 - \varepsilon_6)$, taken from a very recent inelastic neutron scattering study [Donni], is 33meV. The Γ_7 level is considered sufficiently high that it is omitted from the calculation. While investigating the validity of the ZZF approximation for various f-orbital degeneracies, n_f is fixed at 0.94, and the Kondo temperature scale T_0 is determined from Eq.(2.8). When comparing with experiment, T_0 is treated as a free parameter to get the best fit between the theory and experiment, and n_f is appropriately determined from Eq.(2.8).

2.3.1 The validity of the ZZF approximation for low-degeneracy systems

To examine the validity of the ZZF approximation for the low-degeneracy ($N_6 = 2$) YbN system, the behavior of the dynamic susceptibility $\sigma_f(\omega)$ for various lowest f-level degeneracy ($N_6 = 2,3,4,5$ and 6) is investigated (while the effects of any excited f-state are ignored). The result shows that the spectral function of the lowest f-levels $\rho_6(\omega)$ has a well defined single peak at energy ε_6 as expected. Fig. 2.2 is a plot of $\sigma_f(\omega)/\omega$ at $T \ll T_0$ for $N_6 = 3$, 4, 5 and 6. The case $N_6 = 2$, corresponding to YbN, is shown in Fig. 2.4. Despite the very different behavior for different N_6, it is seen that for no degeneracy does the dynamic susceptibility $\sigma_f(\omega)/\omega$ diverge at $\omega = 0$ in the low temperature limit. This is a distinct advantage over the NCA in which $\sigma_f(\omega)/\omega$ diverges as $|\omega|^{-2/(N+1)}$. The Fermi-liquid relation (Shiba relation) [Shiba, 1975]:

$$\frac{\sigma(\omega)}{\omega}\Big|_{\substack{\omega=0\\T=0}} = \frac{3\,\chi^2(T=0)}{N_6\,\mu_6^2} \qquad (2.14)$$

is satisfied within two percent for all values of N_6.

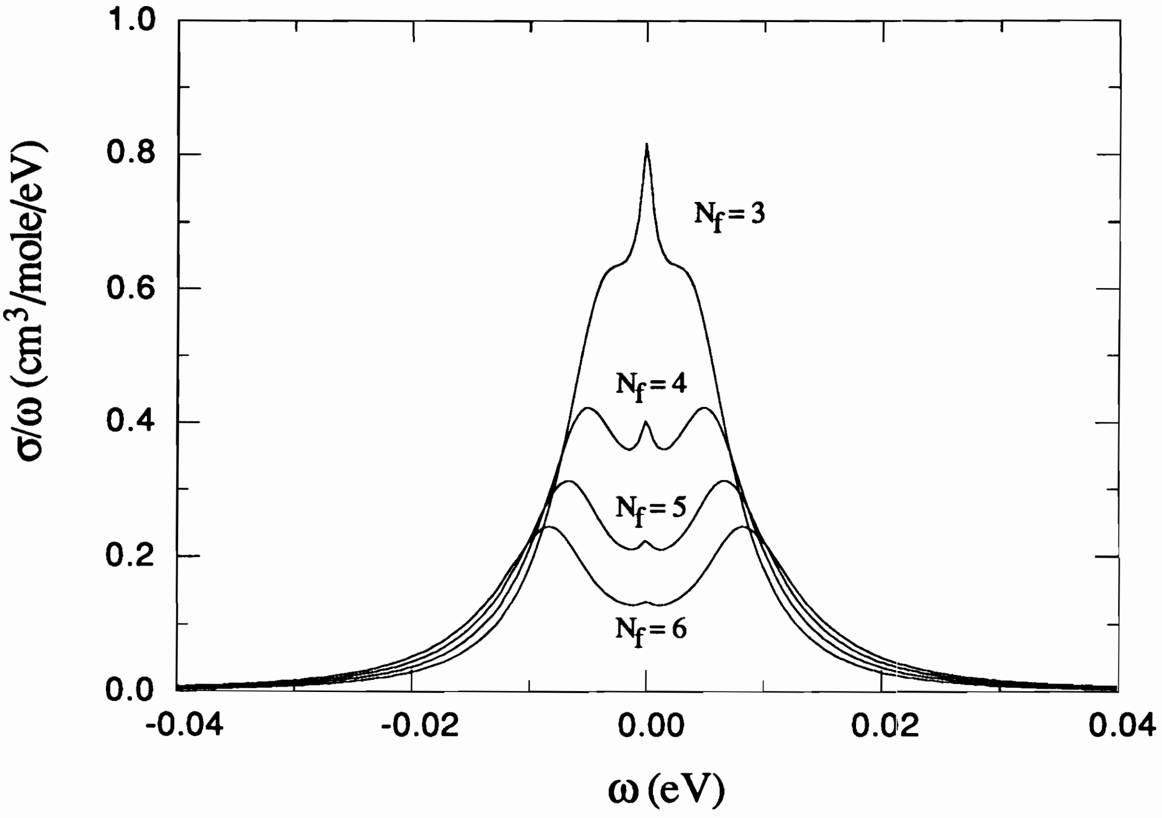

Fig. 2.2 **Low temperature (T=1.5K) behavior of the imaginary part of the dynamical susceptibility divided by frequency.** $\sigma_f(\omega)/\omega$ for f-degeneracies $N_f = 3,4,5$ and 6 are shown. The zero temperature f-occupancy n_f is set to 0.94 for all cases, and the corresponding Kondo temperature scales are T_0 = 40.8K, 55.1K, 69.5K and 84.1K as determined from Eq.(2.8) in the text. The Shiba relation is satisfied within a few percent for all four cases.

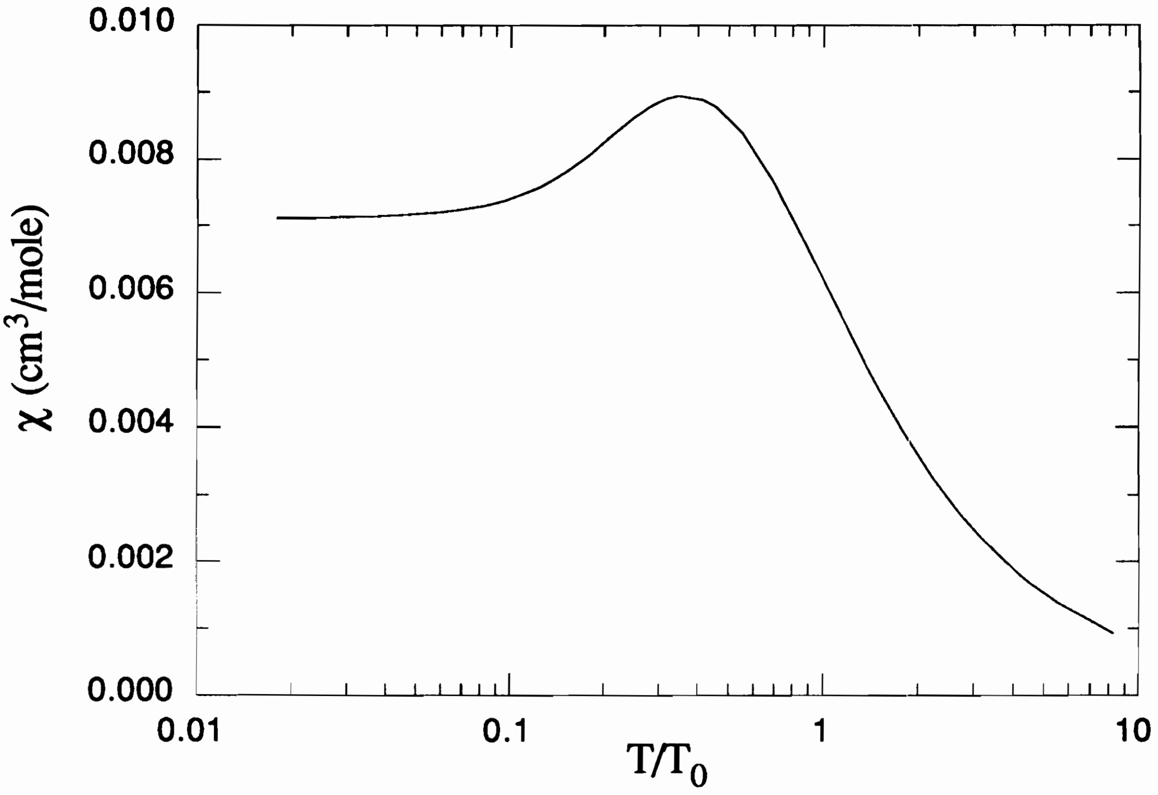

Fig. 2.3 **The static susceptibility $\chi(T)$ versus temperature T for $N_f = 6$.** All parameters are the same as in Fig.2.2. Note that $\chi(T)$ becomes a constant at low temperatures, and that a bump appears similar to the NCA results.

Fig. 2.3 shows $\chi(T)$ as a function of temperature for $N_6 = 6$. For all values of N_6 being studied, the ZZF approximation gives a constant static susceptibility (Pauli law) at temperatures lower than T_0, indicating a non-magnetic Fermi-liquid state. Further, it displays a finite limit as the temperature approaches zero.

2.3.2 Application of the ZZF approximation to YbN

To compare this contribution to the susceptibility with experimental data [Degiorgi, 1990], we subtracted the molecular field contribution from the experimental result using [Degiorgi, 1990; Popielewicz, 1976; Wojciechowski, 1988]:

$$\frac{1}{\chi_m} = \frac{1}{\chi_f} - \lambda \tag{2.15}$$

where χ_m is the measured susceptibility, χ_f is the experimentally derived contribution from the strongly interacting electrons in f-orbitals, and λ is a molecular field constant in the exchange field $H_E = \lambda M$. λ is derived by extrapolating the high temperature $1/\chi_m$ to T=0. From the experimental data of [Degiorgi, 1990], we obtain λ = -10.9 mole/cm^3, with effective moment $\mu_{eff} = 4.85\, \mu_B$ and Curie temperature $T_C = -96.7$K.

$\sigma_f(\omega)/\omega$ vs. ω for $T \ll T_0$ and $\chi(T)$ vs. T are shown for YbN in Fig.2.4 and Fig.2.5. Due to the presence of CF splittings, it is seen in Fig.2.4 that in addition to the low frequency feature of $\sigma_f(\omega)/\omega$, there are two peaks near $\pm(\varepsilon_8 - \varepsilon_6)$, arising from the van Vleck contributions to the susceptibility. $T_0 = 8.49$K is chosen to obtain the optimal fit with the χ_f extracted from the experimental data using Eq.(2.15). This value of T_0 is smaller than the value (10-11K) obtained from the specific heat calculation with NCA. For comparison

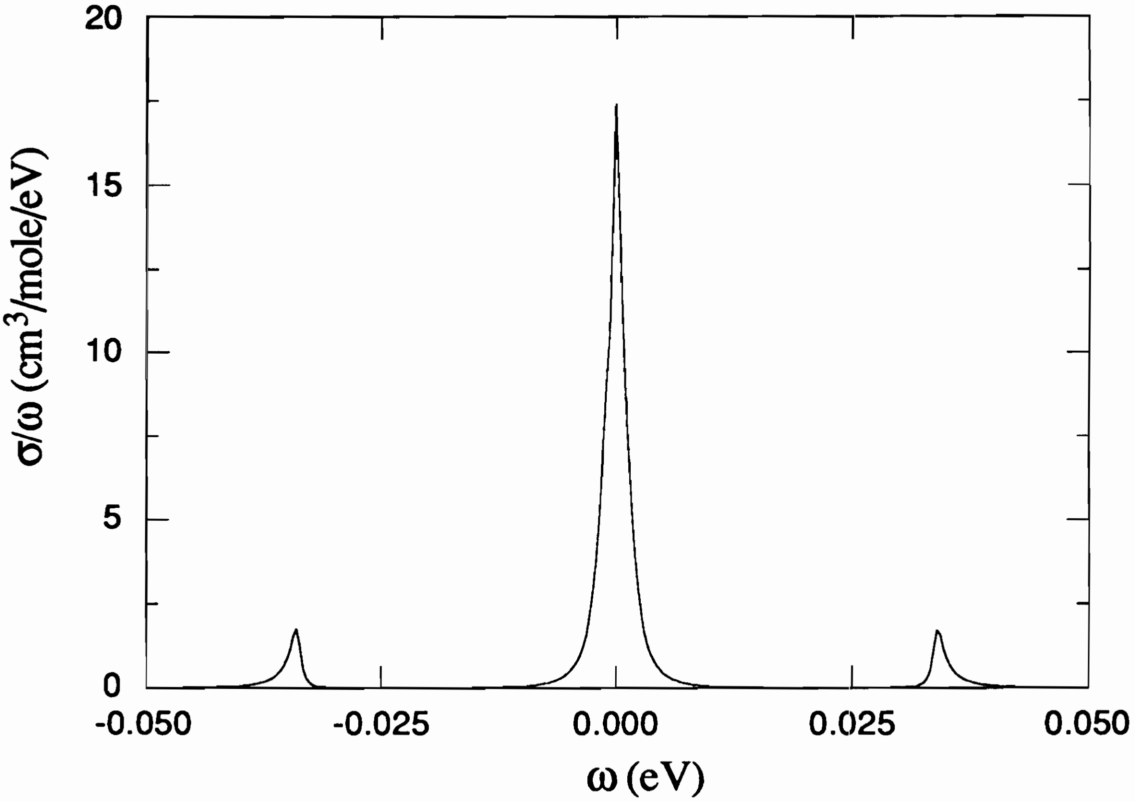

Fig. 2.4 **Low temperature (T = 1.161K) behavior of $\sigma_f(\omega)/\omega$ versus ω for YbN.** It shows a peak at $\omega = 0$ and two small features around $\pm(\varepsilon_8 - \varepsilon_6)$. Kondo temperature $T_0 = 8.49K$ adjusted for best fit with experimental result and $n_f = 0.980$ determined from Eq.(2.8).

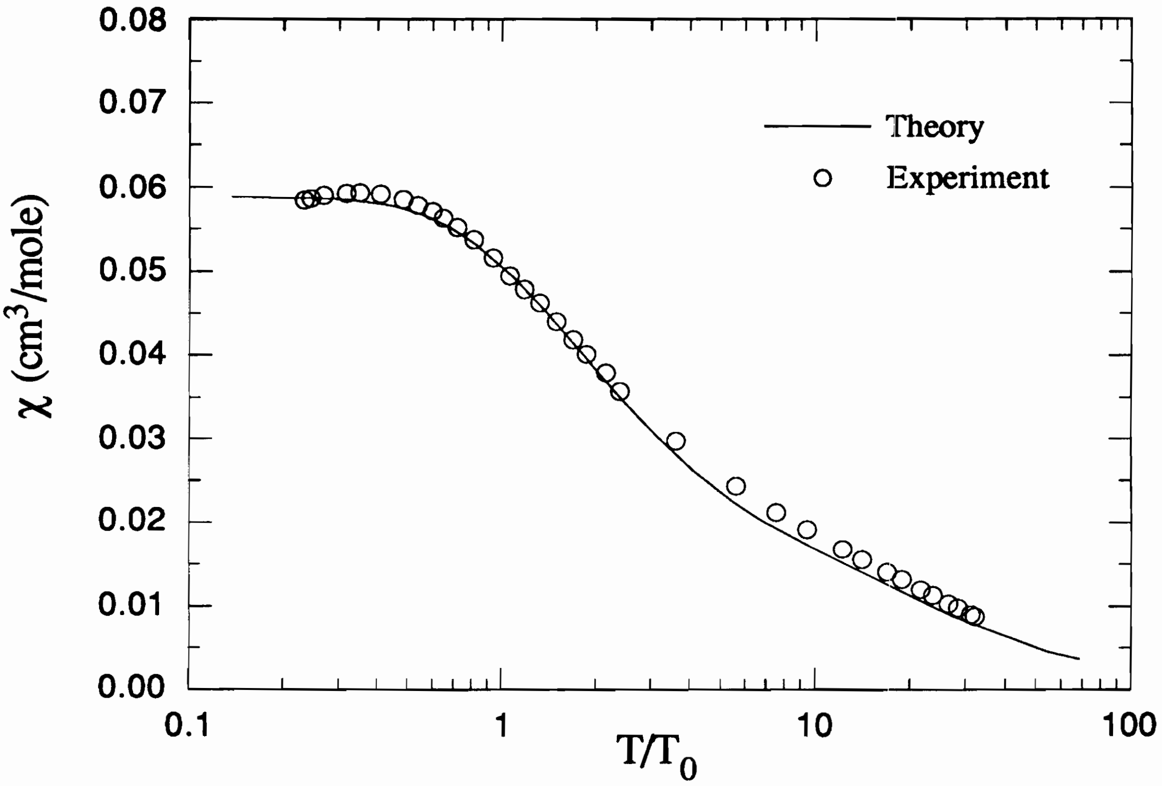

Fig. 2.5 **Magnetic susceptibility χ(T) for YbN.** Parameters are the same as those used in Fig.2.4. Both theoretical χ(T) (solid line) and derived experimental χ_f (circles) results are shown. Good agreement is obtained over the temperature range where the experiment was performed. However, theory does not reproduce the low temperature bump appearing in the experimental result.

χ_f is also shown in Fig.2.5. It is seen that reasonably good agreement is obtained in the temperature range where experiment was performed. The bump observed at low temperature can not be reproduced in the calculation. If an alternative CF splitting (ε_8 - ε_6) = 55meV is used as in [Monnier, 1990], the van Vleck contribution to the susceptibility evaluated with Eq.(2.13) and the second term in Eq.(2.11) is much smaller, and the derived experimental impurity susceptibility is too large for the theory.

The agreement of theory with experiment at low temperature shows that the ZZF approach has removed most of the difficulties encountered in the NCA calculation [Monnier, 1990]. It is a little surprising that the Shiba relation is satisfied for this system with degeneracy as low as 2 since the approximation was derived from the NCA, which is only valid for large degeneracies. Even though the zero-temperature analytic solutions of the NCA offer some insights of why the Fermi-liquid relations are violated [Muller-Hartmann, 1984; Kuramoto, 1985], it is still not clear why the Shiba relation is satisfied within the ZZF approximation regardless of f-degeneracy [Kuramoto, 1985].

2.4 Summary

We have presented a calculation for the magnetic susceptibility of YbN in the presence of crystal fields. Using the ZZF approximation for the spectral function of the empty-f state, the NCA low-temperature divergence of $\sigma_f(\omega)/\omega$ at $\omega = 0$ is removed and the calculational effort greatly reduced. It is found that within this approximation the Fermi liquid relation for the dynamic susceptibility (Shiba relation) is satisfied within a few percent even for a system with f-degeneracy as low as 2, and a constant magnetic susceptibility at temperatures below Kondo temperature is obtained. The ZZF approximation sidesteps the deficiencies of the NCA and seems to yield good agreement with experiment even for small degeneracies. Using coupling functions V(ω) determined from a tight binding fit to a band structure calculation, the theoretical magnetic susceptibility of YbN clearly exhibits a non-magnetic Fermi-liquid state in good agreement with experiment. The full explanation of its success has not yet been found.

Chapter 3

Variational Calculations of the Anderson Lattice

It has been a success to study the electromagnetic properties of some materials with highly localized orbitals such as YbN by solving the Anderson model, as described in the last chapter. However, the Anderson model Hamiltonian (eq.(2.1)) does not include the intersite interactions between the localized electrons, thus it is not able to describe the low temperature magnetic ordering observed in certain transition metal compounds. For example, Malik et.al. (1991) saw evidence that CePdSb orders ferromagnetically and GdPdSb orders antiferromagnetically around 15-17K. This is a consequence of the interaction between the localized 4f electrons and the itinerant conduction electrons. Also, it was found [Kuramoto, 1989] that the momentum dependence in the magnetic response of certain heavy fermion systems is mainly due to the Ruderman-Kittel-Kasuya-Yosida (RKKY) interaction, a type of interaction between two localized electrons through the conduction band. Therefore, it is necessary to investigate a magnetic moment lattice model which is based on the Anderson single impurity Hamiltonian described by Eq.(2.1), that leads to the Anderson lattice model. In this chapter, the Anderson lattice Hamiltonion is discussed, and variational calculations of its ground state energies and wavefunctions for both one- and two-dimensional systems are presented.

3.1 The Anderson lattice Hamiltonian

There has been much interest in the ground state properties of a lattice of localized moments as a description of mixed-valence systems [Stewart, 1984; Varma, 1985a; Varma, 1985b]. The interesting physics of such systems arises from the interaction of the localized f-orbitals (with energy close to the Fermi energy) with the conduction d-bands and by the f-orbital intrasite Coulomb energy. At high temperature they tend to have isolated moments. A model appropriate to describe such systems is the Periodic Anderson Model (PAM). The Hamiltonian for the non-degenerate one dimensional periodic Anderson model has the form

$$H = \sum_{k\,s} \varepsilon_{ks} c^{\dagger}_{ks} c_{ks} + \sum_{l\,s_l} E_l f^{\dagger}_{ls_1} f_{ls_1} + U \sum_{l} f^{\dagger}_{l\uparrow} f_{l\uparrow} f^{\dagger}_{l\downarrow} f_{l\downarrow}$$

$$+ \frac{V}{\sqrt{N}} \sum_{k\,l\,s_l} (e^{ik \bullet R_l}\; f^{\dagger}_{ls_1} c_{ks_1} + \text{h.c.}) \tag{3.1}$$

where $c^{\dagger}$ (c) and $f^{\dagger}$ (f) are the creation (annihilation) operators for the conduction d-orbital and localized f-orbital electrons, respectively. Here U is the on-site Coulomb energy of the localized f-electrons. V represents the hybridization of the two bands, taken to be k independent, and

$$\varepsilon_{k,s} = -2t\cos(k) \tag{3.2}$$

where t is the intersite hopping energy and $-\pi < k \leq \pi$.

Theoretical work on this model has included perturbation expansions in the Coulomb energy U [Yamada, 1983], various Green's function approaches [Czyzcholl, 1982; Czyzcholl, 1985; Kurata, 1980; Brandow, 1979], functional integration methods [Read, 1984a; Read, 1984b; Coleman, 1985], real-space renormalization [Julian, 1977a; Julian, 1977b; Julian, 1982a; Julian, 1982b] and direct diagonalization of finite clusters [Julian, 1982c; Misra, 1987; Chen, 1988]. An extended non-crossing approximation approach (XNCA), based on the NCA for the Anderson single impurity model which is directly related to last chapter's content, has been pursued by Kuramoto (1989) and Kim et.al. (1991).

A wide variety of variational schemes have also been applied to this model [Brandow, 1986]. These include a number of Gutzwiller-type approaches [Fazekas, 1987; Rice, 1987; Oguchi, 1987] whereby an initial trial function is chosen to project out the two-particle states on the localized f-orbitals. Such an approach represents a mean-field theory and thus no information regarding spin correlations of neighboring localized orbitals may be extracted. Another important work, relevant to the present study, is that of Blankenbecler et.al. [Blankenbecler, 1987] who utilized a stochastic Monte Carlo technique to study the ground state properties of the one dimensional PAM. Comparisons with this work, taken to represent the true ground state, shall be made throughout this chapter.

3.2 Variational formalism

This work, based on the Lanczos variational scheme [Mancini, 1985, 1984, 1983, 1990] is a continuation of an earlier preliminary study [Bowen, 1988] on the Anderson model in which the localized f-orbitals were found to be anti-ferromagnetically correlated in the ground state via an RKKY-type of interaction. Here a variational ground state energy as well as magnetic correlation functions and hybridization matrix elements are evaluated [Zhou, 1991e]. The method utilizes a finite matrix truncations scheme whereby a limited subspace of the full Hamiltonian is generated [Mancini, 1990]. The power of the method lies in the fact that for modest computation times one may study very large systems with extensions to higher dimensions being straightforward. A drawback of the technique is that excitations near the Fermi energy are approximated as average band energies, thus obscuring any information on low lying energies leading to the Fermi liquid behavior of intermediate valence systems. In section 3.3 the ground state properties of the one dimensional PAM for an 8-site, 16-site, 32-site and 64-site lattice are studied. Comparisons are made with a stochastic Monte Carlo calculation performed on a 16-site chain. The variational results are in excellent agreement with those of the Monte Carlo calculations in the Kondo lattice regime (Coulomb energy U large). However, in the mixed valence parameter range our results are rather disappointing. This we argue is a consequence of choosing a finite basis whereby important vectors containing the hybridization matrix elements as well as those which represent excitations close to the Fermi energy have been left out. We shall reserve further discussion on this matter until a later section.

3.2.1 The variational basis vectors

Now we introduce a diagrammatic representation of these vectors which facilitates the choosing of a linearly independent set of vectors as well as rendering the orthogonalization (via a Gram-Schmidt orthogonalization process) of this set more manageable. We denote the filled Fermi sea of conduction electrons with the symbol ◡ and the set of singly occupied localized orbitals by a horizontal line $\overset{l}{-\!\!-\!\!\bullet\!\!-\!\!-}$. Here l denotes a particular site. The initial trial wave function is represented by

$$|\phi_1> \;=\; |\Omega> \;\equiv\; \tag{3.3}$$

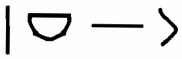

with the normalization $|\phi_1|^2 = 1$.

A truncated basis consisting of various particle-hole excitations may be constructed by repeated operations of Eq.(1) on $|\Omega>$. The set of states generated may be represented diagrammatically, with rules for their construction not given here. Repeated operations of the Hamiltonian [Duncan, 1985] yields a set of nineteen vectors. After checking for linear independence and performing a Gram-Schmidt orthogonalization, the basis was reduced to a set of thirteen independent vectors. Each of these vectors represent a different physical excitation of the ground state. We shall be interested in obtaining the lowest eigenvalue of the 13x13 Hamiltonian matrix within this basis. This matrix is both small and sparse, allowing the calculations to be performed on a desk-top computer using standard matrix routines. It is hoped that such a small amount of computational effort will yield qualitatively useful information on the ground state.

To illustrate the method, we note that explicit operation of the Hamiltonian on the initial vector $|\phi_1>$ yields the following two new vectors. Each vector represents linear combinations of all distinct single particle-hole excitations,

$$\begin{aligned} |\phi_2> &= \frac{1}{\sqrt{N}} \sum_{k<k_F} \sum_{l} e^{ikR_l} f^{\dagger}_{l\bar{s}_1} c_{k\bar{s}_1} |\Omega> \\ |\phi_3> &= \frac{1}{\sqrt{N}} \sum_{k>k_F} \sum_{l} e^{-ikR_l} c^{\dagger}_{ks_1} f_{ls_1} |\Omega> \end{aligned} \tag{3.4}$$

The vector $|\phi_2\rangle$ represents the physical event whereby a conduction electron with momentum $k<k_F$ and spin $\bar{S}_l \equiv -S_l$ hybridizes to a localized f-orbital labeled by l with an already existing spin S_l. Vector $|\phi_3\rangle$ represents the hopping of a localized electron from site l with spin S_l to the conduction band with momentum $k>k_F$. We note that, just as in Oguchi's work [Oguchi, 1987], while the number of f-electrons is not fixed, total electron number is conserved. He uses this condition to determine his variational parameters. The remaining vectors are given below.

We have:

$$|\phi_4\rangle = \frac{1}{\sqrt{N}} \sum_{k>k_F} \sum_{l} e^{-ikR_l} (\varepsilon_{ks_l} - E_{ls_l})\ c^{\dagger}_{ks_l} f_{ls_l} |\Omega\rangle$$

$$|\phi_5\rangle = \frac{1}{N} \sum_{k>k_F} \sum_{l\neq l'} e^{ik(R_{l'}-R_l)} \delta_{s_l \bar{s}_{l'}} f^{\dagger}_{l's_l} c_{ks_l}\ c^{\dagger}_{ks_l} f_{ls_l} |\Omega\rangle$$

$$|\phi_6\rangle = \frac{1}{N} \sum_{\substack{k>k_F \\ k'<k_F}} \sum_{l} e^{i(k'-k)R_l}\ f^{\dagger}_{l\bar{s}_l} c_{k's_l}\ c^{\dagger}_{ks_l} f_{ls_l} |\Omega\rangle$$

$$|\phi_7\rangle = \frac{1}{N} \sum_{\substack{k>k_F \\ k'<k_F}} \sum_{l\neq l'} e^{i(k'R_{l'}-kR_l)}\ f^{\dagger}_{l'\bar{s}_{l'}} c_{k'\bar{s}_{l'}}\ c^{\dagger}_{ks_l} f_{ls_l} |\Omega\rangle$$

$$|\phi_8\rangle = \frac{1}{N} \sum_{k>k_F} \sum_{l\neq l'} e^{-ik(R_{l'}+R_l)} \delta_{s_l \bar{s}_{l'}}\ c^{\dagger}_{ks_{l'}}\ f_{l's_l} c^{\dagger}_{ks_l} f_{ls_l} |\Omega\rangle$$

$$|\phi_9\rangle = \frac{1}{N} \sum_{\substack{k>k_F \\ k'>k_F}} \sum_{l\neq l'} e^{-i(k'R_{l'}+kR_l)}\ c^{\dagger}_{k's_{l'}} f_{l's_{l'}} c^{\dagger}_{ks_l} f_{ls_l} |\Omega\rangle$$

$$|\phi_{10}\rangle = \frac{1}{\sqrt{N}} \sum_{k<k_F} \sum_{l} e^{ikR_l} (E_{l\bar{s}_l} - \varepsilon_{k\bar{s}_l})\, f^{\dagger}_{l\bar{s}_l} c_{k\bar{s}_l} \, |\Omega\rangle$$

$$|\phi_{11}\rangle = \frac{1}{N} \sum_{\substack{k<k_F \\ k'<k_F}} \sum_{l\neq l'} e^{i(k'R_{l'}+kR_l)}\, f^{\dagger}_{l'\bar{s}_{l'}} c_{k'\bar{s}_{l'}}\, f^{\dagger}_{l\bar{s}_l} c_{k\bar{s}_l} \, |\Omega\rangle$$

$$|\phi_{12}\rangle = \frac{1}{N} \sum_{k<k_F} \sum_{l\neq l'} e^{ik(R_{l'}+R_l)} \delta_{s_l \bar{s}_{l'}}\, f^{\dagger}_{l'\bar{s}_{l'}} c_{k\bar{s}_{l'}}\, f^{\dagger}_{l\bar{s}_l} c_{k\bar{s}_l} \, |\Omega\rangle$$

$$|\phi_{13}\rangle = \frac{1}{N} \sum_{\substack{k>k_F \\ k'<k_F}} \sum_{l} e^{i(k'-k)R_l}\, f^{\dagger}_{ls_l} c_{k's_l} c^{\dagger}_{ks_l} f_{ls_l} \, |\Omega\rangle$$

in which k_F is the momentum at the Fermi surface, and δ the Kronecker-delta. The collection of the diagrammatic representations of these 13 many-electron state basis vectors is shown in Fig.3.1.

3.2.2 The Hamiltonian matrix elements

The ground state energy for the truncated basis of thirteen vectors is obtained by finding the lowest eigenvalue of the Hamiltonian matrix $H_{ij} = \langle\phi_i|H|\phi_j\rangle$. With unnormalized basis vectors $|\phi_1\rangle$ through $|\phi_{13}\rangle$ defined in section II, the non-zero elements of the upper-half of the Hamiltonian matrix are:

$$H_{11} = E_0 \, ,$$

$$H_{12} = H_{13} = \frac{N}{2} V \, ,$$

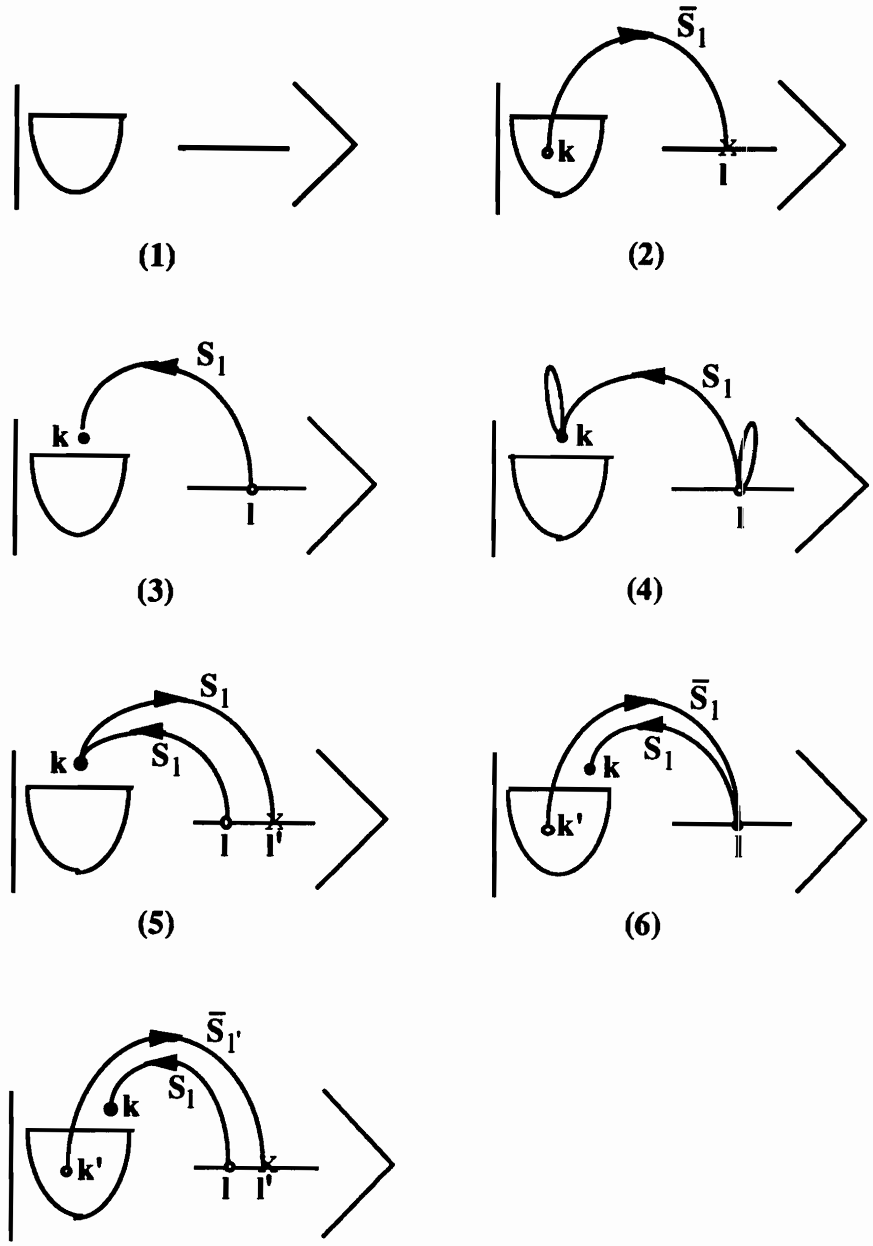
$\bar{S}_l$
k
l
S_l
k
l
S_l
k
l
S_l
k
S_l
l
l'
$\bar{S}_l$
k
S_l
k'
l
$\bar{S}_{l'}$
k
S_l
k'
l
l'

(1) (2) (3) (4) (5) (6) (7)

Fig. 3.1a **Diagrammatic representation of the first seven of thirteen basis states.**

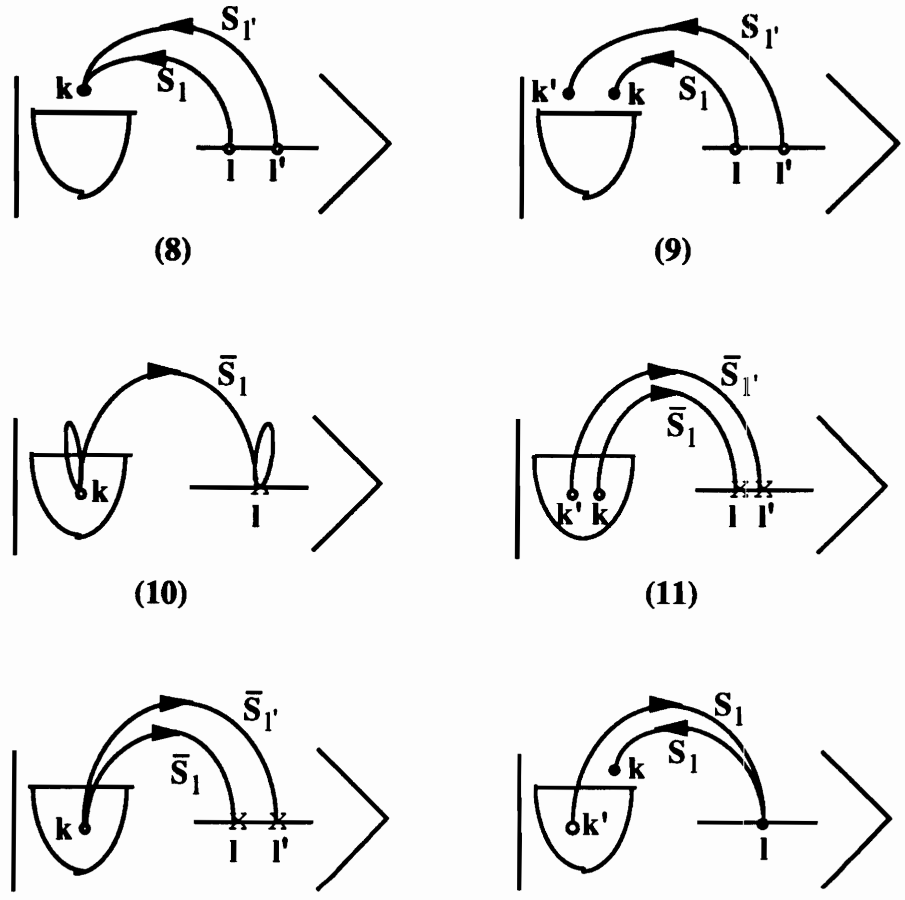
S_l'
k
S_l
l
l'
k'
k
S_l'
S_l
l
l'
S̄_l
k
l
S̄_l'
S̄_l
k'
k
l
l'
S̄_l'
S̄_l
k
l
l'
S_l
k
S_l
k'
l

(8) (9)

(10) (11)

(12) (13)

Fig. 3.1b **Diagrammatic representation of the last six of thirteen basis states.** Up to second order in particle-hole excitations with spin flips have been included. The bubbles appearing in (4) and (10) constitute corrections in self-energies. Diagrams (6) and (13) are vectors which include explicitly the RKKY-type interaction.

$$H_{22} = \frac{N}{2}(E_0 + U - \bar{\lambda}) ,$$

$$H_{25} = \beta^2 V ,$$

$$H_{26} = \frac{N}{4} V , \quad H_{27} = \frac{N^2}{4} V ,$$

$$H_{2,10} = \alpha_<^2 , \quad H_{2,11} = e_<^2 V , \quad H_{2,12} = \Delta^2 V , \quad H_{2,13} = \gamma^2 V ,$$

$$H_{33} = \frac{N}{2}(E_0 + \lambda) ,$$

$$H_{34} = \alpha_>^2 , \quad H_{35} = \beta^2 V ,$$

$$H_{36} = \frac{N}{4} V , \quad H_{37} = \frac{N^2}{4} V ,$$

$$H_{38} = \Delta^2 V , \quad H_{39} = e_>^2 V , \quad H_{3,13} = \gamma^2 V ,$$

$$H_{44} = (E_0 + \lambda)\alpha_>^2 ,$$

$$H_{55} = (E_0 + U)\beta^2 ,$$

$$H_{66} = \frac{N}{4}(E_0 + \mu) ,$$

$$H_{77} = \frac{N^2}{4}(E_0 + U + \mu) ,$$

$$H_{88} = (E_0 + 2\lambda)\,\Delta^2 ,$$

$$H_{99} = (E_0 + 2\lambda)\,e_>^2 ,$$

$$H_{10,10} = (E_0 + U - \bar{\lambda})\;\alpha_<^2 ,$$

$$H_{11,11} = (E_0 + 2U - 2\bar{\lambda})\;e_<^2 ,$$

$$H_{12,12} = (E_0 + 2U - 2\bar{\lambda})\;\Delta^2 ,$$

$$H_{13,13} = (E_0 + \mu)\,\gamma^2 .$$

And the normalization factors are:

$$|\phi_1|^2 = 1 ,$$

$$|\phi_2|^2 = |\phi_3|^2 = \frac{N}{2} ,$$

$$|\phi_4|^2 = \alpha_>^2 , \quad |\phi_5|^2 = \beta^2 ,$$

$$|\phi_6|^2 = \frac{N}{4} , \quad |\phi_7|^2 = \frac{N^2}{4} ,$$

$$|\phi_8|^2 = |\phi_{12}|^2 = \Delta^2$$

$$|\phi_9|^2 = e_>^2 , \quad |\phi_{10}|^2 = \alpha_<^2 ,$$

$$|\phi_{11}|^2 = e_<^2 \ , \qquad |\phi_{13}|^2 = \gamma^2 \ ,$$

The variables used above are defined as:

$$\lambda = \frac{1}{N^2} \sum_{k>k_F} \sum_{l} \left(2\,\varepsilon_{ks_l} - E_{ls_l} \right)$$

$$\bar{\lambda} = \frac{1}{N^2} \sum_{k<k_F} \sum_{l} \left(2\,\varepsilon_{k\bar{s}_l} - E_{l\bar{s}_l} \right)$$

$$\alpha_>^2 = \frac{1}{N} \sum_{k>k_F} \sum_{l} \left(\varepsilon_{ks_l}^2 - \varepsilon_>^2 \right)$$

$$\alpha_<^2 = \frac{1}{N} \sum_{k<k_F} \sum_{l} \left(\varepsilon_{ks_l}^2 - \varepsilon_<^2 \right)$$

$$\varepsilon_> = \frac{2}{N^2} \sum_{k>k_F} \sum_{l} \varepsilon_{ks_l}$$

$$\varepsilon_< = \frac{2}{N^2} \sum_{k<k_F} \sum_{l} \varepsilon_{ks_l}$$

$$e_>^2 = (N-1)\left(\frac{N}{2}-1\right) - \frac{2}{N^2} \sum_{\substack{k>k_F \\ k'>k_F}} \sum_{\substack{l\neq l' \\ k\neq k'}} e^{i(k'-k)(R_l - R_{l'})}\, \delta_{s_l s_{l'}}$$

$$e_<^2 = (N-1)\left(\frac{N}{2}-1\right) - \frac{2}{N^2} \sum_{\substack{k<k_F \\ k'<k_F}} \sum_{\substack{l\neq l' \\ k\neq k'}} e^{i(k-k')(R_l - R_{l'})}\, \delta_{s_l s_{l'}}$$

$$\gamma^2 = \frac{1}{N^2} \sum_{\substack{k>k_F \\ k'<k_F}} \sum_{l,l'} e^{i(k'-k)(R_l - R_{l'})} \delta_{s_l s_{l'}}$$

$$\beta^2 = \frac{1}{N^2} \sum_{\substack{k>k_F \\ k'>k_F}} \sum_{l \neq l'} e^{i(k'-k)(R_l - R_{l'})} \delta_{s_l \bar{s}_{l'}}$$

$$\Delta^2 = \frac{1}{N^2} \sum_{l \neq l'} \delta_{s_l \bar{s}_{l'}}$$

$$\mu = \frac{2}{N} \left(\sum_{k>k_F} \varepsilon_{k\,s} - \sum_{k<k_F} \varepsilon_{k\,s} \right)$$

where N is the number of sites, and E_0 the ground state energy of the half-filled conduction band.

3.3 Ground state of the one-dimensional Anderson lattice

In this section we wish to compare our results [Zhou, 1991e] for the one dimensional PAM with those of the quantum Monte Carlo calculation of Blankenbecler et.al. [Blankenbeckler, 1987], and also with the strong coupling (SC) limit. The values of parameters used are the same as those in [Blankenbeckler, 1987]: $t = 0.5$, and $V = 0.375$. In the strong coupling regime, $U >> \delta$, where the band gap

$$\delta = \sqrt{(1 + 4V^2)} - 1 \tag{3.5}$$

and the ground state energy is given by

$$E_g(U) \;=\; -\frac{1}{2}U + \frac{2}{N}\sum_k \varepsilon_k f(\varepsilon_k) - \frac{2V^2}{N}\sum_k \frac{1 - f(\varepsilon_k)}{\varepsilon_k + \frac{U}{2}} \tag{3.6}$$

with $f(\varepsilon_k)$ the zero temperature Fermi function.

Fig. 3.2 is a plot of the variational ground state energy $E_0(U)$ for the sixteen site lattice. For the large U limit the variational ground state energy converges quite nicely to the Monte Carlo results of [Blankenbeckler, 1987] and for $U \geq 1.8$ are as good or better than the strong coupling theory.

The success of this basis in the large U limit for this symmetric Anderson model is due to the fact that particle hole excitations with a filled f-orbital and 'average' conduction band hole dominate the variational subspace. The energies of these states have the form $(-0.5U + \langle\varepsilon\rangle)$ where $\langle\varepsilon\rangle$ is an average of hole energies over the band. The Coulomb interactions between f-orbitals are also treated exactly in this basis.

It should be noted that the variational basis chosen here does not do well for small U where the actual band structure would begin to dominate. This sequence of vectors represents the band energies by certain averages over the whole band. This characterizes the bands by a sequence of averages closely related to the cumulant expansion well known from statistics. To recover the detailed band structure itself would require large numbers of these vectors. To illustrate this it is useful to examine the simplest complementary variational basis set: one which treats the hybridized bands exactly and treats the f-f Coulomb interaction in mean field only. For this sequence of many-particle states we define hybridized single particle operators $\gamma_{ks}^{\dagger}(\pm)$ which diagonalize the U=0 Hamiltonian.

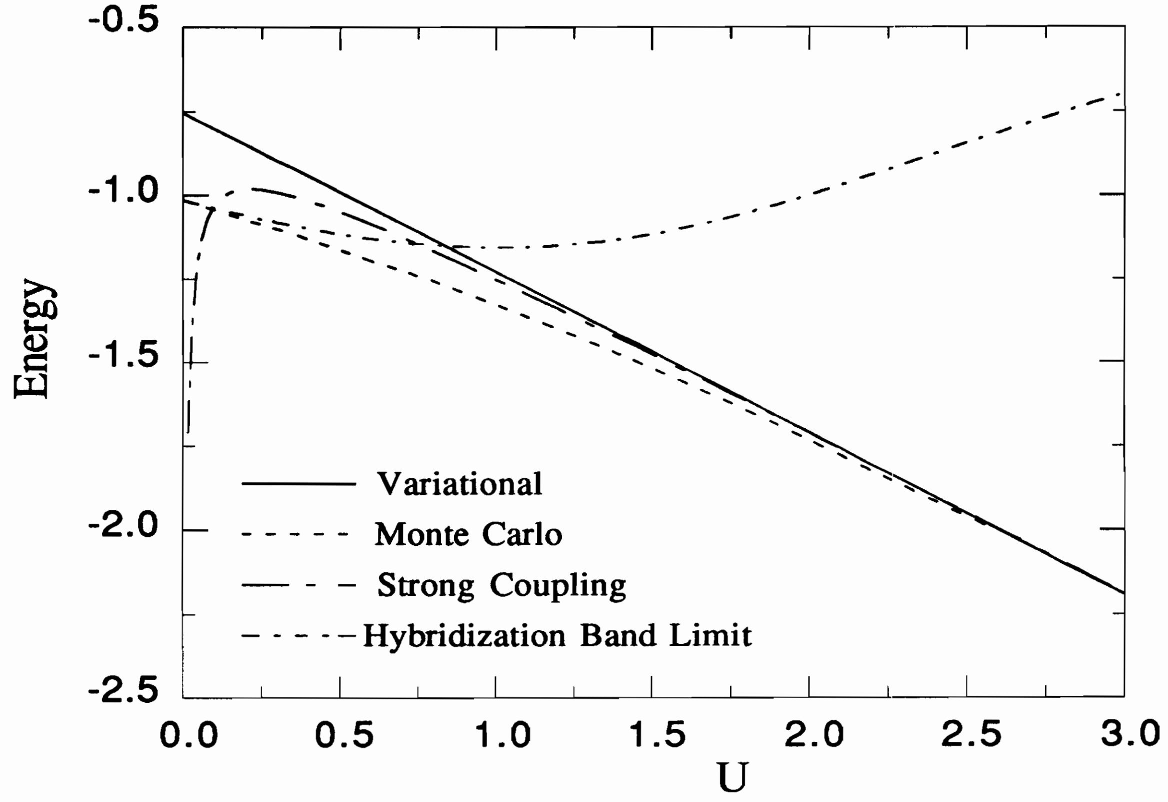

Fig. 3.2 **Ground state energy per site of the 16-site lattice.** Comparing with the Monte Carlo calculation and strong coupling approximation results. The dot-dashed line represents the small U approximation result (Eq.3.10). Parameters used are t = 0.5 and V = 0.375.

The one electron operators are defined as

$$\gamma^{\dagger}_{ks}(\pm) = \frac{Vc^{\dagger}_{ks} + (\lambda_{ks}(\pm) - \varepsilon_{ks})\, f^{\dagger}_{ks}}{\sqrt{V^2 + (\lambda_{ks}(\pm) - \varepsilon_{ks})^2}} \qquad (3.7)$$

where

$$\lambda_{ks}(\pm) = \frac{1}{2}(\varepsilon_{ks} + E_{fs}) \pm \frac{1}{2}\sqrt{(\varepsilon_{ks} - E_{fs})^2 + 4V^2} \qquad (3.8)$$

are the exact energies of the hybridized bands for U=0. The initial variational ground state for this sequence of states is a filled Fermi sea of $\gamma_{ks}{}^{\dagger}(-)$:

$$|G> = \prod_{ks} \gamma^{\dagger}_{ks}(-)\,|0> \qquad (3.9)$$

The dot-dashed line in Fig.3.2 that agrees with the Monte Carlo results at U=0 represents the expectation value of <G|H|G>:

$$E_0(U) = \sum_{ks} \lambda_{ks}(-) + \frac{U}{N}\left[\sum_{k} \frac{V^2 + (\lambda_{ks}(-) - \varepsilon_{ks})^2}{(\lambda_{ks}(+) - \lambda_{ks}(-))^2}\right]^2 \qquad (3.10)$$

In Fig.3.3 we plot the ground state energy for 8, 32, 64 site lattices. In the large U limit where diagonal terms of the Hamiltonian matrix elements dominate and thus where our truncation does well, the energy per site decreases slightly as the size of the lattice increases. As the lattice size is allowed to increase, the number of states present in the true ground state also increases. Thus it is seen that in the mixed-valence regime (small U), for larger and larger lattices our finite basis becomes a poorer approximation.

Further investigation of Fig.3.3 shows that there is another effect to be considered. As U becomes very large the doubly occupied sites which appear in the true ground state will have a vanishingly small amplitude. If one were to ignore such states then the effective number of states in the true ground state would be diminished, tending to improve any finite basis truncation scheme. Thus one needs to investigate the full range of parameter space for a given Hamiltonian before drawing conclusions on size effects and also on the limitations involved in finite-basis methods.

The square of the f-orbital single-site magnetization $<m^f_z(l)^2> = 1 - 2<n^f_{l\uparrow} n^f_{l\downarrow}>$ is shown in Fig.3.4 for a 16-site lattice. Use of the Feynman-Hellman relation enables one to write this function in terms of a derivative of the ground state energy

$$< m^f_z(l)^2 > \ = \ -2\frac{\partial E_g}{\partial U} \tag{3.11}$$

We see that once again our results compare favorably in the large U limit with the Monte Carlo results of [Blankenbeckler, 1987], but fail completely in mixed-valence regime because of the poor approximation to the ground state wavefunction.

It is interesting to investigate the interplay between the Coulomb energy U and the effective hybridization V. As pointed out by Blankenbecler et.al. [Blankenbeckler, 1987], a useful measure of this is given by the ratio of $(f^\dagger_{ls} c_{ls} + c^\dagger_{ls} f_{ls})$ in the interacting ground state to that in the U=0 ground state. Previous results [Blankenbeckler, 1987] demonstrate that the effect of U is to decrease the hybridization. Our calculation of this quantity using the 13x13 basis yields very poor results as expected. We would expect better agreement if more states which couple to the Coulomb energy were added to the basis.

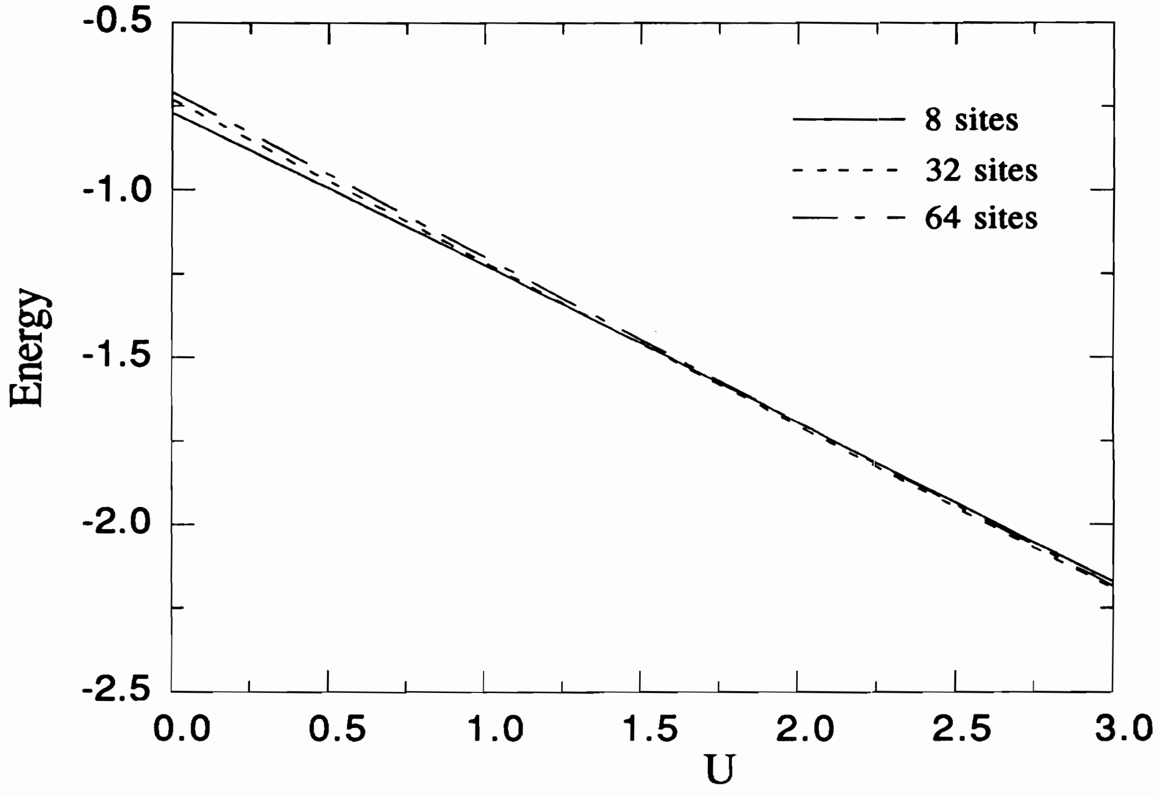

Fig. 3.3 Ground state energy per site of 8, 32 and 64-site lattices. The parameters are the same as those used in Fig.3.2. Note in the mixed-valence regime (small U), the energy of smaller cluster is lower than that of the larger ones in the present approximation.

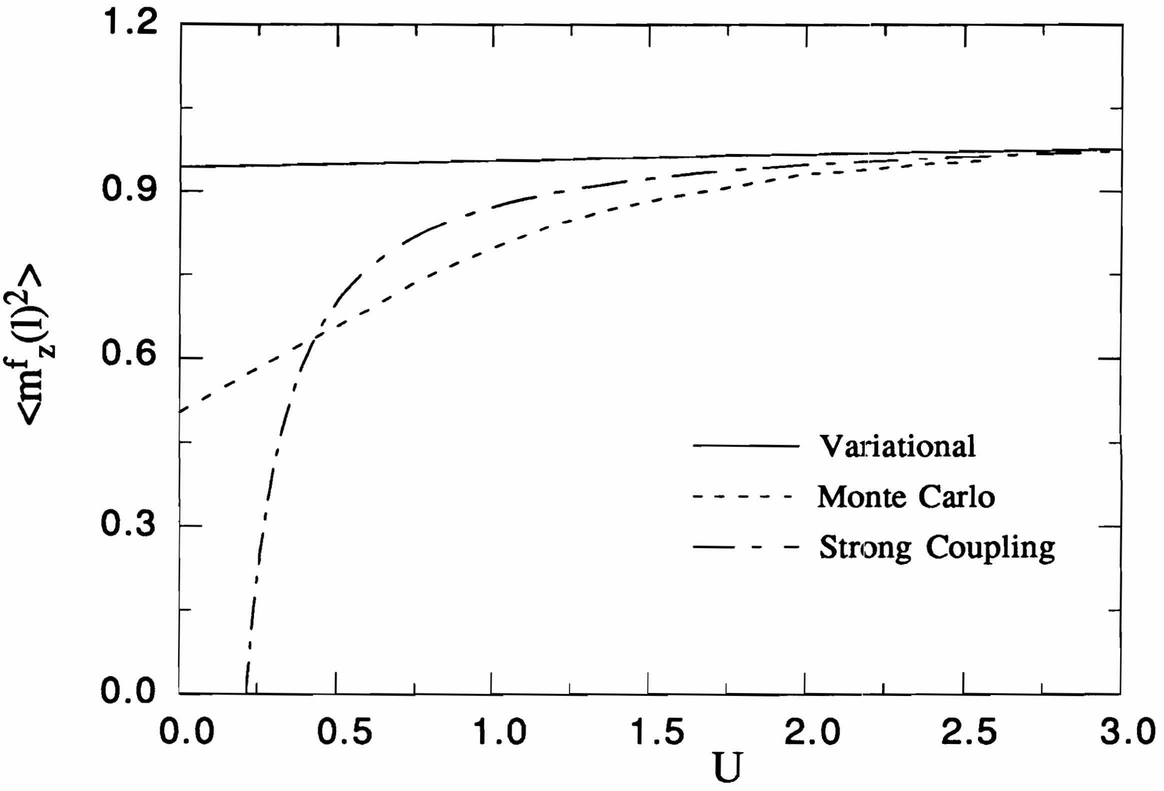

Fig. 3.4 **The square of the f-orbital single site magnetization vs. U for one-dimensional 16-site lattice.** Parameters are the same as those used in Fig.3.2.

3.4 Ground state of the two-dimensional Anderson lattice

With the good agreement between the variational ground state energy and the Monte Carlo result for the one-dimensional periodic Anderson lattice model, one expects this variational scheme to give good estimates for the two dimensional Anderson lattice, a model used extensively for systems with valence electron states [Parks, 1977; Falicov, 1981]. The 2D Hamiltonian has the same form as in one dimension:

$$H = \sum_{k\,s} \varepsilon_{ks} c^{\dagger}_{ks} c_{ks} + \sum_{l\,s_l} E_l f^{\dagger}_{ls_l} f_{ls_l} + U \sum_{l} f^{\dagger}_{l\uparrow} f_{l\uparrow} f^{\dagger}_{l\downarrow} f_{l\downarrow}$$

$$+ \frac{V}{\sqrt{N}} \sum_{k\,l\,s} \left(e^{i\vec{k}\cdot\vec{R}_l} f^{\dagger}_{ls_l} c_{ks_l} + \text{h.c.} \right) \tag{3.12}$$

with the modification that all summations are now two dimensional. The conduction band energy in 2D is

$$\varepsilon_{ks} = -2t\,(\cos(k_x) + \cos(k_y))\,. \tag{3.13}$$

The variatonal basis chosen is a 13 dimensional subspace, and is identical to the basis used for studying the one dimensional model as listed in Fig.3.1. The 13-state basis includes single particle-hole excitations, two particle-hole excitations, and RKKY-type interactions.

Since a fixed 13x13 many-particle basis is kept regardless of the size of a lattice, the calculations can be carried out for moderately large lattice sizes with relatively small amount of computing time. The results for the ground state energies per site as functions of U for

4x4, 8x8 and 16x16 lattices are shown in Fig.3.5, in which we have chosen t=0.5 and V=0.375, consistent with the calculations for one-dimension [Zhou, 1991e; Blankenbecler, 1987]. It is seen that in the vanishing U limit, the larger the lattice size becomes, the higher the variational ground state energy is. We attribute this to the fact that at small U, the true ground state is spanned in a much larger space of states than the subspace of the 13-state-basis used here. And the larger the lattice, the more the basis states there are that overlap the ground state wavefunction. For small U the actual band structure near the Fermi energy should dominate in the system, while the vectors which appear in our calculation represent the band energies by averages over the whole band. For large U (symmetric Anderson model) the ground state will be dominated by singly occupied f states as are the 13x13 basis in this calculation. For this reason we expect that the variational calculation should work well in the large U limit as in the one-dimension case. Similar to the one-dimensional Anderson calculation [Chen, 1988], our ground state energy results here show little size effect in the relevant large U parameter range [Zhou, 1991d].

While we do not expect our results to be valid in the mixed-valence regime (small U), it is useful to apply the simple approximation in this vanishing U limit described by Eq.(3.7)-(3.10) which gives exact ground state energy for U=0, so that an upper bound is given for the ground state energy by combining the results of these two calculations. The results of this simple estimate are shown along with our variational calculations for 4x4, 8x8 and 16x16 lattices in Fig.3.6, Fig.3.7 and Fig.3.8 respectively.

Since results show the similarities between one-dimensional and two-dimensional systems, it should be interesting to compare the ground state energy per site of a two-dimensional lattice with that of a one-dimensional ring with the same number of sites. In

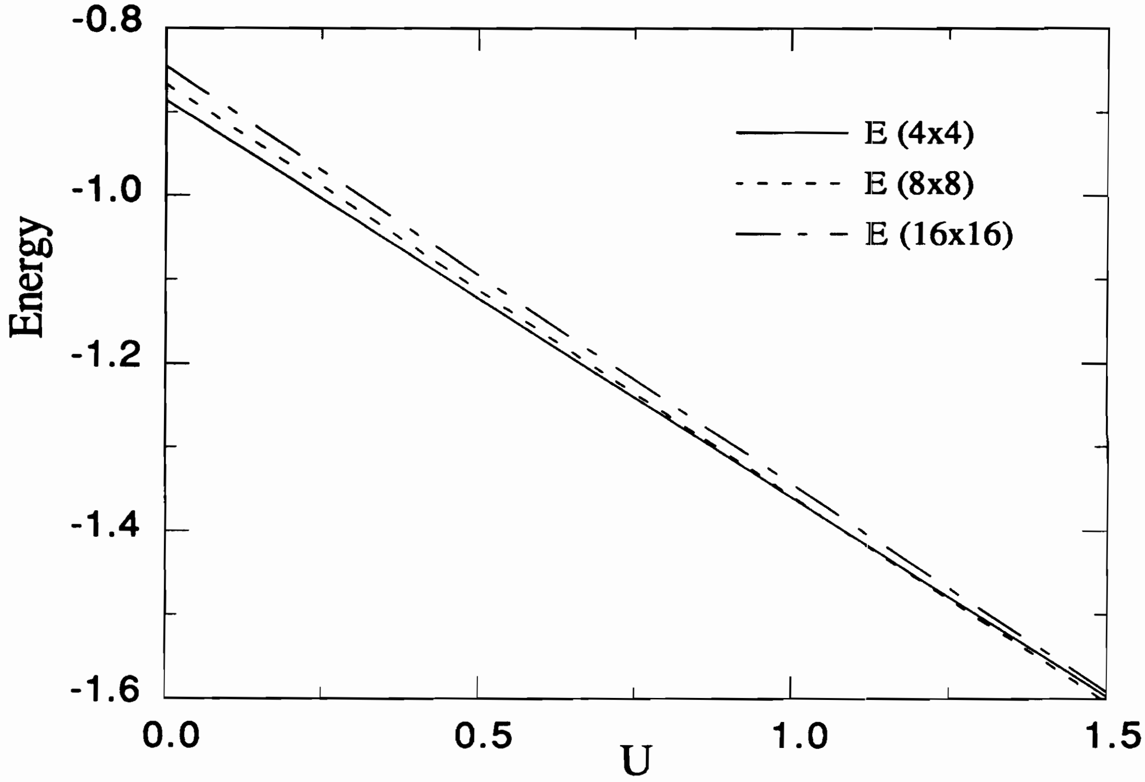

Fig. 3.5 **Ground state energy as a function of U for different two-dimensional lattice sizes.** Retults shown are 4x4 (solid line), 8x8 (dash line) and 16x16 (dot dash line) lattices for t = 0.5 and V = 0.375.

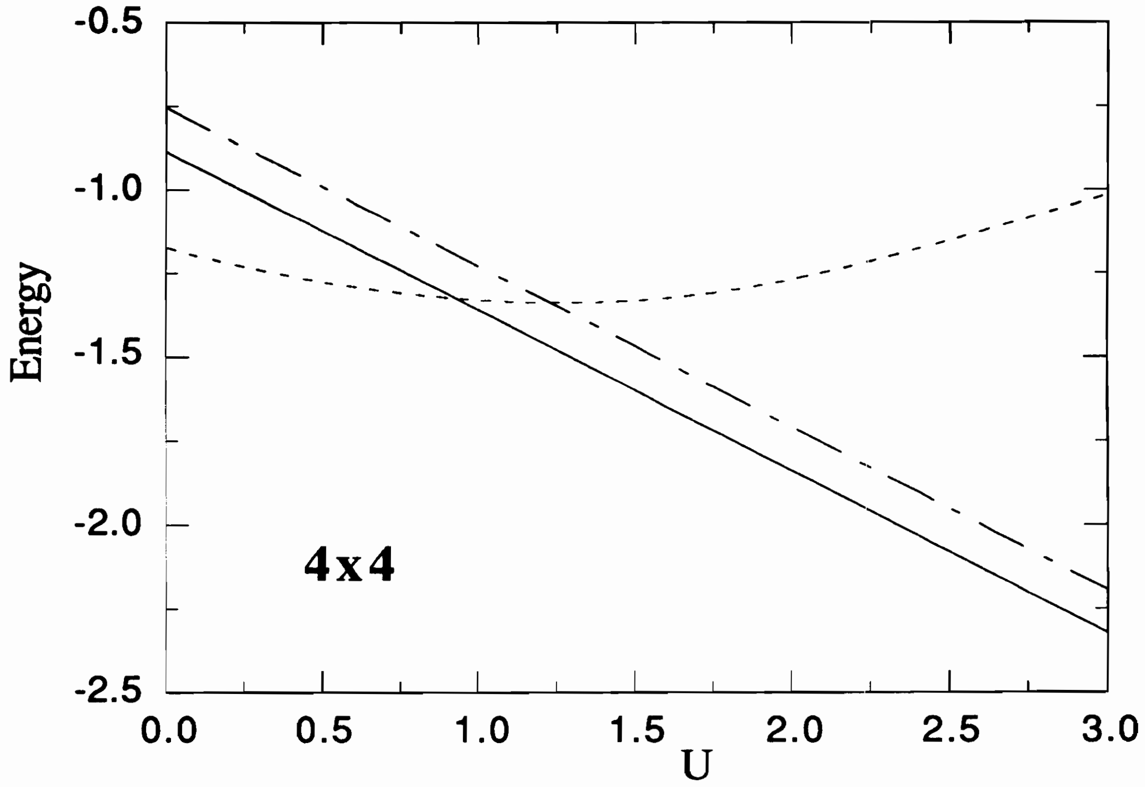

Fig. 3.6 **Ground state energy as a function of U for 4x4 lattice.** The solid line is the result of our variational calculations based on 13x13 matrices. The dashed line is the plot of Eq.(3.10) which approximates the small U ground state. These two lines give an upper bound of the true ground state energy. The variational results for one dimensional 16-site lattice is also plotted (dot-dashed line) for comparison. Parameters are the same as in Fig.3.5.

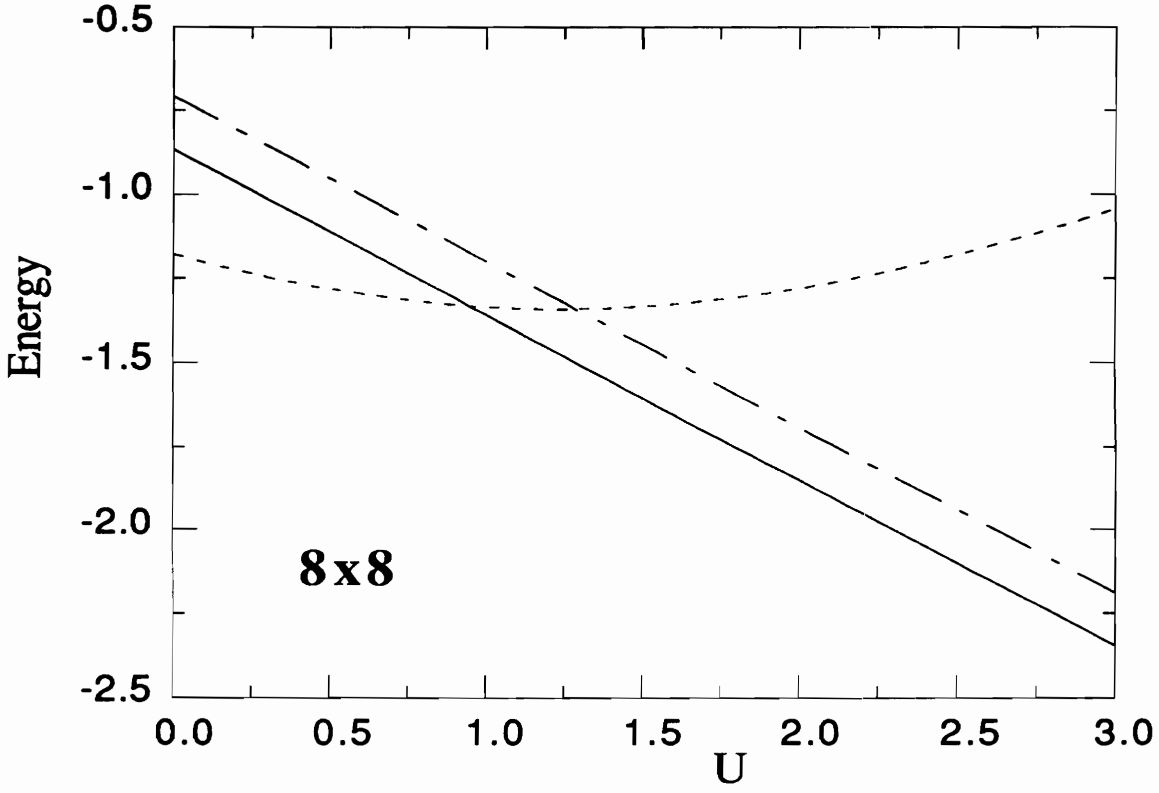

Fig. 3.7 **Ground state energy as a function of U for 8x8 lattice.** The solid line is the result of our variational calculations based on 13x13 matrices. The dashed line is the plot of Eq.(3.10) which approximates the small U ground state. These two lines give an upper bound of the true ground state energy. The variational results for one dimensional 64-site lattice is also plotted (dot-dashed line) for comparison. Parameters are the same as in Fig.3.5.

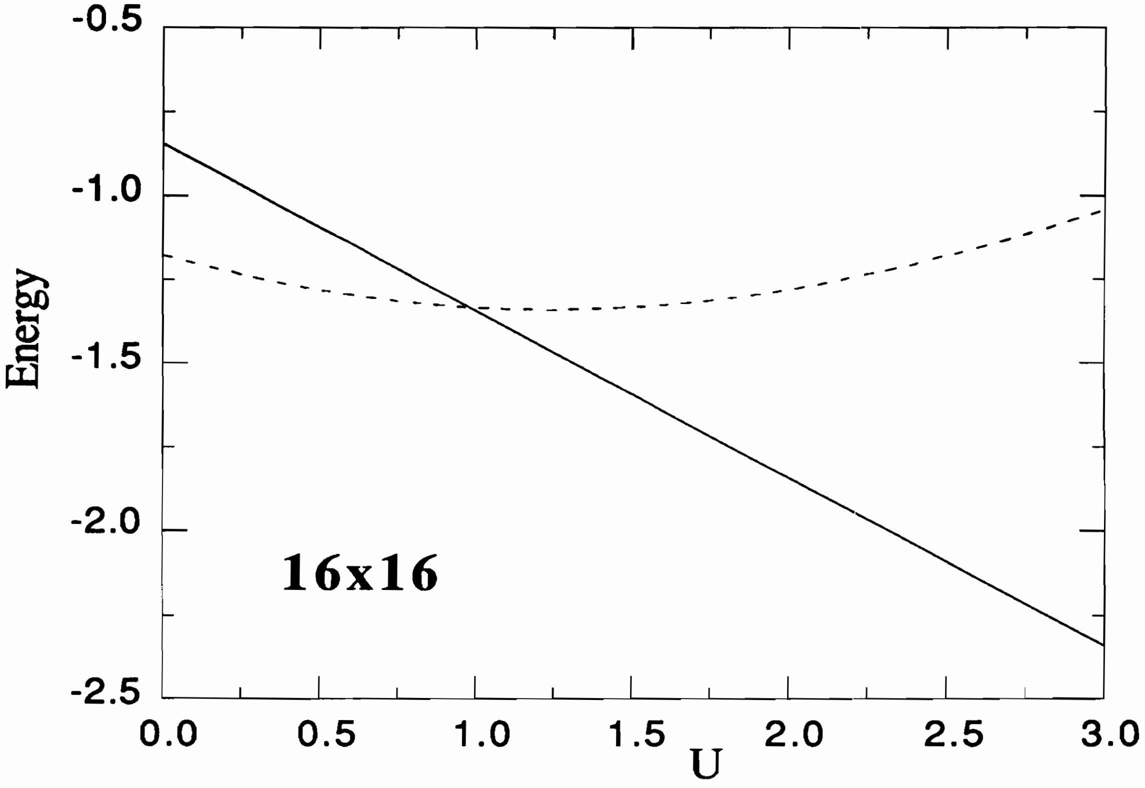

Fig. 3.8 **Ground state energy as a function of U for 16x16 lattice.** The solid line is the result of our variational calculations based on 13x13 matrices. The dashed line is the plot of Eq.(3.10) which approximates the small U ground state. These two lines give an upper bound of the true ground state energy. Parameters are the same as in Fig.3.5.

Fig.3.6 and Fig.3.7, we also compare a 4x4 square lattice ground state energy with that of a 16-site ring, and an 8x8 square with a 64-site ring respectively for our variational calculation in 13 basis states. All of the parameters are the same as those used in Fig.3.5. Despite the similar shapes of the plots, a two-dimensional lattice always has a lower ground state energy than a one-dimensional lattice with the same number of sites. Qualitatively, this is because each atom in a square lattice has 4 nearest-neighbor sites while it has only 2 nearest-neighbors in a ring. Therefore, for a square lattice, each basis state couples with more other states, generating more non-zero off-diagonal elements in the Hamiltonian matrix, which accounts for a lower ground state energy.

As illustrated in the study of one dimensional model, we do not expect to get a good approximation of any ground state property which has a strong dependence on the wavefunction because a small truncated basis has been used, as well as the fact that those vectors representing excitations close to the Fermi energy have been left out. Some of these properties have been studied with exact diagonalization and the Monte Carlo method by Callaway et.al. [Misra, 1987; Zhang, 1988]. However, using a Lanczos variational scheme within a finite basis, we have obtained reasonable results for the ground state energy of square lattices up to 16x16 with a relatively small amount of effort. The approximation can be further improved by choosing a larger basis of states.

3.5 Summary

By using a Lanczos-type of variational method, we have studied the ground state properties of the one and two dimensional periodic Anderson model. With a fairly small amount of computing time, we achieved excellent agreement with the Monte Carlo result on the ground state energy of a 16-site one dimensional lattice in the large U limit. With a fixed number of basis states, this method allows us to carry out the calculation for much larger lattice sizes easily . But for this same reason (limited number of basis states), our results for properties strongly depending on the wavefunction of the ground state are poor. Also, we included particular linear combinations of many-electron states representing a particular phasing (constant phase) of particle-hole excitations both close to the Fermi energy and far away from it in energy. The importance of the other linear combinations of excited states in the variational ground state, particularly for small hybridization, is emphasized by the poor showing of these "fixed phase" excited states that are mixed into the system. We expect improvement by increasing the size of truncated matrix, thus taking into account more basis states.

Chapter 4

One Dimensional Hubbard Model: Exact Diagonalization

The Hubbard model was introduced many years ago [Hubbard,1963], and has been applied to various systems to study their electrical and magnetic properties. Recently it has attracted more attention as a model for high temperature superconductors. The two dimensional (2D) CuO_2 structure in these materials is believed to be the determining factor in making these materials superconducting. The 2D Hubbard model is a candidate for studying the hole movement and the magnetic ordering within the CuO_2 plane. In any case, the Hubbard model is generally regarded as a powerful model for studying strongly correlated and localized electron systems. Within different parameter regions, many other useful models can be derived from the Hubbard Hamiltonion. These include the Heisenburg model, which has been widely used to study surface magnetization, and the t-J model which includes both hole (or electron) movement and the background magnetic ordering in the presence of large Coulomb repulsion energy. Therefore, it is of great importance to understand the properties of the Hubbard model.

In this chapter, a method of exact diagonalization of the Hubbard model Hamiltonian on many-electron Bloch state basis is presented, along with results for small Hubbard rings (one-dimensional Hubbard chains with periodic boundary condition). In contrast to the commonly used single-electron or quasi-particle based approximations, the focal point of our study is the exact many-particle wavefunction. Therefore, unlike other exact diagonalization calculations, the purpose of this study is not to find solutions for relatively large size systems, even though the computer program which has been developed for the task is capable of doing so with sufficient amount of computing time. Instead our attention is focused on the understanding of the properties of many-electron states and what the low-lying eigenstates of the systems consist of, which are essential for other studies of the Hubbard model such as those presented in the following two chapters.

4.1 The Hubbard model

The Hubbard Hamiltonian has the general form:

$$H = \varepsilon \sum_{j,\sigma} n_{j\sigma} + U \sum_{j} n_{j+} n_{j-} + \sum_{j,j',\sigma} t_{jj'} c^{\dagger}_{j\sigma} c_{j'\sigma} \tag{4.1}$$

where j is the lattice site index, $\sigma = \pm$ represents spin up (+) and down(-), c is the electron annihilation operator, and $n_{j\sigma} = c_{j\sigma}{}^{\dagger} c_{j\sigma}$ is the number operator. The energy parameters are the orbital energy ε, the hopping energy between site j and j' $t_{jj'}$, and the Coulomb repulsion U between two electrons at the same site with opposite spins. Normally, ε is set to zero, and $t_{jj'} = t\, \delta_{<j,j'>}$ in the nearest neighbor approximation with sites j and j' being nearest neighbors. This approximation is used to simplify the analysis, even though others, such as the next-nearest-neighbor model which also takes into account hoppings between second nearest neighbor sites, have been studied to investigate the effect of not-so-localized electron motions. Here only the nearest neighbor model is considered, which is sufficient for most of the interesting problems.

Despite the simple form of the Hubbard Hamiltonian, only the ground state of the one-dimensional case has been exactly solved [Lieb, 1968], and using Bethe Ansatz [Lee, 1988] it was found to be an insulating state for the half-filled band ($<n> = 1$). A variety of approximation techniques have been used to study the Hubbard model, among others a variational approach [Coppersmith, 1989], a self-consistant moment expansion method [Nolting, 1989], a functional integral formulations [Cyrot, 1972], and mean-field theories which will be discussed in detail in Chapter 5.

An important approach to the problem is the study of finite Hubbard model systems, where Quantum Monte Carlo (QMC) simulation is a powerful numerical method for this study. Hirsch et.al [Hirsch, 1982; 1983; 1984a; 1984b] have carried out the QMC simulations for one dimensional chains of up to 40 sites. These results are commonly regarded as "exact" results because of their accuracy, even though they suffer difficulties in approaching zero temperature and extrapolating to infinite lattice size (thermodynamic limit).

Another method widely used to solve the finite cluster problem is the diagonalization of the Hamiltonian on the basis of all existing states in the model system. Here the model is solved exactly using a specific basis. Since the computing time increases exponentially with the size of the system, the exact diagonalization method is limited to small clusters, and becomes of limited use in more than one dimension. However, the ground state and excited state wavefunctions which arise can be written explicitly, allowing one to gain more physical insight into the behavior of the system. Other studies can benefit from the exact solution of these small clusters. For example, one can use the ground state wavefunction of a finite system as a guide for choosing the initial state in a variational calculation. Also, the exact diagonalization method is valid for all temperatures, therefore it serves as a compensation and convergence benchmark for QMC simulations. For these reasons, it is not surprising that the small one-dimensional Hubbard chains have been studied intensively, and the exact diagonalization of chains up to 12 sites have been performed [Shiba, 1972; Soos, 1984] with reports of studies of larger sizes underway.

In order to have a better understanding of the properties of low-lying eigenstates, we have diagonalized the Hubbard Hamiltonian in a many-electron Bloch state basis, and have investigated the exact wavefunctions for systems with various numbers of electrons and sites. The details of these calculations and results are presented in the following two sections.

4.2 The many-electron Bloch states of Hubbard rings

The one-electron Bloch state operator is the Fourier transform of the real-space electron operator $c_{l\sigma}{}^{\dagger}$ into momentum space:

$$c_{k\sigma}^{\dagger} = \frac{1}{\sqrt{N}} \sum_{l} e^{ikl} c_{l\sigma}^{\dagger} \tag{4.2}$$

where l and σ are site and spin indices respectively, N the total number of sites. In the basis of $c_{k\sigma}{}^{\dagger}$, the system is described by the band structure solution of the Slater determinant:

$$\det (<0 \mid c_{k\sigma} H c^{\dagger}_{k'\sigma'} \mid 0> - \omega I) = 0 \tag{4.3}$$

in which H is the Hamiltonian, I is the unit matrix, and $|0>$ is the vacuum state.

A failure of the one-electron band structure is that it does not reflect the complex properties of strongly interacting many-particle systems such as the Hubbard model. Thus it is necessary to introduce the relevant many-electron Bloch states:

$$|\Psi_k> = \frac{1}{\sqrt{N}} (\sum_{l'} e^{ikl'} \prod_i c^{\dagger}_{l'+l_i,\sigma_i}) \mid 0> \tag{4.4}$$

$|\Psi_k>$ is an eigenstate of the translation operator T, which translates the lattice by one unit cell and commutes with the Hamiltonian of any system with periodic boundary condition with eigenvalue e^{ika} (where a is the lattice constant).

To have a better understanding of Eq.(4.4), let us illustrate an example of a many-electron Bloch state of a half-filled four-site Hubbard ring [Callaway, 1987a; Mazumdar]:

$$(\otimes O \uparrow \downarrow)_k = \frac{1}{2} [(\otimes O \uparrow \downarrow) - e^{ika} (\downarrow \otimes O \uparrow)$$

$$+ e^{2ika} (\uparrow \downarrow \otimes O) + e^{3ika} (O \uparrow \downarrow \otimes)] \tag{4.5}$$

in which notations ⊗, O, ↑ and ↓ represent doubly-occupied site, empty site, and singly-occupied sites with electron spin $\sigma = +$ and - respectively. The "–" sign in front of the Wannier state (↓ ⊗ O ↑) comes from the fact that it takes three interchanges of electron-pairs to achieve (↓ ⊗ O ↑) from state (⊗ O ↑ ↓), and each interchange would contribute a "–" sign because electrons are fermions. To demonstrate that the the many-electron

Bloch state is indeed an eigenstate of the translation operator T, let us examine the case in Eq. (4.5):

$$\begin{aligned} T(\otimes O \uparrow \downarrow)_k &= \frac{1}{2}[T(\otimes O \uparrow \downarrow) - e^{ika}T(\downarrow \otimes O \uparrow) \\ &\quad + e^{2ika}T(\uparrow \downarrow \otimes O) + e^{3ika}T(O \uparrow \downarrow \otimes)] \\ &= \frac{1}{2}[(O \uparrow \downarrow \otimes) + e^{ika}(\otimes O \uparrow \downarrow) \\ &\quad - e^{2ika}(\downarrow \otimes O \uparrow) + e^{3ika}(\uparrow \downarrow \otimes O)] \\ &= e^{ika}(\otimes O \uparrow \downarrow)_k \qquad (4.6) \end{aligned}$$

Also, Eq.(4.6) shows that

$$T(\otimes O \uparrow \downarrow)_k = (O \uparrow \downarrow \otimes)_k \qquad (4.7)$$

which is exactly the definition of T. Combining Eqs. (4.6) and (4.7), it is easily seen that

$$T^4(\otimes O \uparrow \downarrow)_k = e^{4ika}(\otimes O \uparrow \downarrow)_k = (\otimes O \uparrow \downarrow)_k \qquad (4.8)$$

$$k = 2n\pi/Na, \quad n = 0, 1, 2, ..., N-1 \qquad (4.9)$$

where N = 4 in the case of Eq.(4.8). This implies that wavefunctions with only a finite number of k-points can be obtained from the small-cluster calculations. In the thermodynamic limit ($N \rightarrow \infty$), a continuous spectrum of states emerges.

One advantage of using the periodic boundary condition, and thus translational symmetry, is that the number of basis states is greatly reduced. In Eq.(4.5), one many-electron Bloch state includes N = 4 Wannier states. In the case of the half-filled four-site ring with $S_z = 0$, the total number of many-electron Bloch states is 10, comparing with 36 Wannier states. Therefore the Hamiltonian matrix to be calculated is reduced from 36x36 to 10x10. The reduction factor is not exactly 4 because there are states like $(\uparrow\downarrow\uparrow\downarrow)_k$ which includes only two Wannier states since its translational period is 2a instead of Na. The collection of all 10 basis vectors used in diagonalizing H is listed below:

$$(\uparrow\uparrow\downarrow\downarrow)_k \quad (\uparrow\downarrow\uparrow\downarrow)_k \quad (O\downarrow\uparrow\otimes)_k \quad (O\uparrow\downarrow\otimes)_k \quad (\uparrow O\downarrow\otimes)_k$$

$$(\uparrow\downarrow O\otimes)_k \quad (\downarrow\uparrow O\otimes)_k \quad (\downarrow O\uparrow\otimes)_k \quad (OO\otimes\otimes)_k \quad (O\otimes O\otimes)_k$$

4.3 The exact solutions of small Hubbard rings

Other than the translational symmetry, there are other symmetries in the periodic Hubbard model which may be exploited to reduce the size of the H matrix and to gain more insight about the system. Two symmetries that have been implemented in our calculation are conservation of total spin squared S^2 and the magnetization S_z:

$$[S_z,H] = 0, \quad [S^2,H] = 0 \tag{4.10}$$

where

$$S^2 = \sum_{i,j} \vec{S}_i \cdot \vec{S}_j = \sum_i S_i^2 + 2\sum_{i<j} S_i^z S_j^z + \sum_{i<j} (S_i^+ S_j^- + S_i^- S_j^+) \tag{4.11a}$$

and

$$S_z = \sum_i S_i^z , \qquad S_j^{\pm} = S_j^x \pm i S_j^y \tag{4.11b}$$

in which subindices i and j are site indices. The effect of S_i^+ (S_i^-) is to flip electron spin at site i up (down). The commutation relations of Eq.(4.10) allow one to find the eigenvectors of S^2 as linear combinations of the many-electron Bloch states with fixed S_z, and then construct the Hamiltonian matrix on the basis of these S^2 eigenvectors. Also, because S^2 and S_z commute, only states in the subspace of $S_z = \min(S_z)$ (i.e., $S_z = 0$ for system with even number of electrons, $S_z = 1/2$ for system with odd number of electrons) need to be involved in the calculation since two states with the same value total spin S but different S_z are degenerate. This feature greatly reduces the computational effort. All energy spectrum graphs shown in this chapter are results for $S_z = \min(S_z)$. A complete set of programs has been developed to perform this task, and the results for various lattice sizes and band-fillings are presented below. In all of our calculations, the energy scale is set by defining orbital energy $\varepsilon = 0$ and hopping energy $t = 1$. By using the electron-hole symmetry, the energy of the system with a negative t can be derived from [Callaway, 1987a]:

$$E_{n'}(-t) = E_n(t) + (N-n)\,U \tag{4.12a}$$

where

$$n' = 2N - n \tag{4.12b}$$

in which N is the number of sites and n (n') is the number of electrons. In the graphs shown below, the unit of k-vector is π/a.

4.3.1 Four sites with three electrons

Due to its relatively small number of Bloch states, this system can be solved with little computational effort [Callaway, 1987a], thus it is used as a test of our program. Also by comparing the results with those of the half-filled four site lattice, one can learn about the effect of hole doping in the Hubbard model. Fig.4.1 shows the energies (per site) of all eigenstates of the system at possible k-point within the Brillouin zone ($-1 < k \leq 1$). Because of the symmetry around $k = 0$, the negative k states are omitted in the figure. It is seen that for $U = 4t$ (Fig.4.1a), the ground state $|\psi_1>$ is a $S = 1/2$ state with momentum $k = \pi/2a$, while the first excited state $|\psi_2>$ is located at $k = \pi/a$ within the Brilloin zone with $S = 3/2$. The corresponding wavefunctions are:

$$\begin{aligned} |\psi_1> \;=\;& a_1 (O\downarrow\uparrow\uparrow)_k + a_2 (O\uparrow\downarrow\uparrow)_k + a_3 (\uparrow\downarrow O\uparrow)_k \\ & + a_4 (O O\uparrow\otimes)_k + a_5 (O\uparrow O\otimes)_k + a_6 (\uparrow O O\otimes)_k \end{aligned} \tag{4.13a}$$

$$|\psi_2> \;=\; b[(O\downarrow\uparrow\uparrow)_k + (O\uparrow\downarrow\uparrow)_k + (\uparrow\downarrow O\uparrow)_k] \tag{4.13b}$$

where

$$a_1 = -0.1013 + 0.4707\,i\,; \quad a_2 = -0.3802 - 0.4707\,i\,; \quad a_3 = -0.4815\,;$$
$$a_4 = -0.0413 + 0.1919\,i\,; \quad a_5 = -0.1919 - 0.2375\,i\,; \quad a_6 = 0.1963\,,$$

and

$$b = \frac{1}{\sqrt{3}}\,.$$

As U gets larger and larger, the energy of the low-lying eigenstate at $k = \pi/2a$ becomes higher and higher, surpasses the energy of $S = 3/2$ state at $k = \pi/a$ for $U > 18.6t$. This same critical value of U was found by Callaway et.al [1987a]. The energy spectrum for $U = 24t$ is plotted in Fig.4.1b. By examining the wavefunctions of the two low-lying states, it is found that $|\psi_2>$ in Eq.(4.13b) remains the same, while the weights for Bloch states with double occupancy in $|\psi_1>$ reduce dramatically. The new coefficients of $|\psi_1>$ in

Eq.(4.13a) are:

$$a_1 = -0.2419 + 0.5073\,i\,; \quad a_2 = -0.3201 - 0.5073\,i\,; \quad a_3 = -0.5620\,;$$

$$a_4 = -0.0181 + 0.0379\,i\,; \quad a_5 = -0.0379 - 0.0601\,i\,; \quad a_6 = 0.0420\,.$$

The transition of the ground state from S = 1/2 to S = 3/2 is interesting for the reason that the system is generated by doping a hole into a half-filled lattice. However, for such a small system, one should be cautious trying to draw any conclusions about the transition between magnetic ordered states.

4.3.2 Half-filled four-site system

The system of a four-site ring with four electrons is a typical half-filled Hubbard model with even (number of sites) symmetry. It has been proved by Lieb and Wu [1968] that the ground state of such a system is an antiferromagnetic (AF) state. The many-electron energy spectrum of this half-filled four-site ring is shown in Fig. 4.2 for U = 4t (FIg.4.2a) and U = 10t (Fig.4.2b). In both cases, in contrast to the system with one hole, the ground state is a S = 0 state at k = π/a, which remains the lowest state with increasing Coulomb energy U. It is interesting to note that the Neel state $(\uparrow\downarrow\uparrow\downarrow)_k$ is only part of the S = 0 and k = π/a eigenstate, but not part of the S = 0 and k = 0 eigenstate. By examining the wavefunction it is seen that the ground state is dominated by two Bloch states without double occupancy: $(\uparrow\downarrow\uparrow\downarrow)_k$ and $(\uparrow\uparrow\downarrow\downarrow)_k$. As U gets larger and larger, the energies of the eigenstates dominated by configurations with doubly occupied sites (thus with a diagonal energy U) get higher and higher, creating an energy gap in the eigenstate spectrum, as shown in Fig.4.2b.

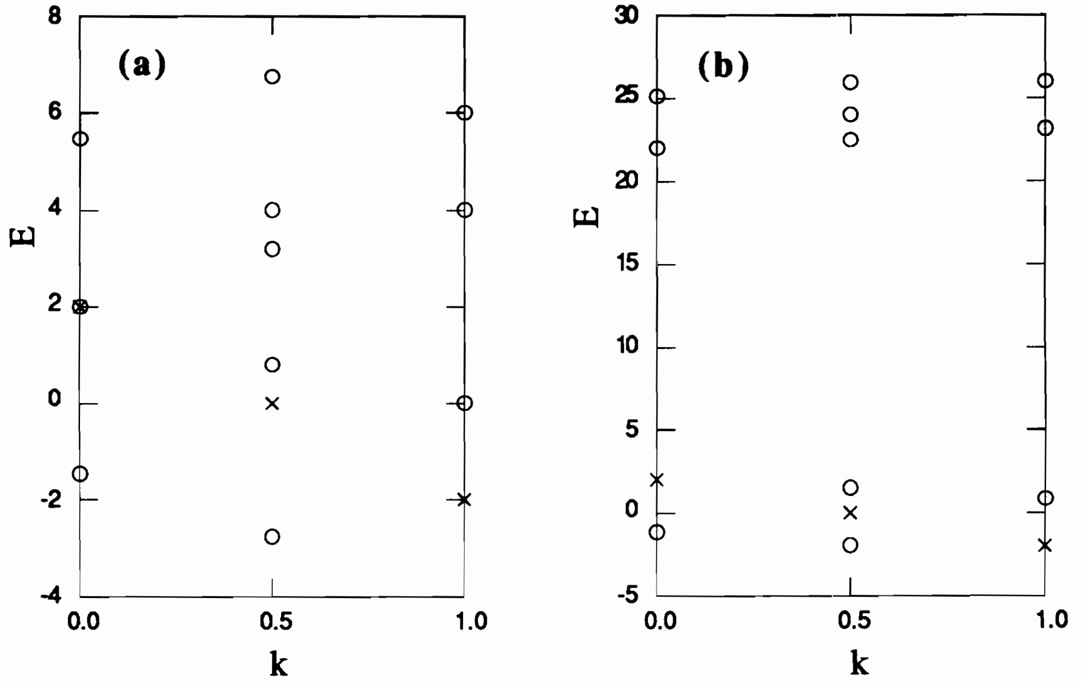

Fig. 4.1 **Eigenstate energy spectrum of the four-site, three-electron Hubbard ring.** Symbols 'o' and 'x' represent S = 1/2 and 3/2 correspondingly. Horizontal axis is k in unit of π/a, and vertical axis is energy per site in unit of t.

(a) U = 4t. The ground state is a S = 1/2 state at k = π/2a.

(b) U = 24t. The ground state is a S = 3/2 state at k = π/a (for U > 18.6t). Notice the gap induced by the large U.

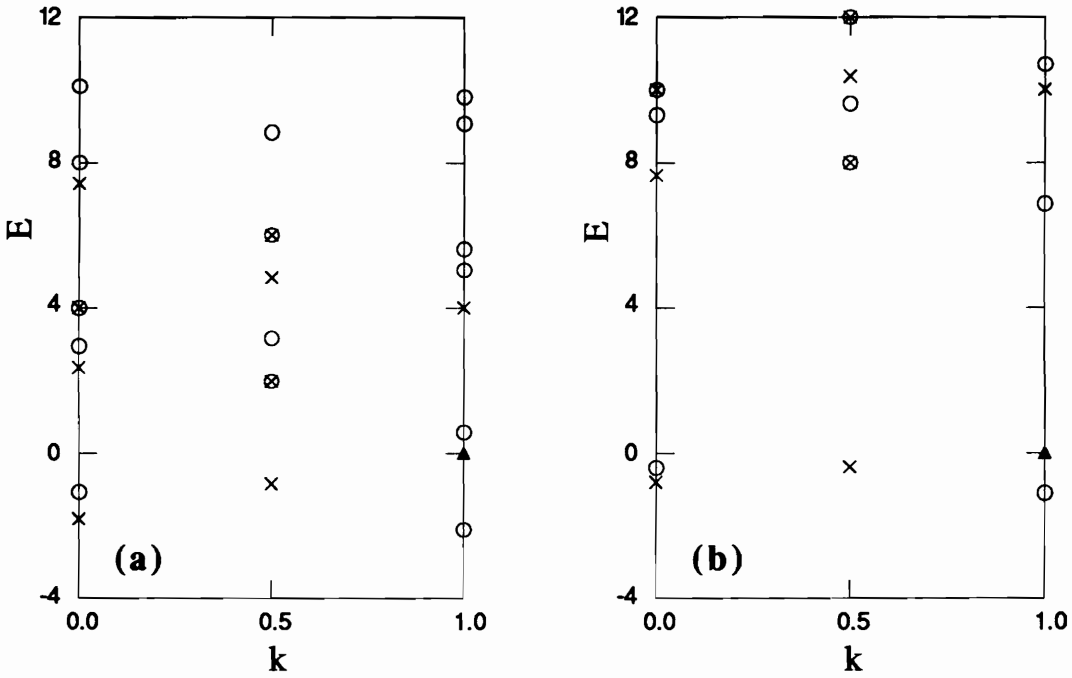

Fig. 4.2 **Eigenstate energy spectrum of the four-site, four-electron Hubbard ring.** Symbols 'o', 'x' and 'Δ' represent S = 0, 1 and 2 correspondingly. Horizontal axis is k in unit of π/a, and vertical axis is energy per site in unit of t.

(a) U = 4t. The ground state is a S = 0 state at k = π/a.

(b) U = 10t. The ground state remains at k = π/a with increasing U.

4.3.3 Four electrons in six- and eight-site rings

With increasing number of sites, fixing the number of electrons is equivalent to introduce more holes in the system. The effect of doping on the low-lying many-electron states can be observed in Fig.4.3, in which the energy spectra for four electrons in six-site (Fig.4.3a) and eight-site (Fig.4.3b) rings are shown with parameter $U = 4t$. As the lattice size gets larger and larger, there are more and more allowed center of mass momentum k points, but the four low-lying states in the half-filled system (Fig.4.2) can be easily identified here. The ground state is now taken over by the $S = 1$ state with momentum $k = 0$. That the energy of the ground state gets lower with increasing lattice size can be easily understood because the many-elelctron basis becomes larger along with the lattice size, electrons are motive, therefore there are more couplings between many-particle states.

4.3.4 Four electrons in five- and seven-site rings

In contrast to cases of four electrons in an even-number-site lattice, the odd-number-site system does not have a many-particle eigenstate at $k = \pi/a$, therefore the energy spectrum looks very different. Fig.4.4 shows the low-lying states of the five-site (Fig4.4a) and seven-site (Fig4.4b) lattices with four electrons for $U = 4t$. In both cases the ground state is a $S = 0$ state with momentum $k = 0$, and the gap between the ground state and excited states is apparent, even though those low-lying excited states are not dominated by double-occupancy. These features are related to different symmetries in the momentum space due to the odd number of k-points, thus any conclusion about effects of hole doping derived from such calculations would not have much physical meaning without the support of calculations for even-number-site lattices. For this reason, it is not surprising to see

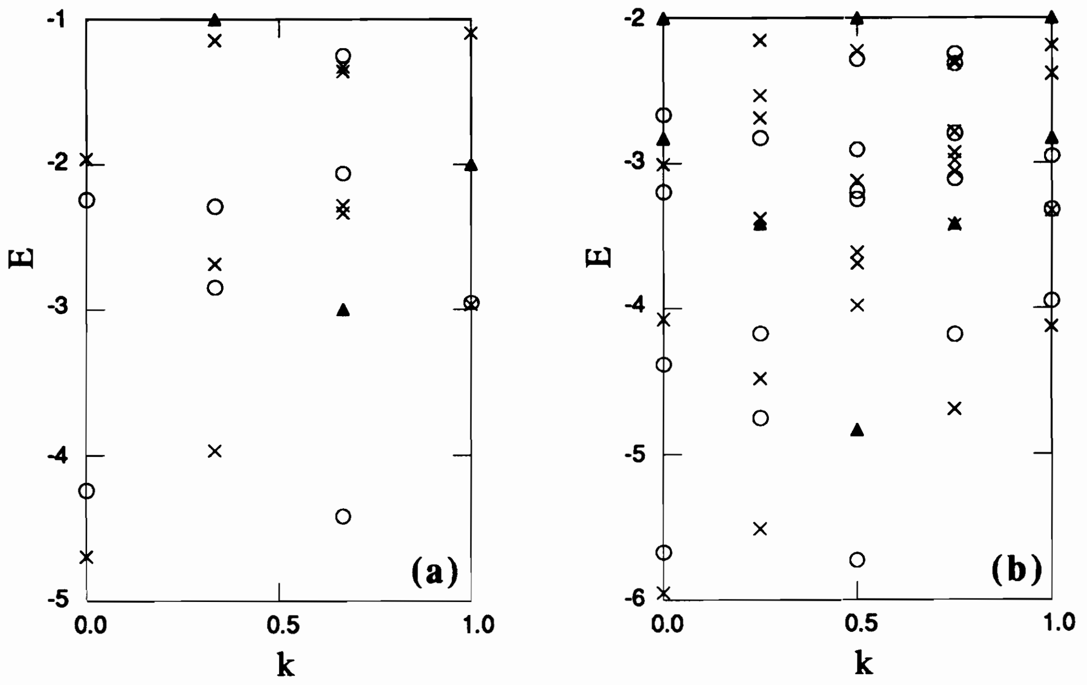

Fig. 4.3 **Eigenstate energy spectra of the six-site (a) and eight-site (b) Hubbard rings with four electrons.** In both cases U = 4t. Symbols 'o', 'x' and 'Δ' represent S = 0, 1 and 2 correspondingly. Horizontal axis is k in unit of π/a, and vertical axis is energy per site in unit of t.

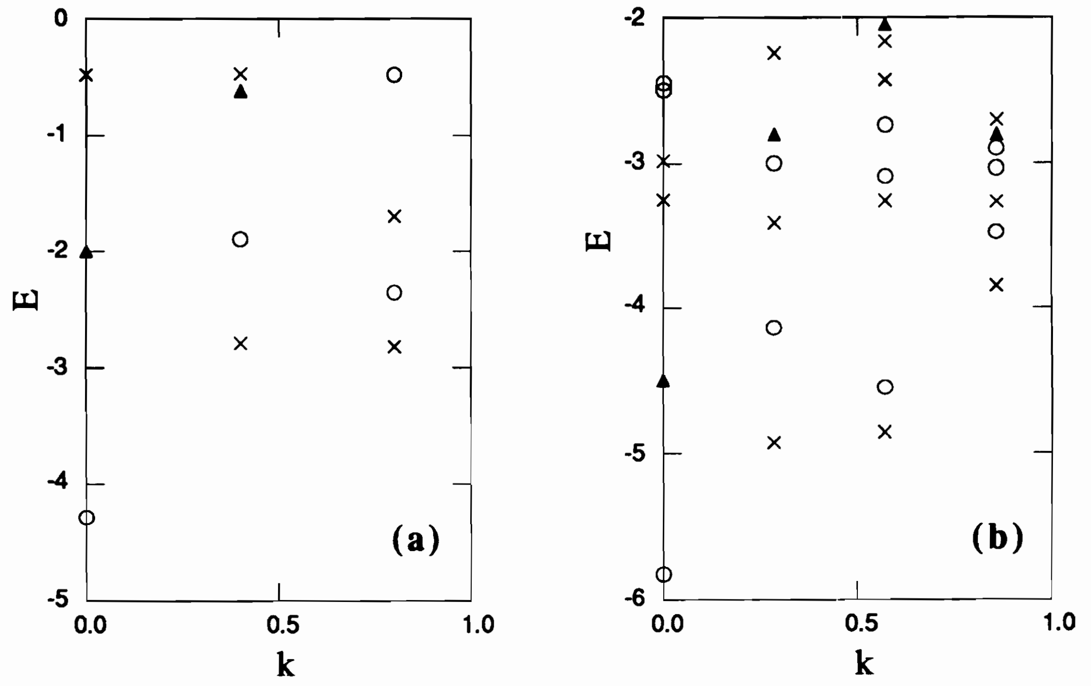

Fig. 4.4 **Eigenstate energy spectra of the five-site (a) and seven-site (b) Hubbard rings with four electrons.** In both cases U = 4t. Symbols 'o', 'x' and 'Δ' represent S = 0, 1 and 2 correspondingly. Horizontal axis is k in unit of π/a, and vertical axis is energy per site in unit of t.

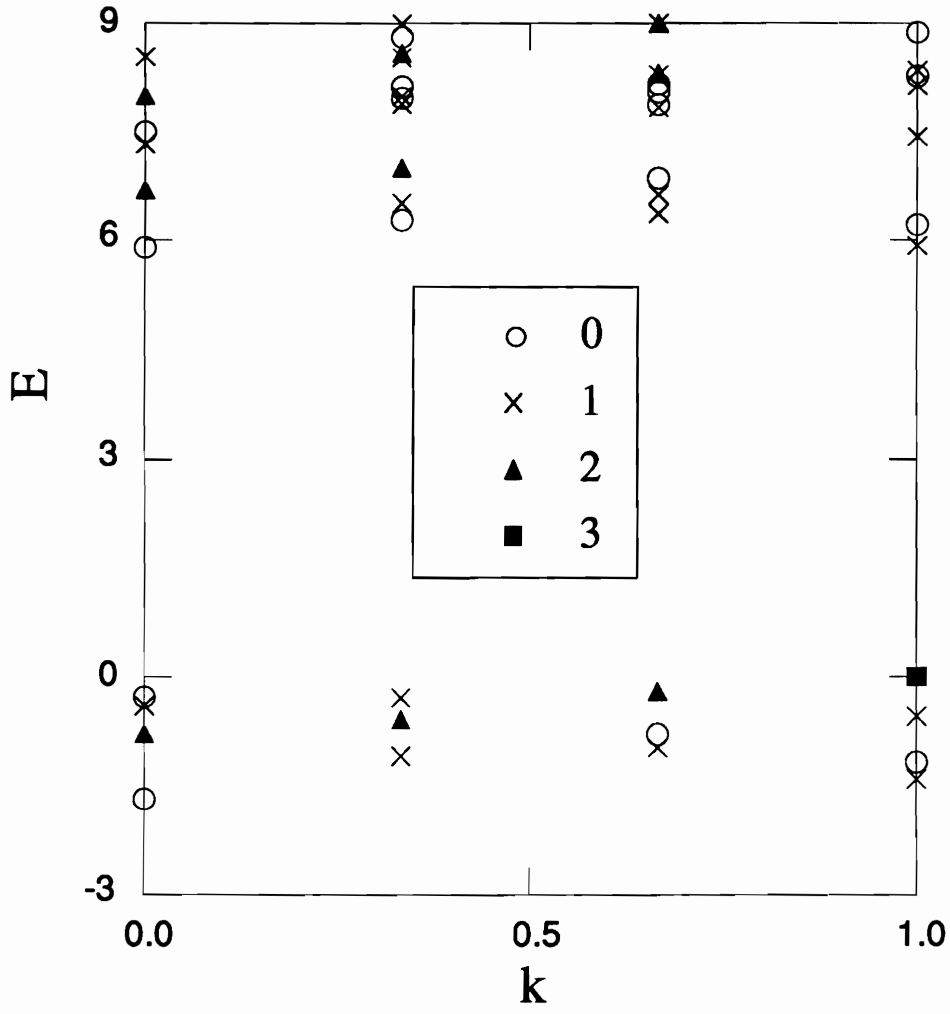

Fig. 4.5 **Eigenstate energy spectra of the half-filled six-site Hubbard ring.** U = 10t. Symbols 'o', 'x', 'Δ' and square represent S = 0, 1, 2 and 3 correspondingly. Horizontal axis is k in unit of π/a, and vertical axis is energy per site in unit of t.

completely different energy spectra for four- and five-site systems with one hole each (Fig.4.1a and Fig.4.4a).

4.3.5 Half-filled six-site system

The last case shown is the energy spectrum of a half-filled six-site ring for U = 10 (Fig.4.5). There is an obvious Hubbard gap due to the relatively large U. Even though the system has an even number of lattice sites, it is found the ground state has momentum $k = 0$ rather than $k = \pi/a$ as seen in a four-site and eight-site ring (results not shown here). This illustrates again the importance (thus the limitations) of symmetry in small cluster calculations. More dicussion on this is presented in the next section.

4.4 Summary

The exact solutions of small one-dimensional Hubbard rings have been found by diagonalizing the Hamiltonian matrices in the basis of many-particle Bloch states. The energy spectra for various lattice sizes and band-fillings are presented, and the effect of hole doping is discussed. It is found that the energy spectrum relies heavily on the symmetry of the lattice. Even though some physical quantities such as the energy and local-magnetization may be extrapolated to the thermodynamic limit without being affected by different symmetries, other important properties including the center of mass momentum and magnetic ordering can be extrapolated only within a particular symmetry. This proves to be rather difficult, especially for higher dimensional systems, since the lattice size and the number of basis states increase rapidly for a given symmetry. However, these limitations do not diminish the roles of exact calculations of small clusters as a guide for variational calculations and as benchmarks of Monte Carlo simulations.

Chapter 5

Two Dimensional Hubbard Model: Projection Operator Mean-Field Calculation

The two dimensional Hubbard model provides one of the simplest models for the electronic structure in high T_C superconductors when one assumes the relevant motion is confined to the Cu-O planes. Since the model was introduced in the early sixties [Hubbard, 1963], many analytical and numerical methods have been used to solve for its dynamics. Exact numerical solutions have been found for small clusters by diagonalizing the Hamiltonian in the basis of many-particle states [Dagotto, 1989; Lin, 1988; Callaway, 1987b]. However, since the size of these matrices increases rapidly with cluster size, it is difficult to examine long range correlations in this way. Monte Carlo simulations [Moreo, 1990; White, 1989; Hirsch, 1985] allow one to obtain reasonably accurate results for somewhat larger cluster sizes, but still the problems of size effects and how to address long range correlations remain. Despite these difficulties and the problem with low temperatures, Monte Carlo results are roughly "exact" in the appropriate parameter range and can serve as a benchmark to test various analytical approximations.

There exist several mean field (MF) theories predicting the nature of the quasiparticle bands in Hubbard-like models, the earliest using the so called Hubbard-I approximation which was introduced along with the model itself [Hubbard, 1963]. Others include a moment expansion technique [Geipel, 1988], the method of irreducible Green's functions [Goryachev, 1982; Yushankhai, 1991], the four-boson theory of Kotliar and Ruckenstein [Kotliar, 1986] and more recently the slave-boson (SB) and slave fermion (SF) theories [Ruckenstein, 1987; Kotliar, 1988; Jayaprakash, 1989; Yoshioka, 1989]. While most of these theories more or less agree on gross average properties such as the energy and double occupancy, many disagree on other more subtle properties such as the momentum distribution, effective mass and the shape and volume of the Fermi surface. Also certain MF theories (e.g. Hubbard-I) have difficulty finding stable antiferromagnetic (AF) solutions in the relevant parameter range. Since MF theories by their very nature involve uncontrolled approximations, it is not easy to compare different MF theories directly or to estimate their validity.

In this chapter the results of a MF calculation on the single-band and three-band two dimensional Hubbard models based on a projection operator scheme [Fedro, 1982; Fedro, 1987; Ruckenstein, 1988] is presented. In this approach, the two usual Hubbard projection operators are defined (involving creation/destruction of a fermion at site j with spin σ either in the presence or absence of the fermion at the same site j with spin $-\sigma$), and the model is solved with an equation of motion method for these operators using a well-defined truncation procedure which treats the complicated statistics of these operators properly. In this way we generate an exact Dyson-like equation for the Green's functions where the self-energy is found to contain both static and dynamic contributions. The effects due to the dynamic terms (in this context termed memory functions) will be ignored within this approach. Thus a MF set of equations for the needed Green's functions are defined. These equations are then solved self-consistently for all band fillings and for possible AF order. It is important to point out that this formulation deals with the physical fermion directly. There is no need to separate the spin and charge degrees of freedom as is done in slave theories. Also it has been shown by Ruckenstein and Schmitt-Rink [Ruckenstein, 1988] that, in the large spin degeneracy (large N) limit, the present approach and the slave boson theory are identical. This theory, however, does not satisfy Luttinger's theorem for finite degeneracy although the deviation is shown not to be significant away from half-filling. It should also be pointed out that this method is essentially equivalent to the method of irreducible Green's functions [Goryachev, 1982; Yushankhai, 1991] which has been used recently in studies of the single-band Hubbard and t-J models.

Recent work by Lilly et.al. [Lilly, 1990] compared the four-boson theory (SBMF) [Kotliar, 1986] to the Monte Carlo (MC) results [Moreo, 1990] on the single band Hubbard model and found excellent agreement for various static and dynamic quantities in both the weak and strong coupling limits. In this chapter a systematic comparison between Hubbard I, SBMF and the projection operator MF approach to the MC results for the single band Hubbard model is made. Properties such as the energy, probability of double occupancy, effective hopping matrix element, momentum distribution function and the Fermi surface are compared with MC results which we will regard as "exact". It is found that the projection operator approach also agrees remarkably well with MC in both limits and provides a good zero order description from which fluctuations can be included.

A distinct advantage of this projection operator-based scheme is that it is easily extended to multi-band Hubbard models used in the theories of high T_c superconductivity with a minimal number of mean field equations compared to slave theories, where additional constraints for the composite "slave particle" must be introduced, making the number of coupled constraint equations unwieldy, especially when describing the superconducting state. Various properties of a CuO_2 lattice model based on the three-orbital two dimensional Hubbard model have been calculated using the projection operator MF scheme [Fedro, 1991], and the results compare well with MC simulations. The study of the density of states of this CuO_2 lattice model shows some interesting results, which is described at the end of the chapter.

5.1 The projection operator based mean field formalism

5.1.1 The multi-band Hubbard Hamiltonian and the projection operator

In general, the multi-band two dimensional Hubbard Hamiltonian has the form

$$H = \sum_{j,\nu,\sigma} \varepsilon_\nu n_{j\nu\sigma} + \sum_{j,\nu} U_{\nu\nu} n_{j\nu,+} n_{j\nu,-} + \sum_{j,j',\nu,\nu',\sigma} t_{j,\nu;j',\nu'} c^\dagger_{j\nu\sigma} c_{j'\nu'\sigma} \tag{5.1}$$

where j denotes the unit cell position, $\sigma = \pm$ represents spin up (+) and spin down (-), and ν is the index of the atoms in the unit cell. In this framework one can also incorporate possible AF order . The hopping matrix elements are real and satisfy $t_{j\nu;j'\nu'} = t_{j'\nu';j\nu}$ with $t_{j\nu;j\nu} = 0$. The site number operators are defined by $n_{j\nu\sigma} = c^\dagger{}_{j\nu\sigma} c_{j\nu\sigma}$. ε_ν are the single electron energies and $U_{\nu\nu}$ the on-site Coulomb repulsions. We now separate the pure fermi excitation operators $c_{j\nu\sigma}$ into two operators $f^\alpha{}_{j\nu\sigma}$ (as done in the original work of Hubbard) with $\alpha = \pm$ as follows:

$$f^{\alpha}_{j\nu\sigma} = n^{\alpha}_{j\nu,-\sigma}\, c_{j\nu\sigma} \quad ; \qquad c_{j\nu\sigma} = \sum_{\alpha} f^{\alpha}_{j\nu\sigma} \tag{5.2a}$$

where we define

$$n^{\alpha}_{j\nu-\sigma} = \begin{cases} n_{j\nu-\sigma} & \alpha = + \\ 1 - n_{j\nu-\sigma} & \alpha = - \end{cases} \tag{5.2b}$$

Then the needed retarded Green's functions $G^{\alpha\alpha'}_{j\nu;j'\nu'\sigma}(t)$ are formed as follows:

$$G^{\alpha\alpha'}_{j\nu;j'\nu'\sigma}(t) = -i \,< [f^{\alpha}_{j\nu\sigma}(t), f^{\alpha'\,\dagger}_{j'\nu'\sigma}]_{+} > \quad ; \qquad t \geq 0 \tag{5.3}$$

where the $f^{\alpha}_{j\nu\sigma}(t)$ are the ordinary Heisenberg operators

$$f^{\alpha}_{j\nu\sigma}(t) = e^{iHt}\, f^{\alpha}_{j\nu\sigma}\, e^{-iHt} \quad ; \qquad f^{\alpha}_{j\nu\sigma}(0) = f^{\alpha}_{j\nu\sigma} \tag{5.4a}$$

and the grand canonical average <·····> is defined in the usual way

$$<\cdots\cdots> = \mathrm{Tr}\, e^{-\beta H}(\cdots\cdots)/\mathrm{Tr}\, e^{-\beta H}\,, \qquad \beta^{-1} = k_B T \tag{5.4b}$$

where T is the temperature and k_B is Boltzmann's constant. To solve for these Green's functions we introduce the projection operator $P^2 = P$ as follows:

$$PX = \sum_{j'',\nu'',\alpha'',\sigma''} f^{\alpha''\,\dagger}_{j''\nu''\sigma''} <[f^{\alpha''}_{j''\nu''\sigma''}, X]_{+}> / <n^{\alpha''}_{j''\nu'',-\sigma''}> \tag{5.5a}$$

which has the property that, for all j,ν,α,σ,

$$P f^{\alpha\dagger}_{j\nu\sigma} = f^{\alpha\dagger}_{j\nu\sigma} \;, \qquad (1 - P) f^{\alpha\dagger}_{j\nu\sigma} = 0 \;. \tag{5.5b}$$

Since the projections defined in Eqns. (7) involve the averages, $\langle n^{\alpha''}{}_{j''\nu''-\sigma''}\rangle$, it is convenient to write the equations of motion for the rescaled Green's functions defined as:

$$\tilde{G}^{\alpha\alpha'}_{j\nu;\,j'\nu'\sigma}(t) = (\langle n^{\alpha}_{j\nu,-\sigma}\rangle \langle n^{\alpha'}_{j'\nu',-\sigma}\rangle)^{-1/2}\, G^{\alpha\alpha'}_{j\nu;\,j'\nu'\sigma}(t) \tag{5.6a}$$

where, by construction,

$$i\,\tilde{G}^{\alpha\alpha'}_{j\nu;j'\nu'\sigma}(t=0) = \delta_{jj'}\,\delta_{\nu\nu'}\delta_{\alpha\alpha'} \;. \tag{5.6b}$$

5.1.2 The equations of motion for the Green's functions

In this section the equations of motion for the Green's functions defined in Eq.(5.6) are derived. In terms of the Liouville operator $LX = [H,X]_-$, the Heisenberg time dependence of an arbitrary operator A can be written as:

$$A(t) = e^{iHt}\, A\, e^{-iHt} = e^{iLt}\, A \quad ; \qquad A(0) = A \;. \tag{5.7}$$

Then the retarded Green's functions $G^{\alpha\alpha'}_{j\nu;j'\nu'\sigma}(t)$ in Eq.(5.3) becomes:

$$G^{\alpha\alpha'}_{j\nu;j'\nu'\sigma}(t) = -i\, \langle [f^{\alpha}_{j\nu\sigma},\, f^{\alpha'\dagger}_{j'\nu'\sigma}(-t)]_+ \rangle \tag{5.8}$$

where the identity

$$<[A, L^n B]_+> \;=\; <[(-L)^n A, B]_+> \qquad n = 0,1,2,... \tag{5.9}$$

has been used.

From Eqs. (5.7) and (5.8), the equation of motion is

$$i \frac{\partial G^{\alpha\alpha'}_{jv;j'v'\sigma}(t)}{\partial t} = -i < [f^{\alpha}_{jv\sigma}, L f^{\alpha' \dagger}_{j'v'\sigma}(-t)]_+ >$$

$$= -i < [f^{\alpha}_{jv\sigma}, L\{P + (1 - P)\} f^{\alpha' \dagger}_{j'v'\sigma}(-t)]_+ > \tag{5.10}$$

for any operator P. In this case P is the projection operator defined in Eqn. (5.5). Now the basic idea of the projection scheme is to write the term P $(f^{\alpha'}{}_{j'v'\sigma})^{\dagger}(-t)$ in terms of the original Green's function at the same time t, resulting in static (mean field) contributions. The remaining term, $\{(1 - P)\}(f^{\alpha'}{}_{j'v'\sigma})^{\dagger}(-t)$, which is orthogonal to this static term (since $P^2 = P$), is then written in terms of an integral of the original Green's function over all earlier times τ such that $\tau < t$, yielding the dynamic (self-energy) terms called memory functions.

From Eqs.(5.8) and (5.5) it is easily seen that

$$P f^{\alpha' \dagger}_{j'v'\sigma}(-t) = i \sum_{j'',v'',\alpha''} [f^{\alpha'' \dagger}_{j''v''\sigma} / < n^{\alpha''}_{j''v'',-\sigma} >] \, G^{\alpha''\alpha'}_{j''v'';j'v'\sigma}(t) \tag{5.11}$$

Now, for any Heisenberg operator, A(-t), there is the operator identity

$$(1 - P)\,A(-t) \;=\; e^{-it(1-P)L}\,(1 - P)\,A(0) \;-\; i\int_0^t d\tau\, e^{-i(t-\tau)(1-P)L}\,(1 - P)LPA(-\tau) \tag{5.12}$$

Obviously this expression is correct at t = 0. To verify that it is valid for all times t, simply differentiate both sides of this expression with respect to time and show that they are equal. Use of Eqns. (5.8), (5.5) and (5.12) yields

$$\begin{aligned} &(1 - P)\, f^{\alpha'\,\dagger}_{j'v'\sigma}(-t) \\ &= \sum_{j'',v'',\alpha''} \int_0^t d\tau \left\{ e^{-i(t-\tau)(1-P)L}\,(1 - P)L\, f^{\alpha''\,\dagger}_{j''v''\sigma} \big/ < n^{\alpha''}_{j''v'',-\sigma} > \right\} G^{\alpha''\alpha'}_{j''v'';j'v'\sigma}(\tau) \end{aligned} \tag{5.13}$$

Now use of Eqs. (5.11) and (5.13) in (5.10) gives the exact equations of motion for the Green's functions, which can be written as follows:

$$\begin{aligned} i\,\frac{\partial\, G^{\alpha\alpha'}_{jv;j'v'\sigma}(t)}{\partial\, t} \;=\; & \sum_{j'',v'',\alpha''} \left\{ \Omega^{\alpha\alpha''}_{jv;j''v''\sigma} \big/ < n^{\alpha''}_{j''v'',-\sigma} > \right\} G^{\alpha''\alpha'}_{j''v'';j'v'\sigma}(t) \\ & + \sum_{j'',v'',\alpha''} \int_0^t d\tau \left\{ M^{\alpha\alpha''}_{jv;j''v''\sigma}(t - \tau) \big/ < n^{\alpha''}_{j''v'',-\sigma} > \right\} G^{\alpha''\alpha'}_{j''v'';j'v'\sigma}(\tau) \end{aligned} \tag{5.14}$$

where the static (mean field) terms are defined by

$$\Omega^{\alpha\alpha''}_{jv;j''v''\sigma} \;=\; < [f^{\alpha}_{jv\sigma},\, L\, f^{\alpha''\,\dagger}_{j''v''\sigma}]_{+} > \tag{5.15}$$

and the memory functions are

$$M^{\alpha\alpha''}_{jv;\, j''v''\sigma}(t) \quad = \quad -i \, \langle [f^{\alpha}_{jv\sigma} , L \, e^{-it(1-P)L} \, (1 - P) \, L \, f^{\alpha''\,\dagger}_{j''v''\sigma}]_{+} \rangle \tag{5.16}$$

The functions defined in Eqs. (5.15) and (5.16) for the various α,α'' combinations can be further simplified. From Eqns. (5.1) and (5.2) one gets

$$\begin{aligned} L \, f^{\alpha\,\dagger}_{jv\sigma} \quad = \quad & \varepsilon^{\alpha}_{v} \, f^{\alpha\,\dagger}_{jv\sigma} \\ & + \sum_{j',v'} t_{jv;j'v'} \, \{ n^{\alpha}_{jv,-\sigma} \, c^{\dagger}_{j'v'\sigma} \; + \; (\delta_{\alpha,+} - \delta_{\alpha,-}) [\, c^{\dagger}_{j'v',-\sigma} \, c_{jv,-\sigma} - c^{\dagger}_{jv,-\sigma} \, c_{j'v',-\sigma}] \, c^{\dagger}_{jv\sigma} \, \} \end{aligned} \tag{5.17a}$$

where the energy

$$\varepsilon^{\alpha}_{v} \quad = \quad \varepsilon_{v} \; + \; U_{vv} \, \delta_{\alpha,+} \tag{5.17b}$$

From Eqs. (5.5) and (5.17) one finds the following identities:

$$\sum_{\alpha} (1 - P) L \, f^{\alpha\,\dagger}_{jv\sigma} \quad = \quad (1 - P) L \, c^{\dagger}_{jv\sigma} \quad = \quad 0 \tag{5.18a}$$

and

$$\langle [-L \, c_{jv\sigma} , (1 - P) \, Z]_{+} \rangle = 0 \tag{5.18b}$$

for any operator Z. Use of Eqns (5.18) in (5.16) gives immediately

$$\sum_{\alpha} M^{\alpha\alpha''}_{jv;\, j''v''\sigma}(t) \quad = \quad 0 \; , \qquad \sum_{\alpha''} M^{\alpha\alpha''}_{jv;\, j''v''\sigma}(t) \quad = \quad 0 \tag{5.19}$$

Therefore,

$$M^{\alpha\alpha''}_{jv;\, j''v''\sigma}(t) \quad = \quad \alpha \, \alpha'' \, M_{jv;\, j''v''\sigma}(t) \tag{5.20a}$$

where

$$M_{jv;\,j''v''\sigma}(t) \quad = \quad M^{--}_{jv;\,j''v''\sigma}(t) \tag{5.20b}$$

A similar analysis can be done for the "mean field" terms $\Omega^{\alpha\alpha''}_{jv;j''v''\sigma}$ defined in Eq. (5.15). From Eqs. (5.9) and (5.17),

$$< [f^{\alpha}_{jv\sigma}, L\, f^{\alpha''\,\dagger}_{j''v''\sigma}]_{+} > \quad = \quad < [-L\, f^{\alpha}_{jv\sigma}, f^{\alpha''\,\dagger}_{j''v''\sigma}]_{+} >$$

$$= \quad \delta_{jj''}\, \delta_{vv''}\, \delta_{\alpha\alpha''}\, \varepsilon^{\alpha}_{v} <n^{\alpha}_{jv,-\sigma}> \; + \; t_{jv;\,j''v''} <n^{\alpha}_{jv,-\sigma}> <n^{\alpha''}_{j''v'',-\sigma}> \; + \; \Delta^{\alpha\alpha''}_{jv;\,j''v''\sigma} \tag{5.21a}$$

where $\Delta^{\alpha\alpha''}_{jv;j''v''\sigma}$ is defined as:

$$\Delta^{\alpha\alpha''}_{jv;\,j''v''\sigma} \quad = \quad <[f^{\alpha}_{jv\sigma}, L_{t}\, f^{\alpha''\,\dagger}_{j''v''\sigma}]_{+}> \; - \; t_{jv;\,j''v''} <n^{\alpha}_{jv,-\sigma}> <n^{\alpha''}_{j''v'',-\sigma}>$$

$$= \quad <[-L_{t}\, f^{\alpha}_{jv\sigma}, f^{\alpha''\,\dagger}_{j''v''\sigma}]_{+}> \; - \; t_{jv;\,j''v''} <n^{\alpha}_{jv,-\sigma}> <n^{\alpha''}_{j''v'',-\sigma}> \tag{5.21b}$$

in which L_t is defined as the commutator with respect to that part of H defined in Eq.(5.1) proportional to the $t_{jv;j'v'}$'s. Use of Eqs. (5.17) in (5.21b) gives, by construction,

$$\sum_{\alpha} \Delta^{\alpha\alpha''}_{jv;\,j''v''\sigma} \; = \; 0 \;, \qquad \sum_{\alpha''} \Delta^{\alpha\alpha''}_{jv;\,j''v''\sigma} \; = \; 0 \tag{5.22}$$

Just as in Eq.(5.20),

$$\Delta^{\alpha\alpha''}_{jv;\,j''v''\sigma} \quad = \quad \alpha\, \alpha''\, \Delta_{jv;\,j''v''\sigma} \tag{5.23a}$$

where

$$\Delta_{jv;\, j''v''\sigma} \quad = \quad \Delta^{--}_{jv;\, j''v''\sigma} \tag{5.23b}$$

Using the results of Eqs.(5.20) and (5.23) in (5.14),

$$\begin{aligned}
\left(i \frac{\partial}{\partial t} - \varepsilon^{\alpha}_{v} \right) G^{\alpha\alpha'}_{jv;j'v'\sigma}(t) \quad = \quad & \sum_{j'',v'',\alpha''} t_{jv;j''v''} < n^{\alpha}_{jv,-\sigma} > G^{\alpha''\alpha'}_{j''v'';j'v'\sigma}(t) \\
& + \sum_{j'',v'',\alpha''} \alpha\, \alpha'' \left[\Delta_{jv;j''v''\sigma} \,/ < n^{\alpha''}_{j''v'',-\sigma} > \right] G^{\alpha''\alpha'}_{j''v'';j'v'\sigma}(t) \\
& + \sum_{j'',v'',\alpha''} \int_{0}^{t} d\tau \left\{ \alpha\, \alpha'' M_{jv;j''v''\sigma}(t-\tau) \,/ < n^{\alpha''}_{j''v'',-\sigma} > \right\} G^{\alpha''\alpha'}_{j''v'';j'v'\sigma}(\tau)
\end{aligned} \tag{5.24}$$

This can be rewritten in terms of the rescaled Green's function $\tilde{G}^{\alpha\alpha'}_{jv;j'v'\sigma}(t)$ defined in Eq.(5.6):

$$\begin{aligned}
\left(i \frac{\partial}{\partial t} - \varepsilon^{\alpha}_{v} \right) \tilde{G}^{\alpha\alpha'}_{jv;j'v'\sigma}(t) \quad = \quad & \sum_{j'',v'',\alpha''} t_{jv;j''v''} \left(< n^{\alpha}_{jv,-\sigma} > < n^{\alpha''}_{j''v'',-\sigma} > \right)^{1/2} \tilde{G}^{\alpha''\alpha'}_{j''v'';j'v'\sigma}(t) \\
& + \sum_{j'',v'',\alpha''} \alpha\, \alpha'' \Delta_{jv;j''v''\sigma} \left(< n^{\alpha}_{jv,-\sigma} > < n^{\alpha''}_{j''v'',-\sigma} > \right)^{-1/2} \tilde{G}^{\alpha''\alpha'}_{j''v'';j'v'\sigma}(t) \\
& + \sum_{j'',v'',\alpha''} \alpha\, \alpha'' \int_{0}^{t} d\tau \; M_{jv;j''v''\sigma}(t-\tau) \left(< n^{\alpha}_{jv,-\sigma} > < n^{\alpha''}_{j''v'',-\sigma} > \right)^{-1/2} \tilde{G}^{\alpha''\alpha'}_{j''v'';j'v'\sigma}(\tau)
\end{aligned} \tag{5.25}$$

For arbitrary function A, its Laplace and spatial transforms are defined by:

$$A_{j\nu;j'\nu'}(\varpi) = \int_0^{\infty} dt\, e^{i\varpi t} A_{j\nu;j'\nu'}(t) \quad , \qquad \varpi = \omega + i0^+ \tag{5.26a}$$

and

$$A_{j\nu;j'\nu'} = \frac{1}{N} \sum_k e^{ik(j-j')} A_{k\nu\nu'} \tag{5.26b}$$

where N is the number of unit cells. The desired exact equations of motion for the momentum and frequency dependent Green's functions are obtained by using Eq.(5.26) in Eq.(5.25):

$$\sum_{\alpha''\nu''} \{ \varpi\, \delta_{\nu\nu''}\delta_{\alpha\alpha''} - E^{\alpha\alpha''}_{k\nu\nu''\sigma}(\varpi) \}\ \tilde{G}^{\alpha''\alpha'}_{k\nu''\nu'\sigma}(\varpi) = \delta_{\nu\nu'}\delta_{\alpha\alpha'} \tag{5.27a}$$

where

$$\begin{aligned} E^{\alpha\alpha''}_{k\nu\nu''\sigma}(\varpi) = {} & \delta_{\nu\nu''}\, \delta_{\alpha\alpha''}\, \varepsilon^{\alpha}_{\nu} + t_{k\nu\nu''} \left(< n^{\alpha}_{\nu,-\sigma} > < n^{\alpha''}_{\nu'',-\sigma} > \right)^{1/2} \\ & + \alpha\alpha'' \left[\Delta_{k\nu\nu''\sigma} + M_{k\nu\nu''\sigma}(\varpi) \right] \left(< n^{\alpha}_{\nu,-\sigma} > < n^{\alpha''}_{\nu'',-\sigma} > \right)^{-1/2} \end{aligned} \tag{5.27b}$$

in which

$$\varepsilon^{\alpha}_{\nu} = \varepsilon_{\nu} + U_{\nu\nu}\, \delta_{\alpha,+} \tag{5.28}$$

and it has been assumed that the "n" averages are independent of the unit cell. The static mean field corrections $\Delta_{k\nu\nu''\sigma}$ in Eq.(5.27b) are the spatial transforms of

$$\Delta_{j\nu;\, j''\nu''\sigma} = <[f^{-}_{j\nu\sigma}\, , L_t\, f^{-\dagger}_{j''\nu''\sigma}]_+> - t_{j\nu;\, j''\nu''} <n^{-}_{\nu,-\sigma}> <n^{-}_{\nu'',-\sigma}> \tag{5.29}$$

and the dynamic memory functions $M_{k\nu\nu''\sigma}(\varpi)$ are the Laplace and spatial transforms of

$$M_{j\nu;\,j''\nu''\sigma}(t) \;=\; -i\,\langle[f^{-}_{j\nu\sigma},\, L\, e^{-it(1-P)L}\,(1-P)\,L\, f^{-\dagger}_{j''\nu''\sigma}]_{+}\rangle \tag{5.30}$$

In the energy matrix of Eq.(5.27b), if the $\Delta_{k\nu\nu''\sigma}$'s and $M_{k\nu\nu''\sigma}(\varpi)$'s are set to zero, one gets the Hubbard I solution. Notice that the Hubbard I solution misses these static and dynamic terms due to the naive truncation in the original Hubbard paper which essentially treats the "f" operators as if they were pure fermions. The complicated statistics of the $f^{\alpha}_{j\nu\sigma}$'s are automatically handled correctly when one truncates the equations of motion by using the the projection operator given in Eq. (5.5), leading to the solutions given in Eq. (5.27). Finally, the projection operator mean field solution is that generated by setting all the memory functions $M_{k\nu\nu''\sigma}(\varpi)$ to zero in Eq. (5.27), so that the resulting energies in Eq. (5.27b) are independent of ϖ:

$$E^{\alpha\alpha''}_{k\nu\nu''\sigma}(\varpi) = E^{\alpha\alpha''}_{k\nu\nu''\sigma} \quad . \tag{5.31}$$

5.2 Calculations of the 2D single-band Hubbard model

For the single band Hubbard model, there is only one atom per unit cell, thus the atom index ν in Eq.(5.1) is supressed. Its Hamiltonian has the simple form:

$$H \;=\; \varepsilon_d \sum_{j,\sigma} n_{j\sigma} \;+\; U \sum_{j} n_{j+}\, n_{j-} \;+\; \sum_{j,j',\sigma} t_{jj'}\, c^{\dagger}_{j\sigma}\, c_{j'\sigma} \tag{5.32}$$

and in the nearest hopping case, $t_{jj'} = -t$ for nearest neighbor (j,j'), zero otherwise. In all calculations the unit of energy is defined by setting $t = 1$. The value of inverse temperature β is chosen according to the available MC results [Moreo, 1990] which we will compare to the three mentioned MF calculations. In all of the figures, we use the notations MC, SBMF, HI and POMF to represent the Monte Carlo results, the four-boson theory of Kotliar and Ruckenstein, the Hubbard I approximation and our current projection-operator-based MF theory respectively.

Fig.5.1 shows the energy versus band-filling $\langle n\rangle$ for $U = 4$ and $\beta = 6$. We see at best minor differences among the various MF results to the MC simulation, thus the energy does not provide a good criterion for choosing one MF calculation over another. In Fig.5.2 we plot the on-site squared local moment $\langle m_z^2\rangle = \langle(n_\uparrow - n_\downarrow)^2\rangle$ versus $\langle n\rangle$ for the same set of parameters as in Fig.5.1. It is seen that the present calculation yields results in reasonably good agreements with those of MC and SBMF except around half-filling, $\langle n\rangle = 1$, (the reason will be discussed later in this section), while the Hubbard I approximation is failing badly as $\langle n\rangle$ approaches 1.

An important quantity, which estimates the effect of U on the bandwidth, is t_{eff}/t, defined as the ratio of hopping probability in the presence of U to that in the absence of U, i.e.,

$$\frac{t_{eff}}{t} = \frac{\langle c_{i\sigma}^\dagger c_{j\sigma} + c_{j\sigma}^\dagger c_{i\sigma}\rangle_{U\neq 0}}{\langle c_{i\sigma}^\dagger c_{j\sigma} + c_{j\sigma}^\dagger c_{i\sigma}\rangle_{U=0}} \tag{5.33}$$

for (i,j) near neighbors. The results for t_{eff}/t as a function of U for $\langle n\rangle = 1$ and $\beta = 10$ are shown in Fig.5.3, in which the Hubbard I curve is obtained from the paramagnetic case, since no AF solution is found in this range of U. Going beyond Hubbard I, by including

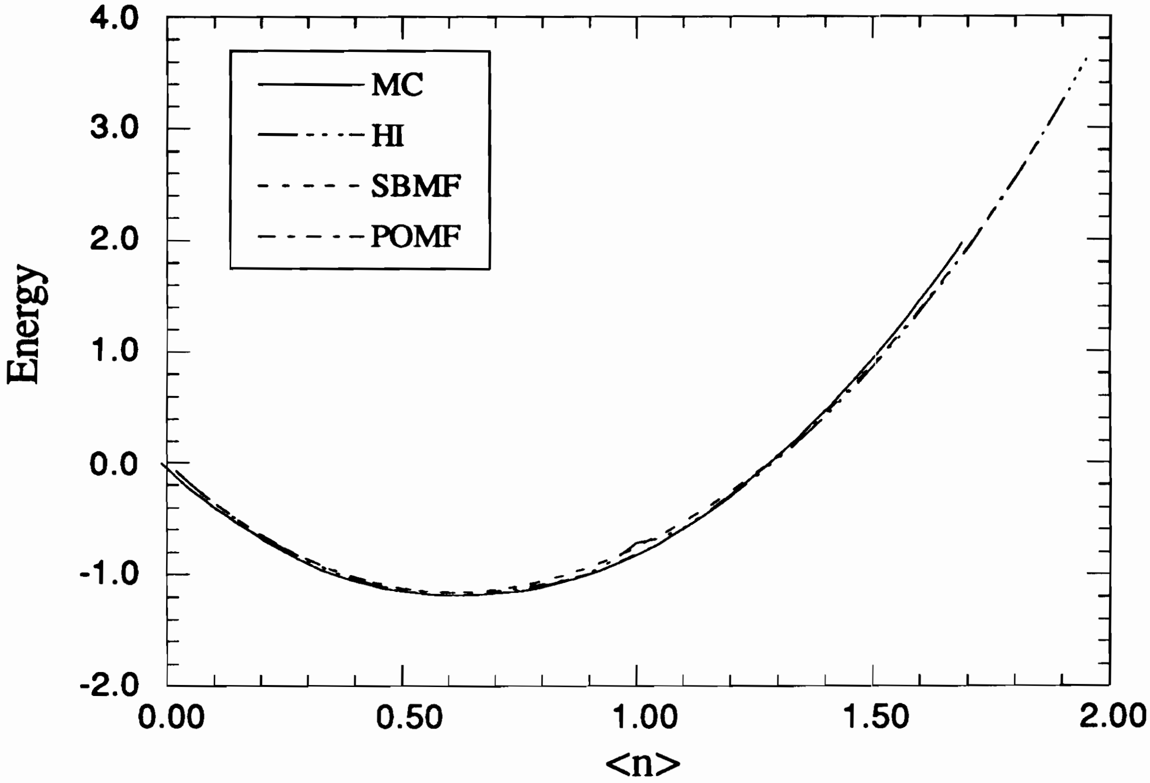

Fig. 5.1 **Energy per site versus band filling <n> for U = 4 and β = 6.** The results shown include those of Monte Carlo (MC) simulations [Moreo, 1990], the slave-boson MF (SBMF) theory [Lilly, 1990], the Hubbard I approximation (HI) and our projection-operator-based calculation (POMF). Little difference is seen among these approaches.

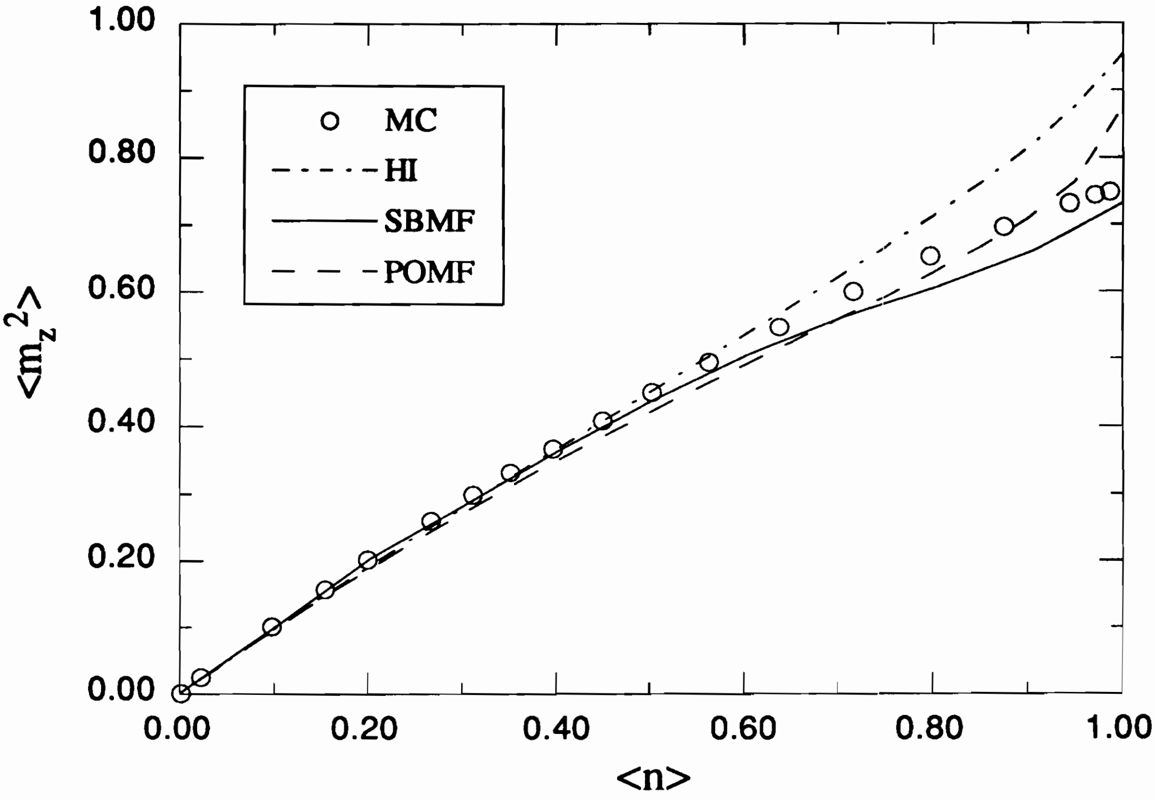

Fig. 5.2 **Local magnetic moment $\langle m_z^2 \rangle$ vs. band filling <n> for U = 4 and β = 6.** The projection operator result agrees well with Monte Carlo simulation and four-boson MF theory except around half-filling (<n> = 1). Hubbard I fails badly as <n> approaches 1.

the static energy shifts Δ resulting in the projection operator MF formalism (POMF), AF solutions are obtained for U's as small as 5. Results for t_{eff}/t as a function of <n> for U = 4 and $\beta = 10$ are plotted in Fig.5.4, where both the Hubbard I and POMF curves shown are for the paramagnetic case. The fact that no AF solution is found for U < 5 also explains the poor fit of POMF to the MC curve around <n> = 1 in Figure 5.2. In both Fig.5.3 and Fig.5.4 our results agree reasonably well with that of SBMF, but the Hubbard I result overemphasizes the suppression of the hopping at all U and all fillings. We also point out here that the suppression in Fig.5.3 at large U is occurring for different reasons in the SBMF and POMF formalisms. In the SBMF theory, the bands are becoming severely narrowed since they are proportional to $\delta = 1 - \langle n \rangle$ for large U, but, in the POMF scheme, the effective hopping is going to zero because the lower Hubbard sub-band is being filled while retaining a finite bandwidth.

A more severe criterion for the applicability of MF is shown in Fig.5.5, where the momentum distribution function $\langle n_{\mathbf{k}\sigma} \rangle$ versus **k** along the (1,1) direction ($k_x = k_y$) is plotted for the quarter filled band case <n> = 0.5, with U = 4 and $\beta = 6$. It is apparent that the Hubbard I curve lies well below the MC curve for states below the chemical potential. Since this feature holds true in other directions as well, ones finds that, in order to accommodate a fixed number of electrons, the Fermi volume in Hubbard I must be significantly larger than the MC volume which is approximately equal to the Luttinger volume. This is a manifestation of the breakdown of Luttinger's theorem. However, within the POMF scheme, where the effect of the static energy Δ term defined in Eq.(5.29) is included, the calculation tends to recover the Luttinger volume since the resulting $\langle n_{\mathbf{k}} \rangle$ curve is almost identical to the MC result and slightly higher than the SBMF result. The expansion of the Fermi surface volume is again illustrated in Fig.5.6 for <n> = 0.87. It is

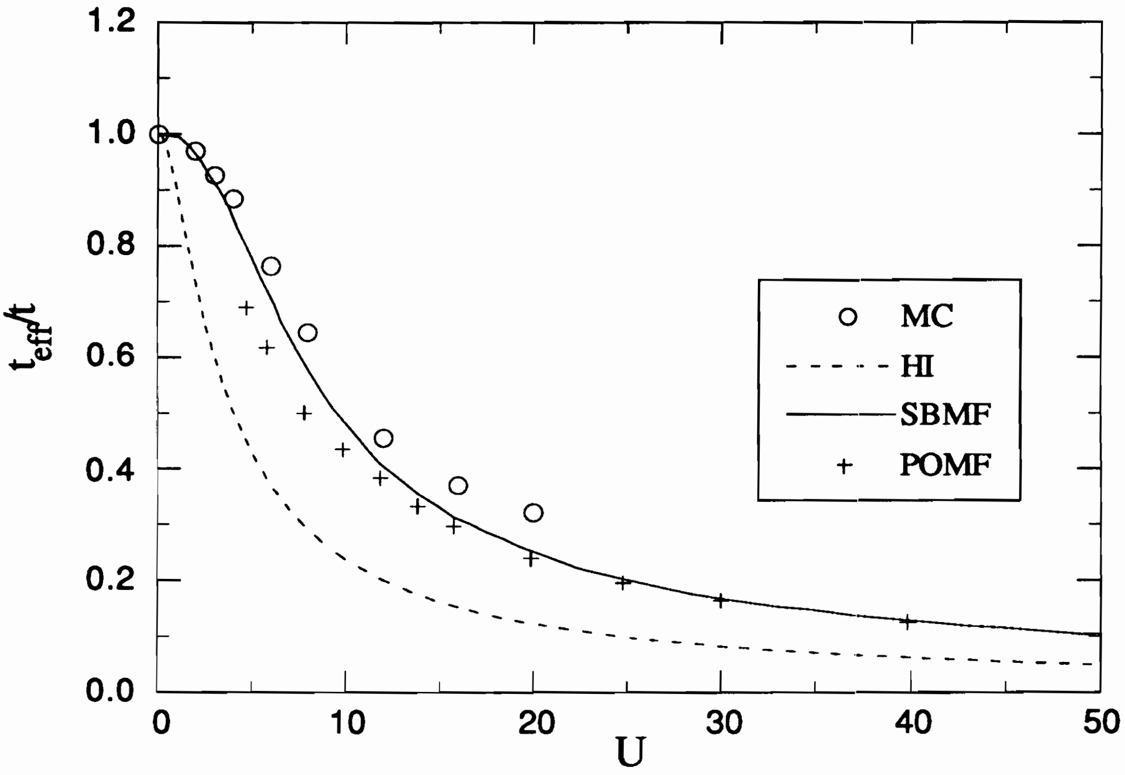

Fig. 5.3 **Effective hopping energy vs. U for half-filled case.** t_{eff}/t is defined in Eq.(5.33). <n> = 1 and $\beta = 10$. The Hubbard I (HI) curve is obtained from the paramagnetic solution.

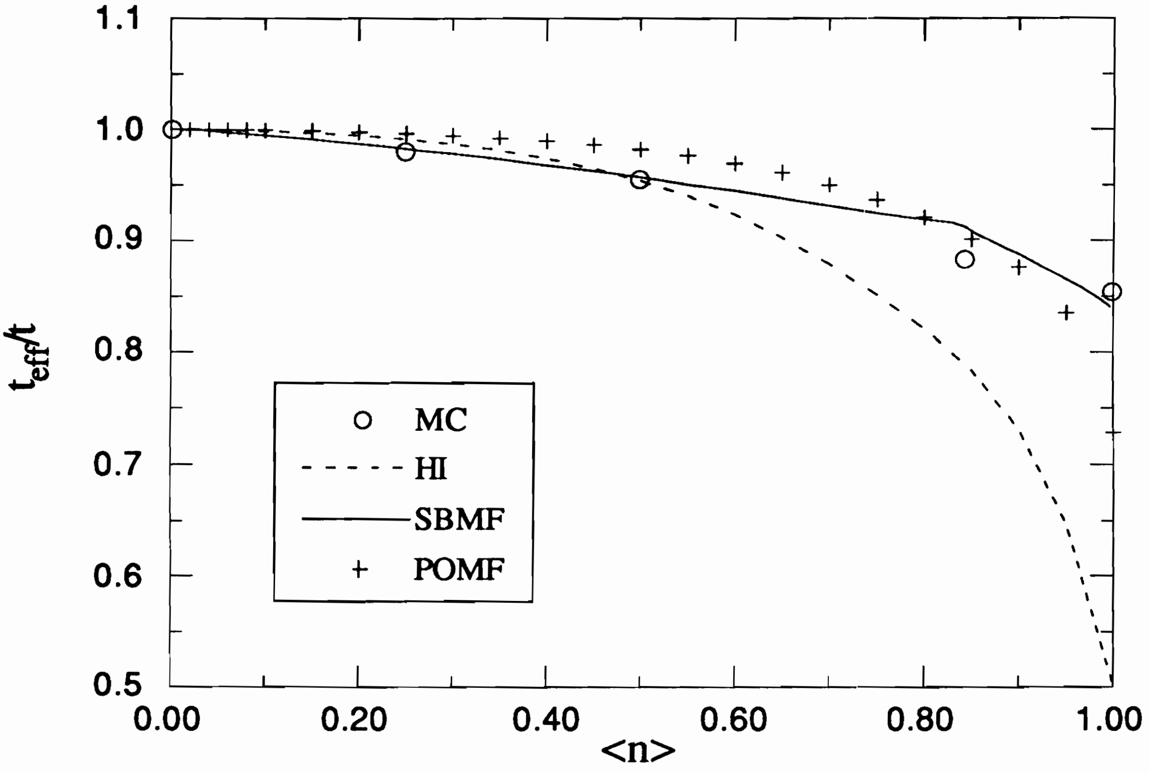

Fig. 5.4 **Effective hopping energy t_{eff}/t vs. <n> for U=4 and β = 10.** Both projection operator MF and Hubbard I curves shown are derived from paramagnetic solutions because of the small U.

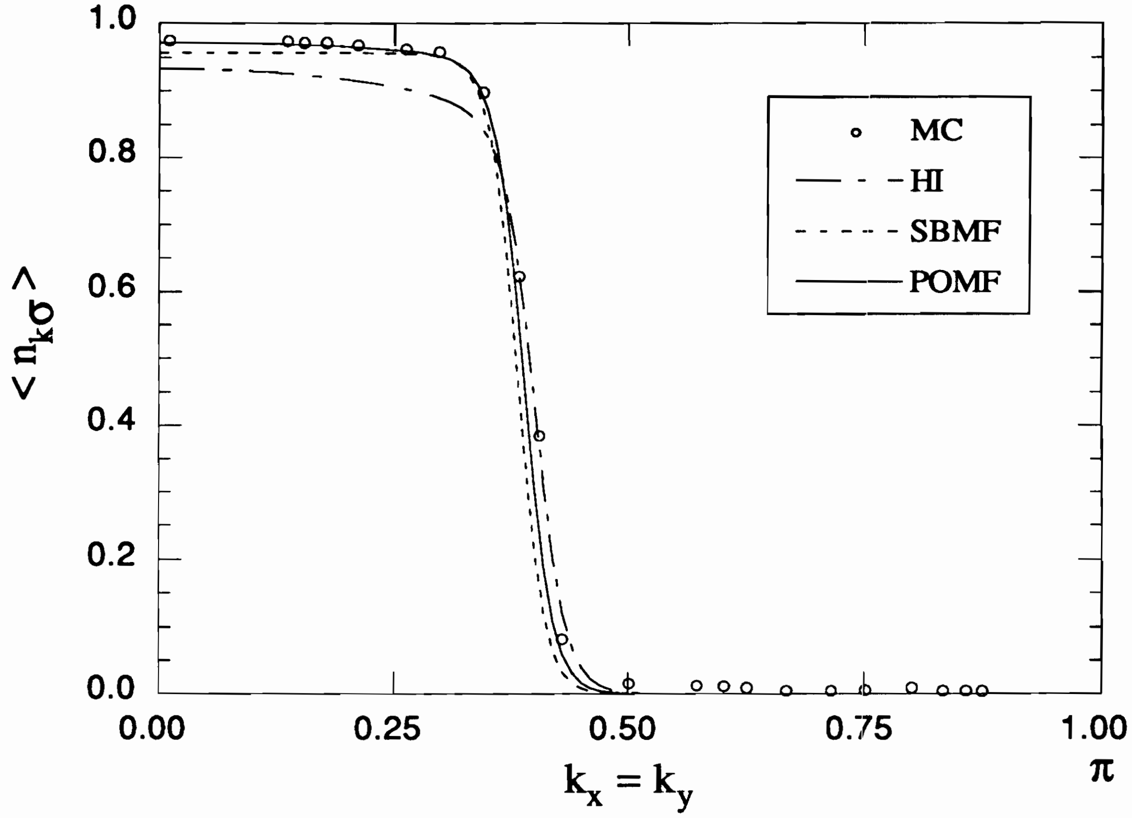

Fig. 5.5 **Momentum distribution function $<n_k>$ vs. k along (1,1) direction ($k_x = k_y$).** The parameters used here are: $<n> = 0.5$ (quarter-filling), U=4 and $\beta = 6$. The POMF result agrees very well with that of MC while Hubbard I and SBMF under estimate the density inside Fermi surface.

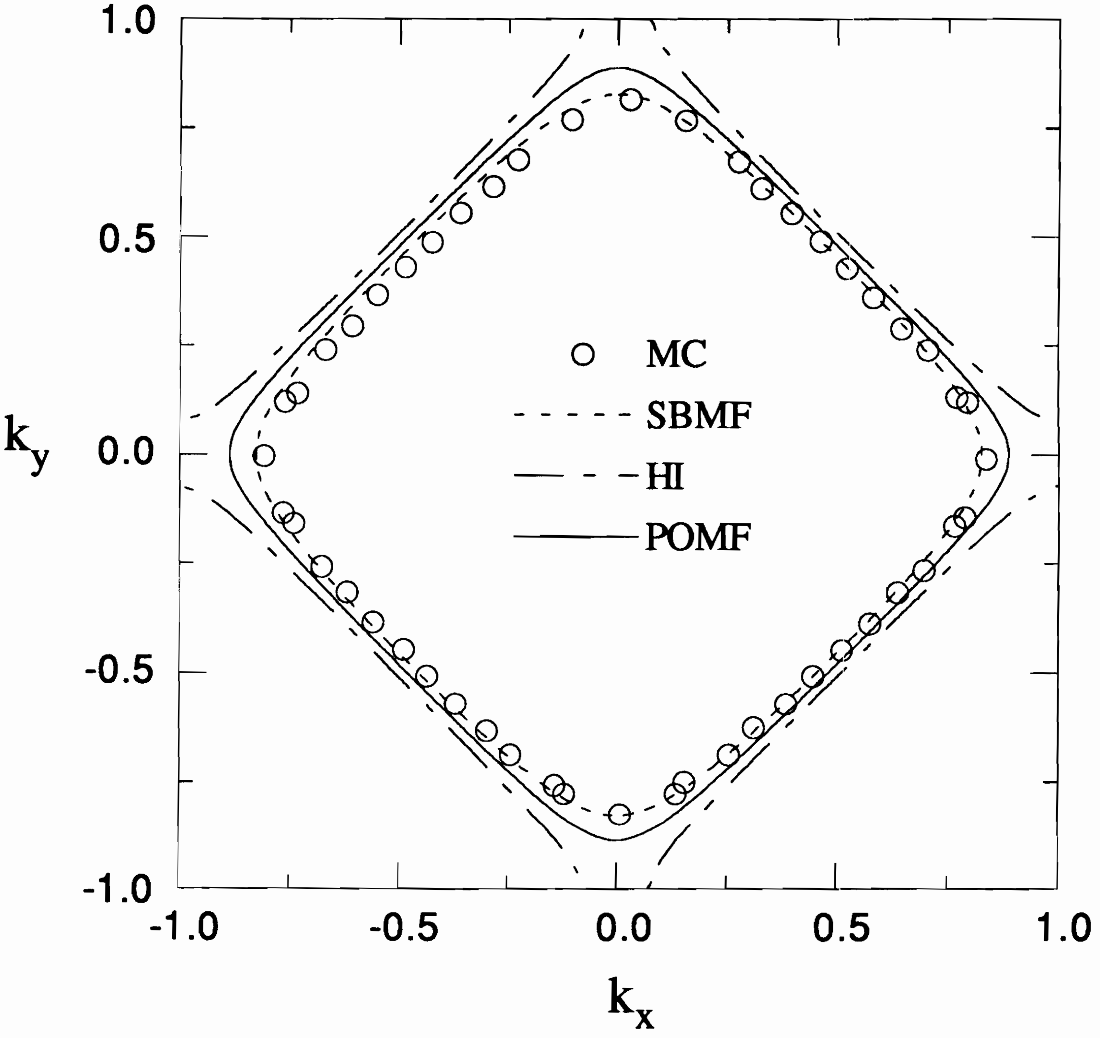

Fig. 5.6 **Fermi surface for <n> = 0.87, U = 4 and β = 6.** Both POMF and Hubbard I calculations over estimate the volume inside Fermi surface, even though POMF does not violate the Luttinger theorem as severely as Hubbard I.

seen that present result POMF overestimates the Fermi volume compared to MC and SBMF while the Hubbard I volume severely overestimates this volume at this filling. In fact, as <n> goes to 1, the deviation from the Luttinger Fermi volume for both Hubbard I and POMF is becoming more significant.

5.3 Calculations of the CuO_2 lattice model

The two dimensional multi-band Hubbard models have been used intensively for studying the high T_c superconductors. Recent Monte Carlo (MC) studies [Scalettar; Dopf, 1990], using the three-band Hubbard model to describe this motion, have been done in a wide parameter range for various values of doping δ away from half-filling ($\delta = 0$ is defined as one hole per Cu site). Their results show that if one defines the on-site O energy as ε_p and the Cu on-site energy as ε_d, then there are two basic regimes depending on whether the on-site energy difference ε between the O and Cu sites ($\varepsilon = \varepsilon_p - \varepsilon_d$) is greater or less than the on-site Cu Coulomb repulsion U_{dd}. If $U_{dd} >> \varepsilon$ the behavior of the system is controlled by ε (charge transfer limit). In this case, at half-filling, they found strong antiferrromagnetic correlations and evidence of a charge transfer gap ($\approx \varepsilon$). The antiferromagnetic correlations decrease rapidly as one dopes away from half-filling as it should. In the other case $\varepsilon >> U_{dd}$ the behavior is controlled by U_{dd}. Here the O occupation is always small and it is essentially an effective single band model with a Mott-Hubbard gap which depends on U_{dd}.

In this section the calculation for the multi-band Hubbard model of the CuO_2 lattice based on the projection operator scheme [Fedro, 1982; Fedro, 1987; Ruckenstein, 1988] as described in detail in section 5.1 is presented. A detailed comparison of our MF results to the above-mentioned MC simulations which are regarded as "exact" is made. The density of states results are presented in the end, along with the comparison with the Hubbard I approximation and the four-boson mean field theory results.

5.3.1 The 3-orbital Hubbard model of the CuO_2 lattice

In general, the Hamiltonian for the 2D CuO_2 lattice can be written in hole notation as follows [Varma, 1987; Emery, 1987]:

$$
\begin{aligned}
H \;=\; & \varepsilon_d \sum_{j,\sigma} n_{j,\sigma} + U_{dd} \sum_{j} n_{j,+}\, n_{j,-} + \varepsilon_p \sum_{j,\lambda,\sigma} n_{j+\lambda/2,\sigma} + U_{pp} \sum_{j,\lambda} n_{j+\lambda/2,+}\, n_{j+\lambda/2,-} \\
& + U_{dp} \sum_{j,\alpha,\lambda,\sigma,\sigma'} n_{j,\sigma}\, n_{j+\alpha\lambda/2,\sigma'} - t_{dp} \sum_{j,\alpha,\sigma} [\, d^{\dagger}_{j\sigma} (\, p_{j+\alpha x/2,\sigma} - p_{j+\alpha y/2,\sigma}) + \mathrm{H.c.}] \\
& + t_{pp} \sum_{j,\sigma} [\, (\, p^{\dagger}_{j+x/2,\sigma} - p^{\dagger}_{j-x/2,\sigma}) (\, p_{j+y/2,\sigma} - p_{j-y/2,\sigma}) + \mathrm{H.c.}]
\end{aligned}
\tag{5.34}
$$

where $\lambda = x,y$ and $\alpha = \pm$. Here the Cu d-hole operator for site j and spin σ is given by $d_{j\sigma}$ with the corresponding number operator $n_{j\sigma} = d^{+}{}_{j\sigma}\, d_{j\sigma}$. The oxygen p-hole operators surrounding the j-th Cu site are defined by $p_{j+\alpha\lambda/2,\sigma}$ with the corresponding number operators given by $n_{j+\alpha\lambda/2,\sigma} = p^{+}{}_{j+\alpha\lambda/2,\sigma}\, p_{j+\alpha\lambda/2,\sigma}$. ε_p and ε_d are the on-site O and Cu energies respectively, U_{pp} and U_{dd} the corresponding on-site Coulomb repulsions, and U_{dp} the near neighbor Cu-O repulsion. t_{dp} is the near neighbor Cu-O hopping matrix element and t_{pp} the O-O near neighbor hopping matrix element. The orbital sign convention is such that the LDA values for both t_{dp} and $t_{pp} > 0$. We define the space lattice to be that of the Cu's, i.e., a 2D square lattice of spacing a. The four surrounding oxygens are then at a distance a/2 from the central Cu atom. The LDA numbers for the parameters are given by [Hybertsen, 1989; McMahan, 1988]

$$\begin{aligned} &U_{dd} = 10.5\text{ eV} \quad ; \quad U_{pp} = 4.0\text{ eV} \quad ; \quad U_{dp} = 1.2\text{ eV} \\ &t_{dp} = 1.3\text{ eV} \quad ; \quad t_{pp} = 0.65\text{ eV} \quad ; \quad \varepsilon_p - \varepsilon_d = 3.6\text{ eV} \end{aligned} \tag{5.35}$$

It is generally believed that the effect of U_{dp} is solely to shift the entire energy spectrum without significantly disturbing the relevant physical properties. Therefore, in most calculations it is set to zero to simplify the analysis. We also set $U_{dp} = 0$ throughout our calculations so that the multi-band Hamiltonian in Eq.(5.34) can be written in the form:

$$H = \sum_{j,v,\sigma} \varepsilon_v n_{jv\sigma} + \sum_{j,v} U_{vv} n_{jv,+} n_{jv,-} + \sum_{j,j',v,v',\sigma} t_{j,v,j',v'} c^{\dagger}_{jv\sigma} c_{j'v'\sigma} \tag{5.36}$$

which is exactly the Hamiltonian discussed in Eq.(5.1). Thus the entire projection operator mean-field formalism can be applied to this CuO_2 lattice model without any alteration.

Various physical properties have been calculated by using this mean-field formalism, and comparison is made between its results and those of quantum Monte Carlo simulations and other MF theories. In all figures shown in this section, notations MC, POMF and SBMF are used to represent the data points of the Monte Carlo simulation, the projection operator mean field calculations and the four-boson mean field theory, just as in Figs.5.1-5.6. Temperature T is defined through $\beta = 1/T$.

5.3.2 Static properties and comparison with MC results

Since the parameters used in the aviailable MC results are not the LDA parameters, also U_{pp}, U_{pd} as well as t_{pp} are set to zero. The comparison between the results of POMF and that of the MC [Scalettar; Dopf, 1990] is made by keeping the parameters in the MC simulations. In all results shown in this section, the unit of energy is defined by $t_{dp} = 1$ and we set $U_{pp} = U_{dp} = 0$.

In Fig.5.7 the Cu and O site occupation numbers versus band filling $<n> = <n_{Cu}> + 2<n_O>$ are shown for $\beta = 8$. In the hole picture, $<n> = 1$ is the half-filled case. The result is obtained for charge transfer regime: $U_{dd} = 6$ and $\varepsilon = \varepsilon_p - \varepsilon_d = 2$ where the insulating state is characterized by a charge transfer gap, and there is an excellent agreement between the POMF and MC results. At half-filling, the hole occupation on the Cu site is much larger than that on the O site because of the low lying singly-occupied Cu d state. When the hole doping $\delta = <n> -1$ gets larger, it is seen that $<n_{Cu}>$ has little increase, most of the doped holes go to the O site. The opposite happens when there is electron doping ($\delta<0$).

The Cu and O hole occupation versus band filling $<n>$ is shown for another parameter regime, the Mott-Hubbard limit, in Fig.5.8 with $U_{dd}= 6$ and $\varepsilon = 8$. Here it is seen that there is little change in the hole occupation on the O sites with doping since the O p-states have higher energy than the doubly-occupied Cu d-states, so that added holes tend to fill the Cu sites. Notice again that the MC and POMF data points are essentially indistinguishable.

To examine the effect of t_{pp}, we repeat the calculation of Fig.5.7 for $t_{pp} = 0.5$, and the comparison between the two cases is shown in Fig.5.9. Due to the hopping of p-electrons, thus to the broadening of the O p-band, there is a greater portion of p-states mixed into the low-lying Cu d-states, resulting in a larger $<n_o>$ and smaller $<n_{Cu}>$ comparing with $t_{pp} = 0$ in the half-filled case. With hole doping, the increase in $<n_o>$ is not as rapid as when $t_{pp} = 0$, nonetheless most of the doped holes still go to the O site.

Fig.5.10 is the plot of the Cu hole-occupation number $<n_d>$ as a function of the charge transfer energy ε for the half-filled case with $U_{dd} = 6$ and $\beta = 10$, the transition from the charge transfer limit ($\varepsilon = 0$) to the Mott-Hubbard limit (ε large) is continuously shown. As ε becomes larger and larger, the O p-states are higher and higher in energy, therefore Cu sites tend to be occupied. For $t_{pp} = 0$, where MC results are available, our MF calculation again yields good agreement. When t_{pp} is finite, the hole occupation on the Cu sites is suppressed dramatically in the charge-transfer limit as observed in Fig.5.9, while this suppression is much smaller in the Mott-Hubbard limit because the p-state energy is much higher than the Cu d-state, thus the broadening of p-band does not affect the whole system significantly.

In Fig.5.11, the squared local moment $<m_z^2> = <(n_\uparrow - n_\downarrow)^2>$ on the Cu site vs. U_{dd} (Fig.5.11a) and vs. ε (Fig.5.11b) at half filling with $\beta = 10$ is shown. Parameters used are $\varepsilon = 2U_{dd}/3$ in (a) and $U_{dd} = 6$ in (b). Similarly to the single band Hubbard model case, there is no antiferromagnetic (AF) solution for a certain parameter range within POMF. For parameters where the AF ground state can be found, POMF results for the Cu squared local moment agree very well with those of MC simulations. It is seen that both U_{dd} and t_{dp} tend to localize the spin on the Cu site. With a non-zero t_{pp}, the hole occupation on the Cu site becomes smaller, and the Cu $<m_z^2>$ is suppressed. This is readily shown in the

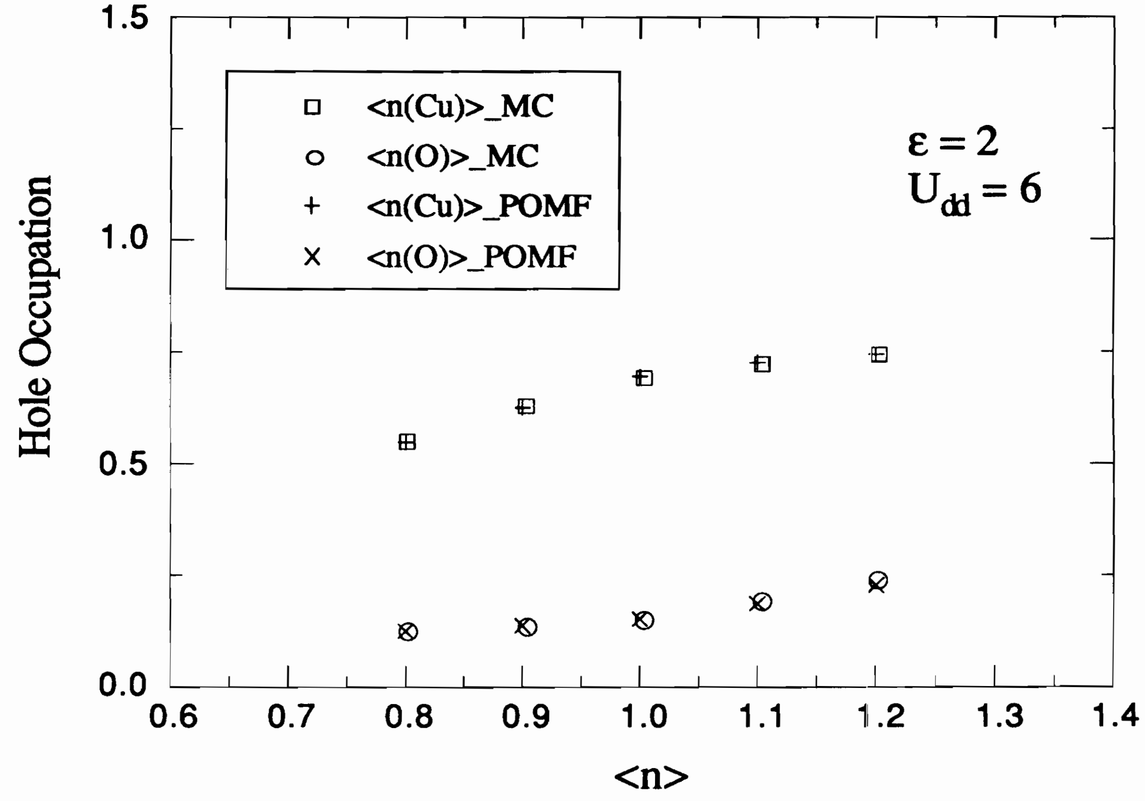

Fig. 5.7 **Charge transfer regime: the hole occupation numbers on the Cu site $<n_{Cu}>$ and O site $<n_O>$ vs. band filling $<n> = <n_{Cu}> + 2<n_O>$.** Both of the Monte Carlo [Scalettar et.al] and the projection operator mean field results for $t_{dp} = 1, U_{dd} = 6, \varepsilon = 2, t_{pp} = 0, U_{pp} = 0$, and $\beta = 8$ are shown.

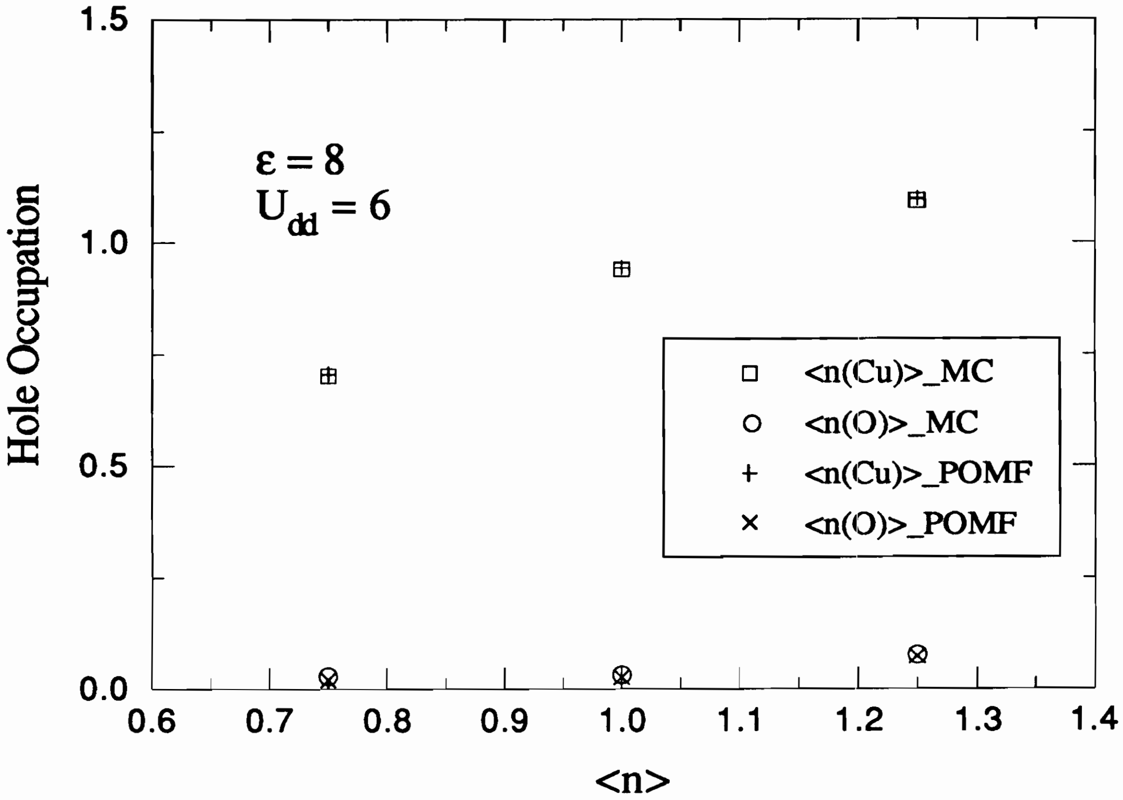

Fig. 5.8 **Mott-Hubbard regime: the hole occupation numbers on the Cu site $<n_{Cu}>$ and O site $<n_O>$ vs. band filling $<n> = <n_{Cu}> + 2<n_O>$.** Both of the Monte Carlo [Scalettar et.al] and the projection operator mean field results for $t_{dp} = 1, U_{dd} = 6, \varepsilon = 8, t_{pp} = 0, U_{pp} = 0$, and $\beta = 8$ are shown.

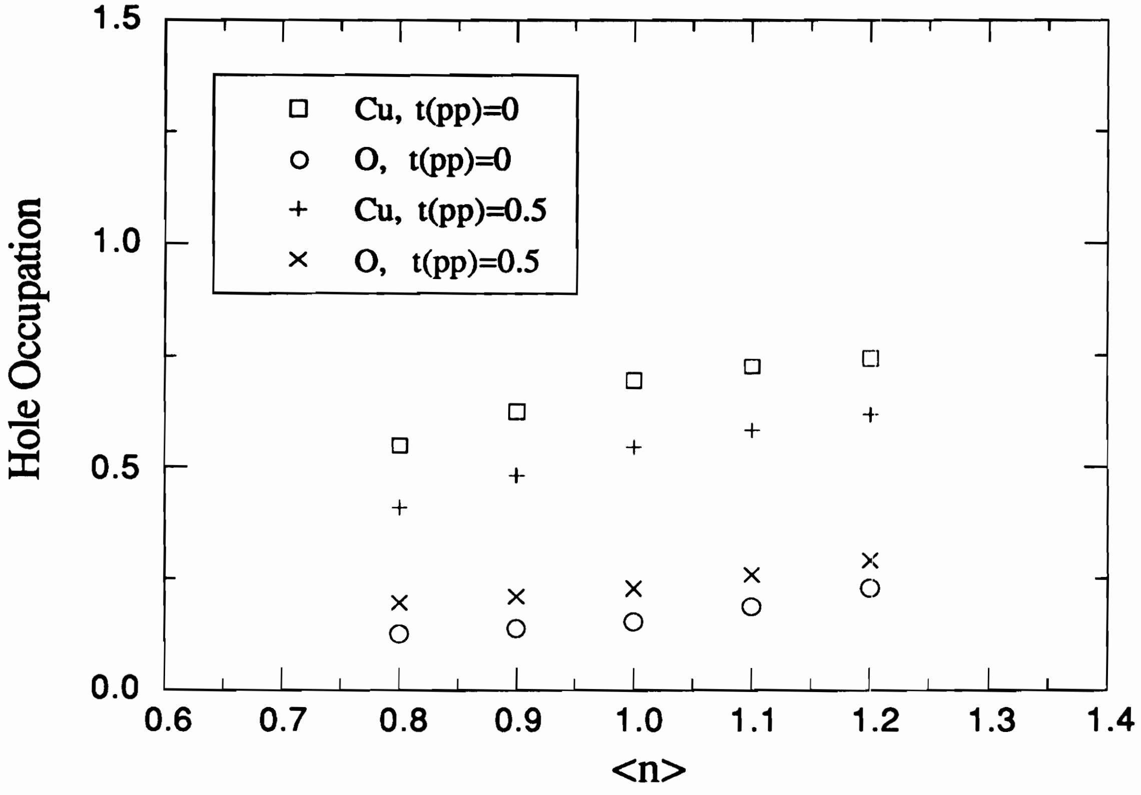

Fig. 5.9 **Effect of t_{pp} on the hole occupation at the Cu and O sites versus band filling in the charge transfer limit.** All parameters are the same as those given in Fig.5.7 except for finite t_{pp}.

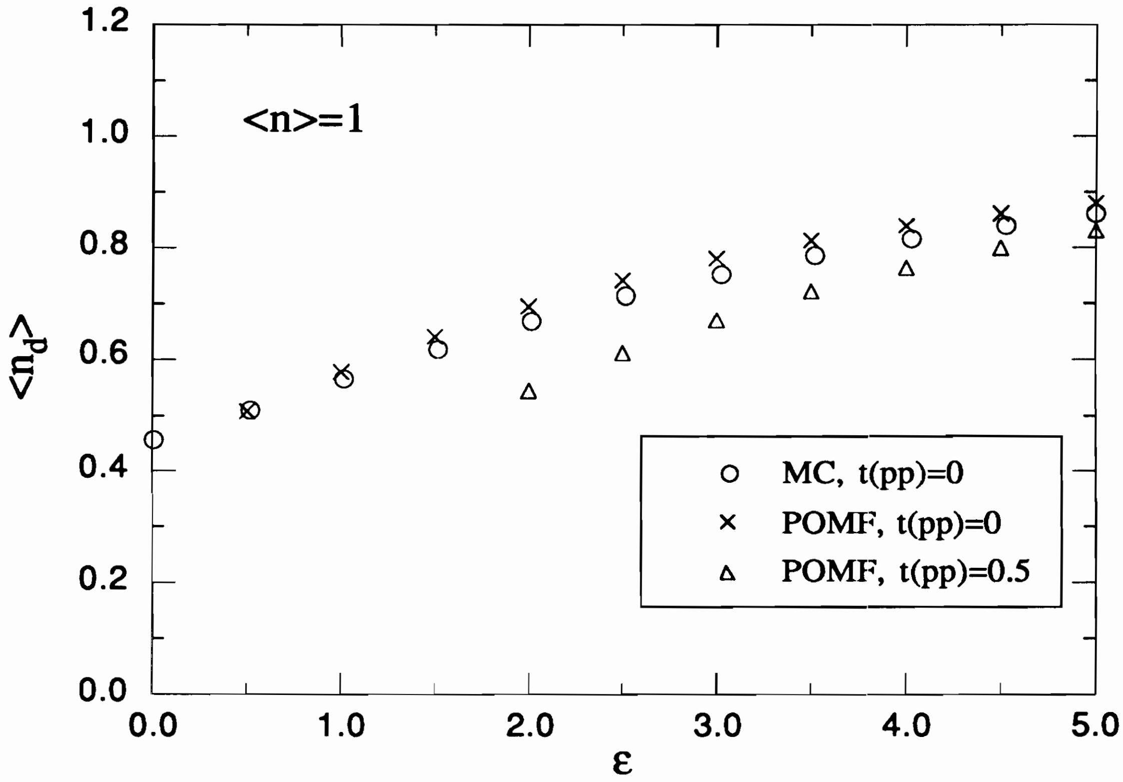

Fig. 5.10 **Hole-occupation number on the Cu sites $\langle n_d \rangle$ as a function of the charge transfer energy ε.** Half-filled case with $t_{dp} = 1$, $t_{pp} = 0$, $U_{pp} = 0$, $U_{dd} = 6$ and $\beta = 10$. t_{pp} significantly suppresses $\langle n_d \rangle$ in the charge transfer limit.

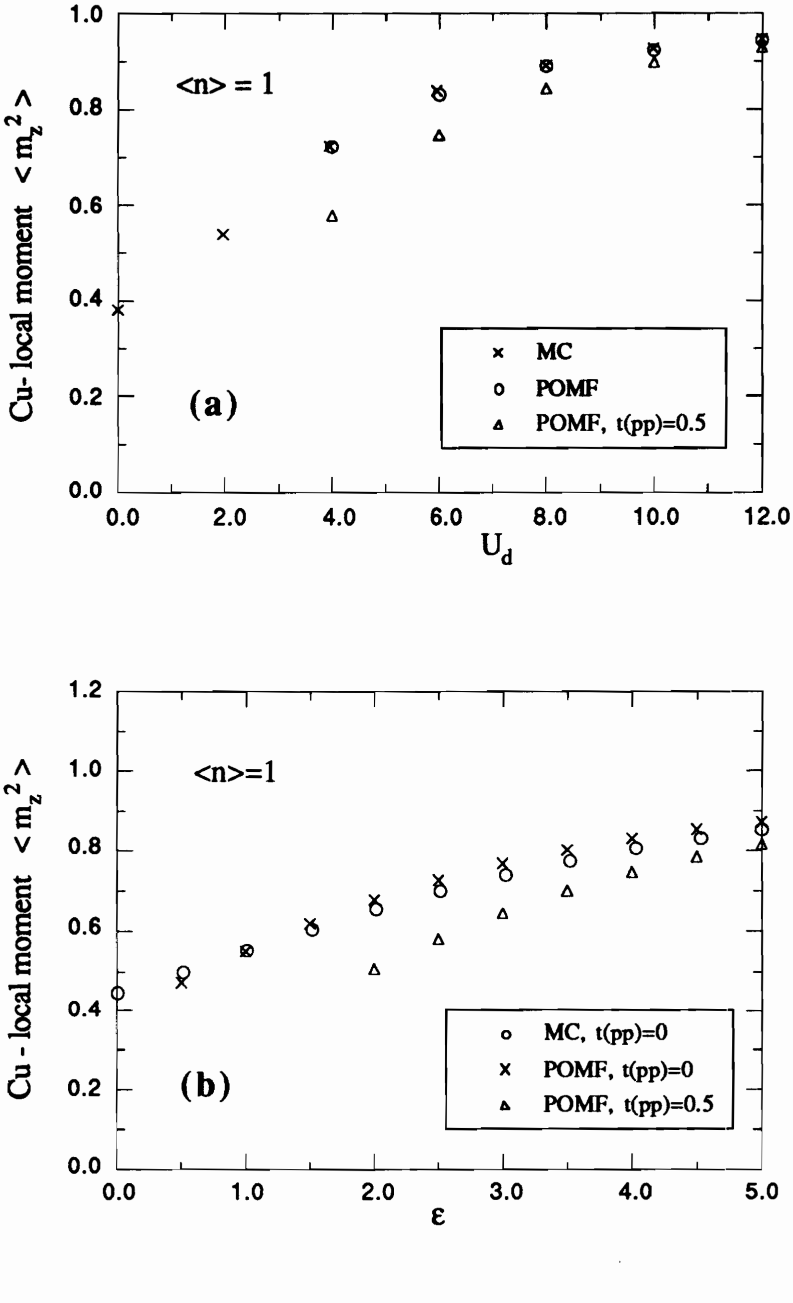

Fig. 5.11 **The squared local moment on the Cu site $<m_z^2> = <(n_\uparrow - n_\downarrow)^2>$.** (a) $<m_z^2>$ vs. U_{dd}, (b) $<m_z^2>$ vs. ε. $t_{dp} = 1$, $t_{pp} = 0$, $U_{pp} = 0$, $\beta = 10$. In (a) $\varepsilon = 2U_{dd}/3$. In (b) $U_{dd} = 6$. Symbol Δ are the data points for $t_{pp} = 0.5$. The Monte Carlo result in (a) is by Scalettar et.al., in (b) is by Dopf (1990).

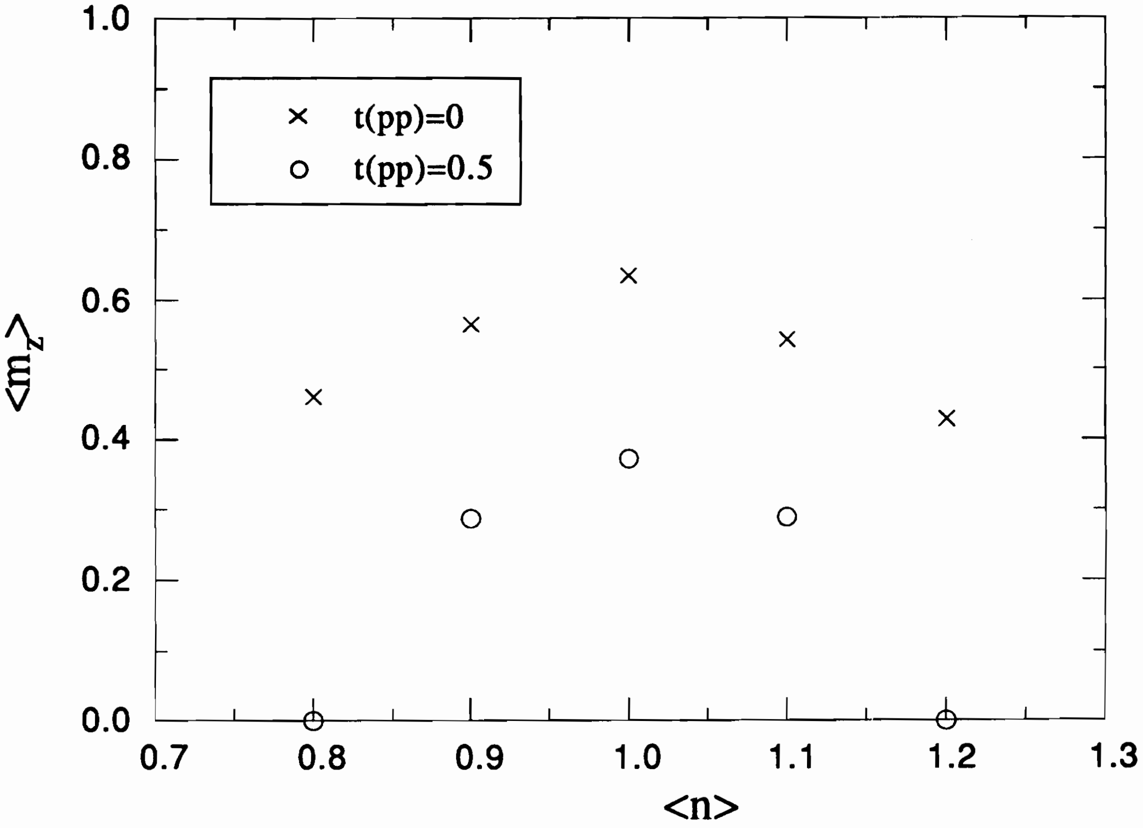

Fig. 5.12 **The staggered magnetic moment $<m_z> = |<n_\uparrow - n_\downarrow>|$ on the Cu site vs. band filling <n>.** Parameters are the same as those used in Fig.5.7. Note that in the hole picture, <n> > 1 corresponds to hole doping, <n> < 1 corresponds to electron doping.

figure. This suppression of $<m_z^2>$ is more severe in the charge transfer limit, similar to what has been observed in Fig.5.10.

The result of the staggered magnetization $<m_z> = |<n_\uparrow - n_\downarrow>|$ on the Cu sites versus band-filling $<n>$ is shown in Fig.5.12 with $U_{dd} = 6$, $\varepsilon = 2$ and $\beta = 8$. The system has its maximum magnetization at half-filling. As the system gets away from half-filling by either hole doping or electron doping, $<m_z>$ decreases and vanishes eventually. It is also seen that turning on t_{pp} not only suppresses the value of $<m_z>$ but makes it vanish much more rapidly with doping.

5.3.3 Density of states of the CuO_2 lattice model

To gain a better understanding of the physical properties presented above, it is useful to study the density of states (DOS) of the three-band CuO_2 lattice model with proper LDA parameters [Zhou, 1991c]. Unless specified otherwise, the LDA parameters listed in Eq.(5.35) are used with $U_{dp} = 0$.

Fig.5.13 shows the Cu, O and total density of states for the paramagnetic (PM) state and Fig.5.14 for the AF state in the half-filled case with $\beta = 10$. In the PM state, the calculation clearly shows the three-band structure, with a mostly O p-state band in between the two bands dominated by singly occupied and doubly occupied Cu d-states. For $<n> = 1$, the Fermi energy (set to zero in the figures, also indicated by the vertical line) lies in the middle of the d-band. In the AF state, this low lying band splits, leaving the Fermi level in the gap. Since the AF state has a lower energy, therefore the undoped system is an insulator.

As discussed in section 5.1, the difference between Hubbard I and POMF is a static energy shift Δ. For the single band Hubbard model, the POMF result [Zhou, 1991b] shows a systematic improvement over that of Hubbard I. In Fig.5.15 we make a comparison between the results for the total DOS for the AF ground state of the undoped system ($<n> = 1$) from POMF, Hubbard I and the four-boson theory (SBMF) [Zhang, 1990]. The parameters used here are the same as those used by Zhang et.al., which are $U_{dd} = 6eV$, $\varepsilon = 1.5eV$, $t_{dp} = 1.085eV$, $t_{pp} = 0.2$ eV, and $U_{pp} = 0$. All Fermi levels (vertical line) are set to zero in the figure. It is seen that the DOS from POMF and SBMF are similar (Fig.5.15a), except that in SBMF there is no high energy Hubbard-like band for the doubly occupied Cu d-states which always exists in the POMF and the Hubbard I approximation (not shown in the figure). Both the POMF and SBMF results indicate an insulating system, with the Fermi energy inside the AF band gap. But the DOS results obtained from the Hubbard I calculation show a rather different structure around the Fermi energy (Fig.5.15b), yielding an unphysical conducting ground state at half filling. Thus, as in the single band Hubbard model case, the static energy shift Δ used in POMF is important for getting the correct physical properties.

In order to examine the effect of doping on the density of states, the staggered magnetization $<m_z>$ on the Cu site versus $<n>$ with LDA parameters and $\beta = 10$ is calculated, and the result is shown in Fig.5.16. Starting from $<n> = 1$, $<m_z>$ becomes smaller with the increase of hole doping, and the ground state of the system changes from an AF state to a PM state around 30% doping within this calculation. This effect of doping induced transition from the AF ground state at $\delta = 0$ to a PM ground state can be better understood by examining the density of states of the system. The total DOS for $\delta = 0, 0.2$ and 0.4 is plotted in Fig.5.17 with the same parameters as those used in Fig.5.16. As

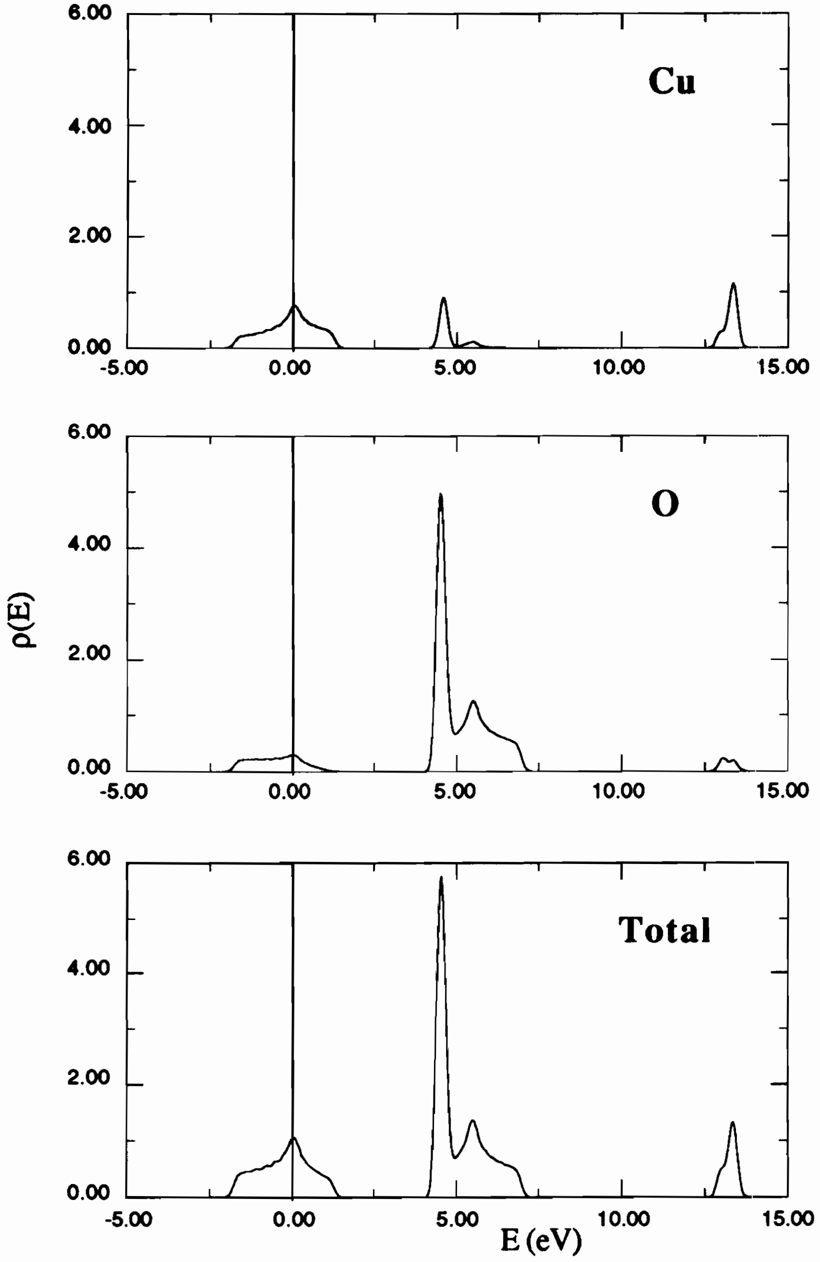

Fig. 5.13 **The Cu, O and total density of states for the paramagnetic half-filled system.** The LDA parameters are used along with β = 10. The Fermi energy is set to be zero and marked by a vertical line.

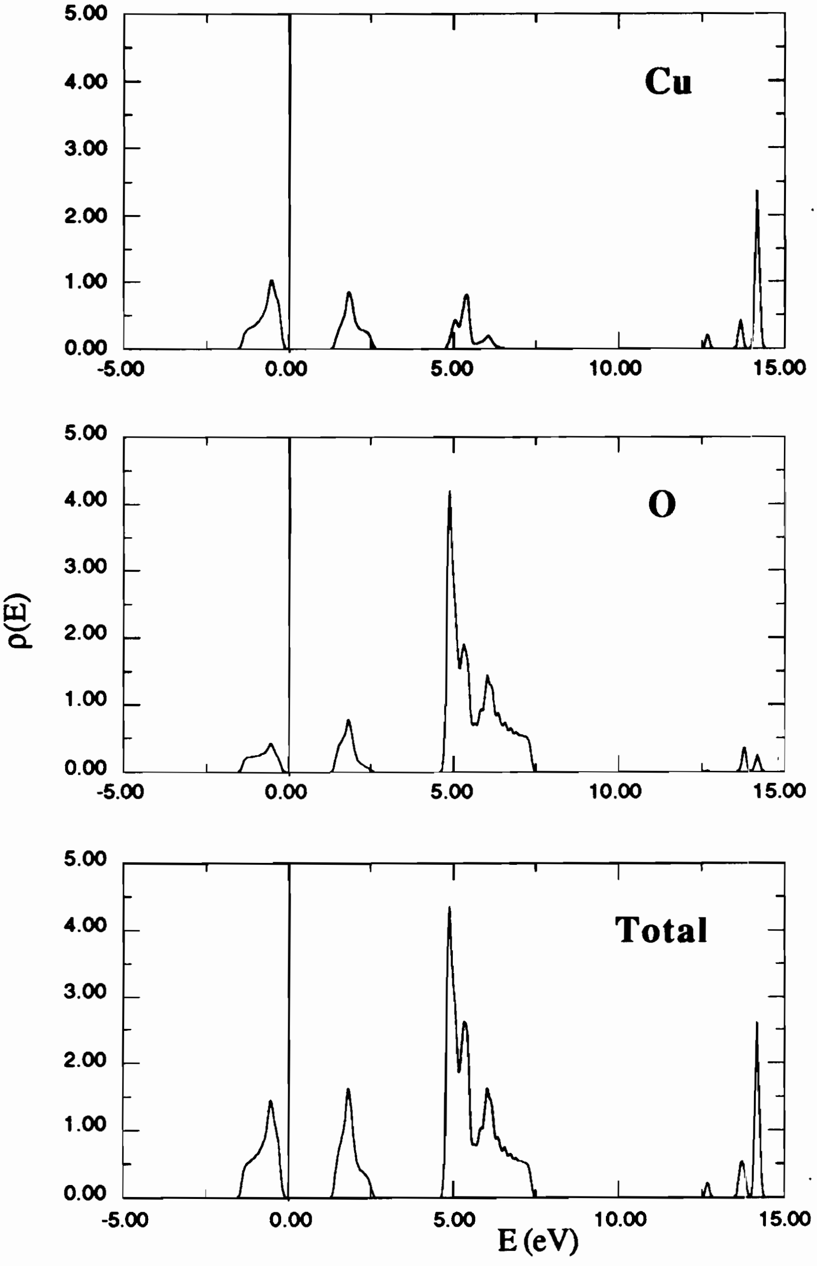

Fig. 5.14 **The density of states for the anti-ferromagnetic half-filled system.** Parameters are the same as those used in Fig.5.13.

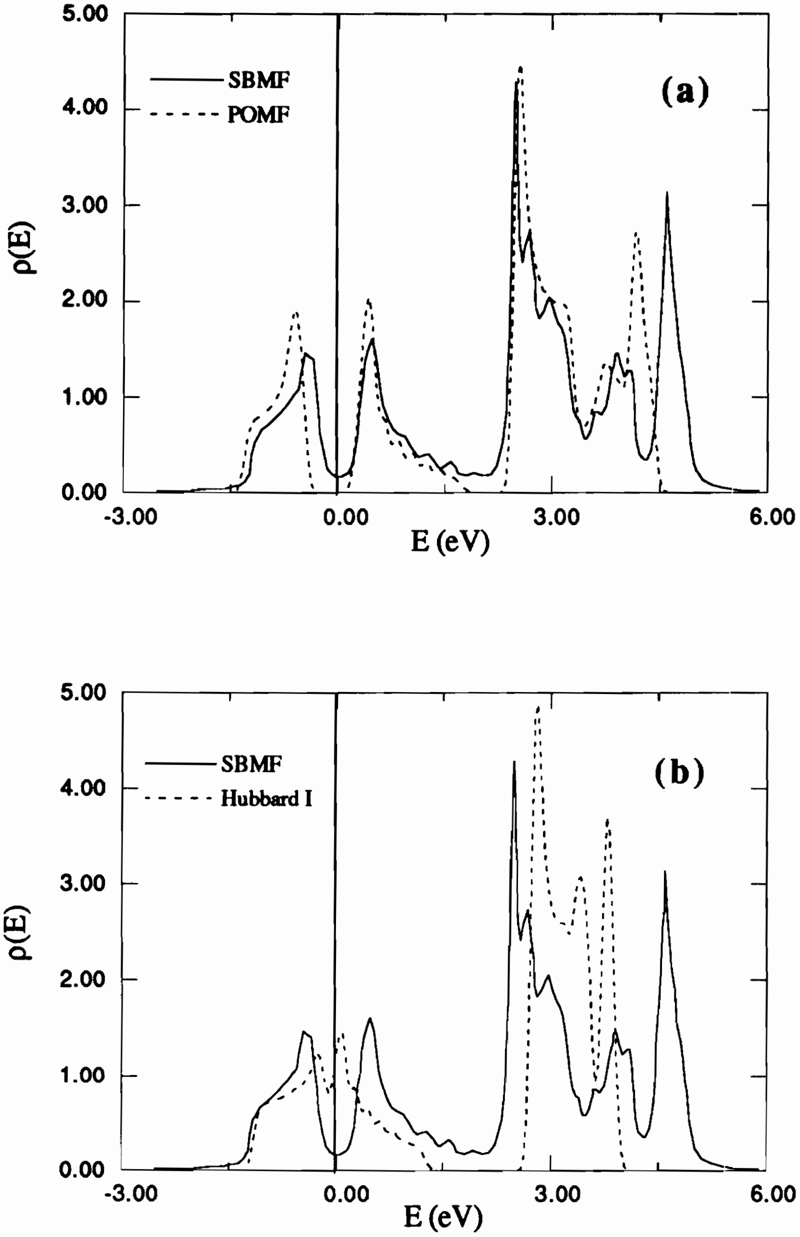

Fig. 5.15 **Density of states obtained from SBMF [Zhang, 1990], POMF and the Hubbard I approximation for half-filling.** Parameters used are: U_{dd} = 6eV, ε = 1.5eV, t_{dp} = 1.085eV, t_{pp} = 0.2 eV and U_{pp} = 0. The high energy structures in POMF and Hubbard I results are not shown in the graph. (a). The DOS from SBMF and POMF are very similar. β = 10 in POMF. (b). β = 40 is used in the Hubbard I calculation in order to get the AF solution.

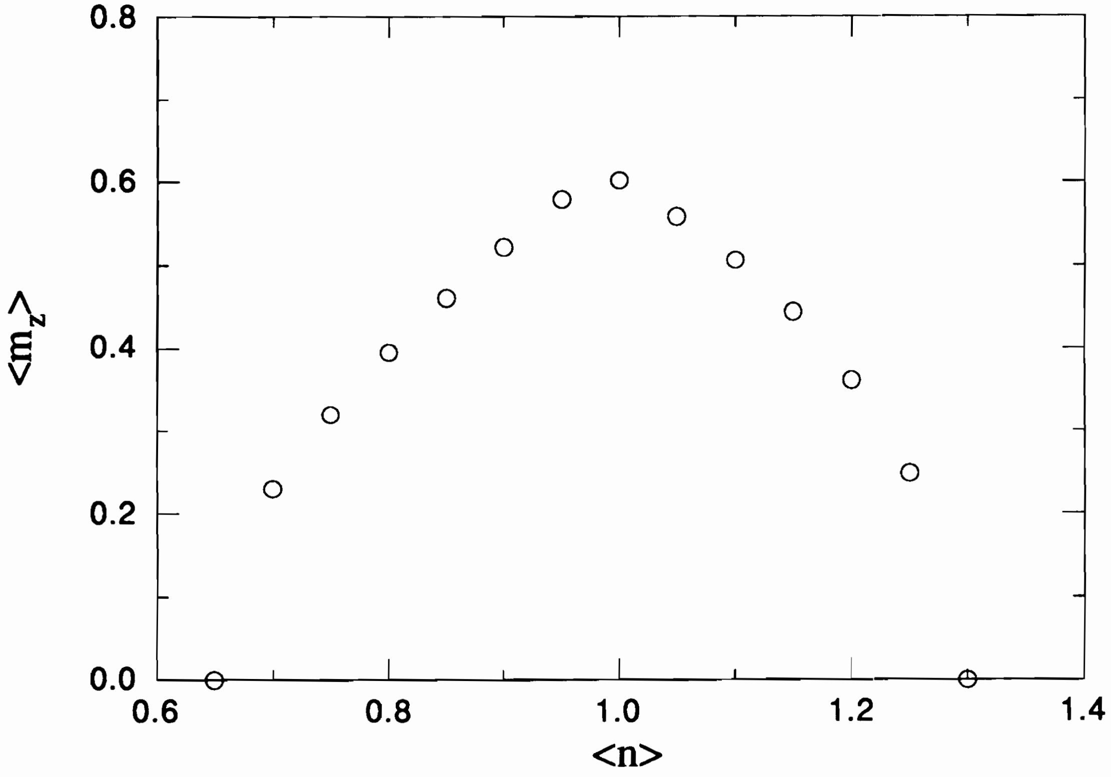

Fig. 5.16 **The staggered magnetic moment <m_z> on the Cu site vs. <n> using the LDA parameters.** β = 10. Note that in the hole picture, <n> > 1 corresponds to hole doping, <n> < 1 corresponds to electron doping.

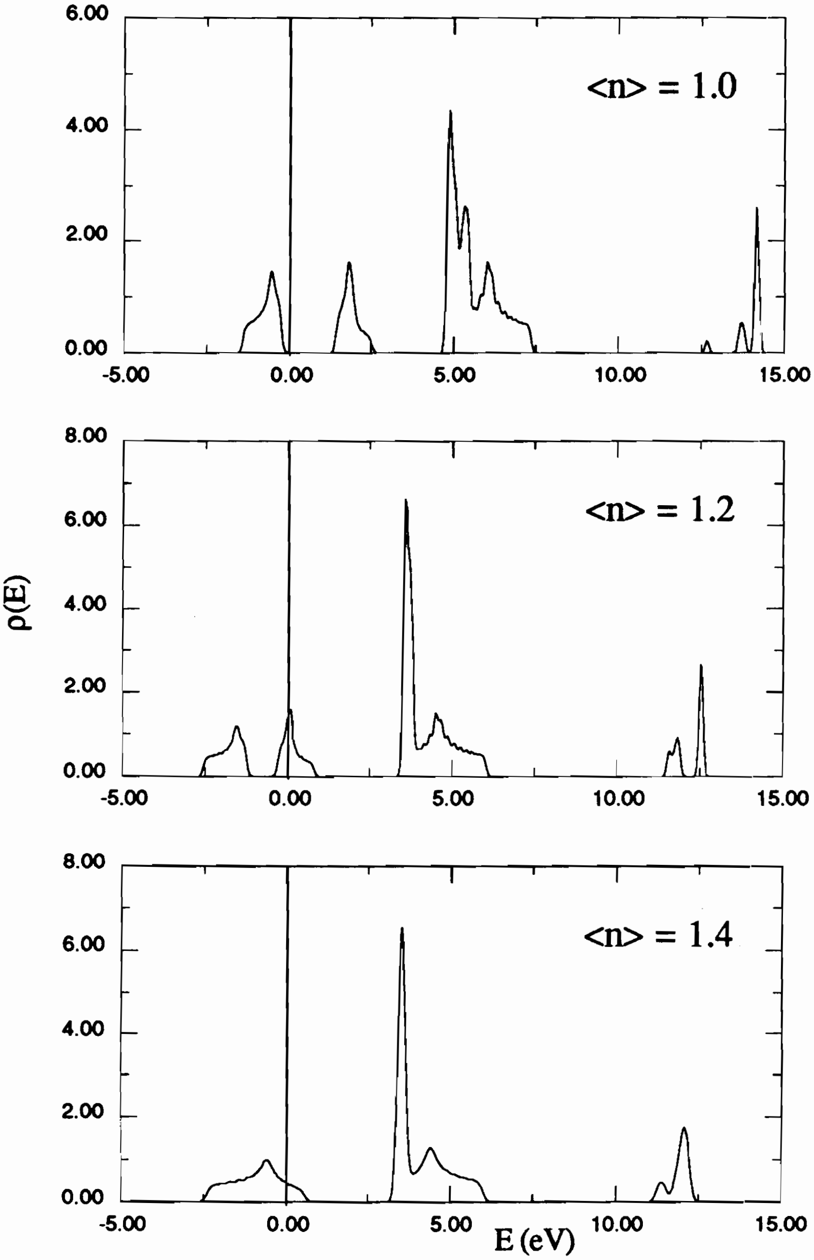

Fig. 5.17 **The total density of states for band fillings <n> = 1.0, 1.2 and 1.4.** Parameters are the same as those used in Fig.5.16. The Fermi energy is set to zero (vertical line). The ground states for <n> = 1.0 and 1.2 are AF states, for <n> = 1.4 a PM state.

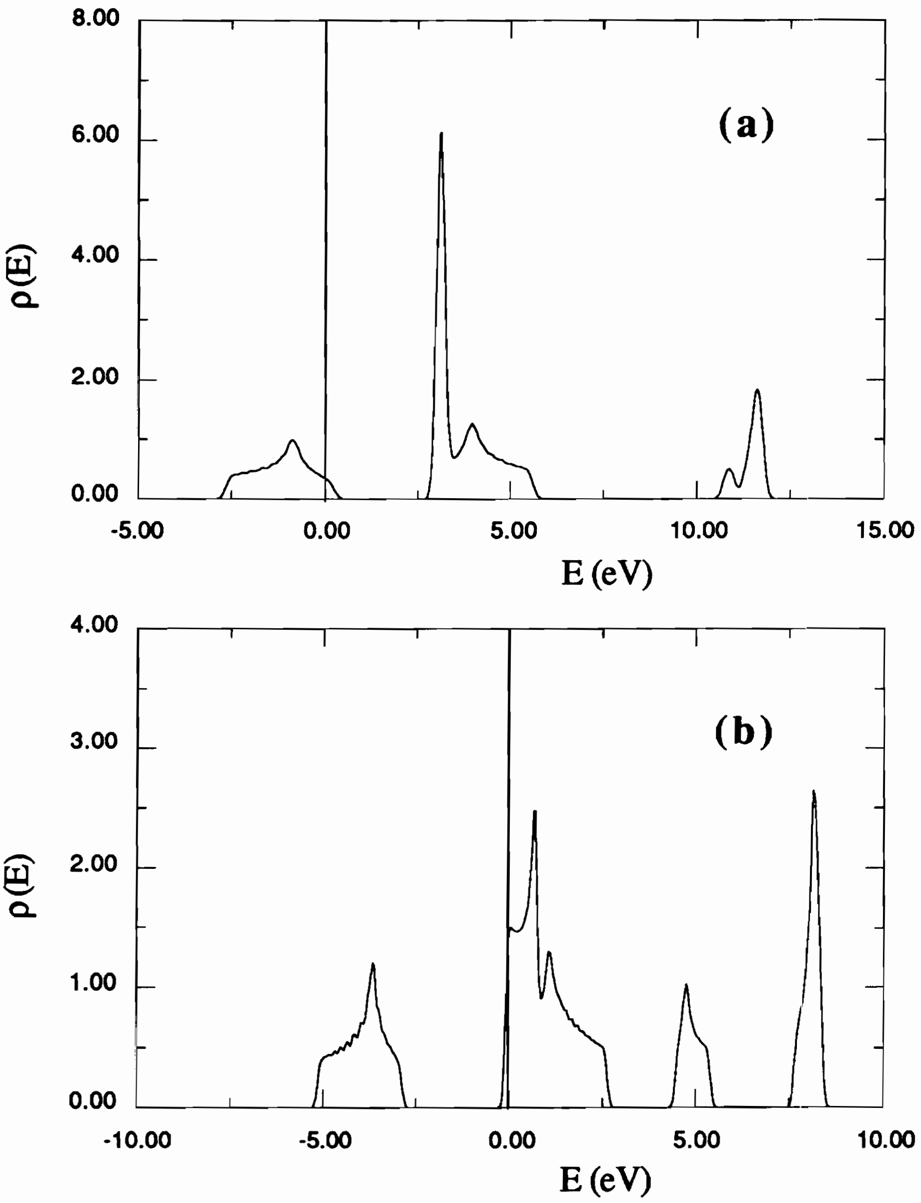

Fig. 5.18 **The total density of states obtained from the POMF** (a) **and the Hubbard I** (b) **calculations for <n> = 1.5.** LDA parameters are used with temperature T = 100K. The ground state is a PM state in this case.

discussed earlier, the system is an insulator with its Fermi level in the AF band gap when $\delta = 0$. With 20% hole doping, the ground state is still an AF state. Now the Fermi level moves into the upper singly occupied Cu AF band. Meanwhile the AF band gap is smaller when δ gets larger. Eventually this gap vanishes, thus the system becomes a PM state. This is seen in the $\delta = 0.4$ case.

In Fig.5.15, the distinct difference between the total DOS obtained from the POMF and the Hubbard I scheme has been shown for an AF ground state. For a PM ground state, their difference can be seen in Fig.5.18, where $\langle n \rangle = 1.5$ and temperature T = 100K. The Fermi level is inside the low-lying d-band for POMF (Fig.5.15a), but for Hubbard I it lies inside the p-band (Fig.5.15b). Also comparing with the DOS of POMF, the Hubbard I calculation yields a separate p-state dominated band around 5eV. It is interesting to see that even though the Coulomb repulsion U_{dp} between electrons on Cu and O sites is not incorporated in this current calculation, the resulting total DOS in Fig.5.18b is similar to those in Fig.4b and Fig.8b of Entel et.al. (1990) in which all parameters used are the same as those in Fig.5.18 except $U_{dp} = 1.2$eV. This implies that even with certain restrictions (as those used by Entel et.al.), the Hubbard I approximation may yield a qualitatively different position of Fermi level in the DOS result from the POMF and SBMF calculations, therefore it is necessary to be cautious when interpretating the experimental data using the Hubbard I result.

5.4 Summary

A mean-field calculation of the two dimensional Hubbard model based on a projection operator formalism has been presented. For the single-band case, it is found that, for various physical properties, its results agree very well with those of the four-boson theory and the quantum Monte Carlo simulations, showing a systematic improvement over the Hubbard I approximation. Unlike the Hubbard I approximation where no anti-ferromagnetic solution can be found at half-filling in the relevant parameter range, the AF ground state is obtained for U's as small as 5 in this current treatment. By examining the Fermi surface of the system, we found that Luttinger's theorem is still violated (especially around half-filling) within the projection operator formalism, even though the violation is not as severe as in Hubbard I.

Comparing with the four-boson theory, the number of equations to be solved in this projection operator-based theory is much smaller, thus the calculation can be easily extended into multi-band models such as the three-band CuO_2 lattice model. The results of this MF calculation agree remarkably well with the Monte Carlo simulation results in the parameter range where MC results are available. In addition, we have examined the effect of hopping between Oxygen sites, and found that t_{pp} suppresses the hole occupation at the Cu sites and the AF order when moving away from half-filling, especially in the charge transfer limit. The study of the density of states shows good agreement between the POMF and SBMF calculations, while the Hubbard I approximation yields rather different and unphysical results.

Chapter 6

Many-Electron Partition Function

From calculations presented in previous chapters, it is apparent that finding solutions for strongly correlated electron systems is a very difficult task. The many-body interaction effects may not show up in the standard independent single-particle state results. Therefore it is appealing to develop a systematic derivation of many-electron partition functions for various models so that their thermodynamic properties can be extracted directly and accurately [Bowen,1991]. In this chapter, the cumulant expansion calculation of the low temperature quantum mechanical partition functions of degenerate many-electron systems is presented, and its application to other interacting systems is discussed in the last section.

The initial motivation behind this calculation was to provide a possible approximation for partition functions in the Canonical and Grand Canonical Ensembles that would not require the usual starting assumption of independent single particle states. As a test for this methodology, it was first decided to calculate both partition functions for the degenerate free electron gas for which the grand canonical partition function is well known. There does not appear to be any other direct calculation of the free electron canonical partition function for low temperatures in the literature. This absence of canonical ensemble calculations is quite natural, given the difficulty in counting states and the well known "proof" in the standard quantum statistical mechanics literature [Huang, 1963; Yamamoto, 1956] on the equivalence of the two partition functions. However, it is found that the direct, approximate calculations of the canonical partition function and the grand canonical partition function starting from the same ground state for N electrons yield different results at low temperatures, where the cumulant expansion method is valid. This surprising result can be understood by looking into the difference between the two emsembles and the usual "proof" of their equivalence, which has been done in this study.

6.1 The cumulant expansion formula

There have been a large number of applications of the concept of the cumulant [Kubo, 1962; Brout, 1959], most of them having been made in classical statistical mechanics [Yvon, 1969] and in the study of the interacting gas [Mayer, 1940], leading to expansions that are valid in the high temperature regime. For the application in this chapter to low temperatures, the cumulant expansion can be regarded as a rearrangement theorem for a sum which closely resembles the expansion of an exponential, except that the terms are not products of the argument of the exponential. Let us consider a series of the form

$$e^{\Theta} = 1 + \sum_{n=1}^{\infty} \frac{t_n}{n!} \tag{6.1}$$

where the terms t_n are not simple powers of some variable to the n-th power. In our application t_1 is extensive (thermodynamically) and each other term t_n has dominant terms of order N^n. The re-arrangement of this series to find Θ, which is the variable whose powers give the usual series expansion for the exponential, yields the following sum:

$$\Theta = \sum_{n=1}^{\infty} \frac{\kappa_n}{n!} \tag{6.2}$$

where the κ_n are given by:

$$\begin{aligned}
\kappa_1 &= t_1 \\
\kappa_2 &= t_2 - t_1^2 \\
\kappa_3 &= t_3 - 3\,t_2\,t_1 + 2\,t_1^3 \\
\kappa_4 &= t_4 - 4\,t_3\,t_1 + 12\,t_2\,t_1^2 - 3\,t_2^2 - 6\,t_1^4 \\
\kappa_5 &= t_5 - 5\,t_4\,t_1 - 10\,t_2\,t_3 + 20\,t_3\,t_1^2 + 30\,t_1\,t_2^2 - 60\,t_2\,t_1^3 + 24\,t_1^5
\end{aligned} \tag{6.3}$$

Determiniation of the r-th cumulant uses all the t_n up to r in the original series. A listing of the first few cumulants can be found in several handbooks [Abramowitz, 1970; Korn, 1968] and a formula for the general cumulant is given by Mattis [Mattis, 1985]. If the series of κ's are quickly converging, finite sums have the potential of providing good approximations for the partition functions of interacting systems. In those systems the t_n will roughly correspond to the sum of terms with n excitations present.

The partition function Q_N for the canonical ensemble for a Hamiltonian H in contact with an energy reservoir with temperature β^{-1} is defined as

$$Q_N = \mathrm{Tr}_N\,(e^{-\beta H}) \tag{6.4}$$

where the trace is taken over states with N particles.

The grand partition function Z is defined for a system that is in contact with a particle reservoir at chemical potential μ which allows the exchange of particles and energy with the system. For systems described by the grand canonical ensemble the number of particles for the system is not definite, but may fluctuate. The average number of particles <N> in the system is determined by the chemical potential. The grand partition function is defined as

$$Z = \sum_{N=1}^{\infty} Q_N e^{\beta\mu N} \tag{6.5}$$

From the definition of the grand canonical partition function it is straightforward to derive the following useful formulas for the average energy U = <E> and the average number of particles <N>:

$$U = \mu \langle N\rangle - \left(\frac{\partial \ln Z}{\partial \beta}\right)_{\mu} \tag{6.6a}$$

$$\beta \langle N\rangle = \left(\frac{\partial \ln Z}{\partial \mu}\right)_{\beta} \tag{6.6b}$$

where the subscripts indicate the variable held constant in the partial derivative.

From the earliest literature [Fermi, 1926], the grand canonical partition function for the free electron gas has been calculated by using the product theorem of statistical mechanics, which states that the partition function representing two independent sub-systems is the product of the partition functions of the systems. For the grand partition function of an electron gas with one-electron energies of ε_{ks} we may write:

$$Z = \prod_{\vec{k},\, s} \{ 1 + \exp[-\beta (\varepsilon_{k,s} - \mu)] \} \tag{6.7}$$

Applying Eq. (6.6) to this product yields the standard definition for the energy and average particle number:

$$U = \sum_{\vec{k}\, s} \varepsilon_{ks}\, f(\varepsilon_{ks}) = \int g(\varepsilon)\, \varepsilon\, f(\varepsilon)\, d\varepsilon \tag{6.8a}$$

$$\langle N \rangle = \sum_{\vec{k}\, s} f(\varepsilon_{ks}) = \int g(\varepsilon)\, f(\varepsilon)\, d\varepsilon \tag{6.8b}$$

where f(ε) is the Fermi function and g(ε) is the one electron density of states for both spin states.

The standard procedure [Huang, 1963] is to take these two equations and carry out an integration by parts, yielding an integral of g(ε) against the derivative of the Fermi function. At low temperatures this derivative is so sharply peaked at the chemical potential μ that the density of states can be expanded in a Taylor series about μ. The resulting integrals of powers of the energy with the sharply peaked factor leads to a (usually) asymptotic power series in temperature.

Using these series and calculating the heat capacity at constant particle number and constant volume gives

$$C_{<N>} = \left.\frac{\partial U}{\partial T}\right|_{<N>} = \gamma T = \left(\frac{\pi^2}{3}\, g(\mu)\, k_B^2\right) T \tag{6.9}$$

where k_B is the Boltzmann constant. Usually this calculation is quite complicated, but straightforward.

A simpler more direct calculation can be obtained by first calculating the grand canonical partition function directly from Eq. (6.7). The first step is to seek the logarithm of Z, converting the products to sums and integrals over the density of states $g(\varepsilon)$. By separating the integrals into two types: particle excitations $(\varepsilon - \mu) > 0$ and hole excitations $(\varepsilon - \mu) < 0$ one obtains integrals of $g(\varepsilon)$ multiplied by the logarthm of 1 plus something small. A useful asymptotic expansion can be obtained from these integrals by first expanding the logarithms in a series expansion and then also expanding the density of states in a Taylor series in $(\varepsilon - \mu)$ and carrying out the resulting integrals of $(\varepsilon - \mu)$ powers and exponentials. The resulting expression for the grand partition function is

$$\ln(Z) = -\beta \left(E(\mu) - \mu \langle N(\mu) \rangle \right) + 2 \sum_{r=1}^{\infty} \frac{g^{[2r]}(\mu)\, \eta_r}{\beta^{2r+1}} \qquad (6.10a)$$

where $g^{[n]}(\mu)$ is the n-th derivative of the density of states evaluated at the chemical potential and η_r is defined as

$$\eta_r = \sum_{l=1}^{\infty} \frac{(-1)^{l+1}}{l^{2r+2}} \qquad (6.10b)$$

and

$$E(\mu) = \int_{\varepsilon_0}^{\mu} \varepsilon\, g(\varepsilon)\, d\varepsilon \qquad (6.10c)$$

$$N(\mu) = \int_{\varepsilon_0}^{\mu} g(\varepsilon)\, d\varepsilon \qquad (6.10d)$$

with ε_0 the energy at the bottom of the band.

Using Eq. (6.6) it is easy to derive the following expression for the energy,

$$U = E(\mu) + 2 \sum_{r=1}^{\infty} \frac{\left[g^{[2r]}(\mu) + \mu\, g^{[2r+1]}(\mu)\right] \eta_r}{\beta^{2r+2}} \tag{6.11a}$$

and for the average number of particles

$$<N> = N(\mu) + 2 \sum_{r=1}^{\infty} \frac{g^{[2r+1]}(\mu)\, \eta_r}{\beta^{2r+2}} \tag{6.11b}$$

For use in our later discussion it is appropriate to note that the heat capacity at constant chemical potential can be obtained easily from Eq. (6.11a),

$$C_\mu = 2k \sum_{r=1}^{\infty} \left[g^{[2r]}(\mu) + \mu\, g^{[2r+1]}(\mu)\right] \eta_r\, (kT)^{2r+1} \tag{6.12}$$

The heat capacity at constant particle number, Eq. (6.9), and corrections may be obtained easily from these equations by first determining the temperature derivative of the chemical potential so that <N> is constant in temperature.

It is currently standard practice to use $C_{<N>}$ for interpreting experiments instead of C_μ. This practice is based on the standard argument in statistical mechanics that the canonical partition function is essentially the same as the grand canonical partition function for large systems. The results of this study contradict this argument.

Let us now re-examine this argument. The key step in the argument is the unverified assumption [Huang, 1963] that the dominant term in the grand canonical partition function is $Q_N\, e^{\beta\mu N}$ where for simplicity we write N = <N> for the average particle number. Because the Helmholtz free energy is extensive, this dominant term can be written in the form $\exp(V\phi(\beta,V/N))$ where ϕ is intensive with respect to the volume V and/or particle number N. Two rather weak inequalities are applied at this point to bound Z. The first inequality simply states that the whole series must be larger than the single dominant term. The second inequality rather weakly dominates Z. It is argued that for some large number of particles N_0 in the volume V the interactions raise the energy so much that Q_{N_0+r} is as small as desired. In this case one can argue that Z must be smaller than N_0 times the maximum term. It is further argued that N_0 must be proportional to the volume, $N_0 = aV$. These arguments can be combined to yield

$$e^{V\phi} < Z < aV\, e^{V\phi}$$

Taking the logarithm and dividing by V gives

$$\phi < \ln(Z)/V < \phi + \ln(aV)/V$$

As the volume becomes very large, the second term on the right side of the equality goes to zero and Z is approximated well by $\exp(V\phi)$. The possibility that is ignored in this general argument is that there are systems where combinations of terms involving small fluctuations in particle number may combine to make a contibution to Z that dominates the Q_N contribution.

In the case of the electron gas it is found that the collection of terms for small m

$$\exp(\Theta_m) = \sum_{r=-m}^{m} Q_{N+r} \exp[\beta\mu(N+r)] \tag{6.13}$$

gives rise to an extensive Θ_m which converges to a Θ as $m \rightarrow \infty$, which dominates the Helmholtz Free energy for N particles obtained from the canonical ensemble. Later we will see that the cumulant formula applied to m=5 recovers the grand canonical result to within about 2 percent at low temperatures.

The "standard" proof of the equivalence of the canonical and grand canonical ensembles only determines the sum to order ln(V). However, the cumulant series used here involves individual terms which are valid in the thermodynamic limit and the series thus converges in this limit more quickly than the t_n series itself. If T_N is the partial sum of the series of the t_n terms and if Z is the sum, then, if $|T_N - Z| < \varepsilon$ for large enough N and if K_N is the partial sum of the cumulant series, we have that $|K_N - \ln(Z)| < \varepsilon / Z$. This means that approximations determined by the cumulant series are much more strongly convergent to the partition function than the standard argument which only gives equality to within corrections of order 1/V.

For the low temperatures of interest here, the temperature dependence of the first cumulant κ_1 dominates the partition function. Higher order κ_n give either corrections to the coefficient of the temperature dependence of κ_1 or contribute higher powers of temperature. When we examine the canonical ensemble below, we will explicitly evaluate only κ_1 and κ_2.

In order to see how the terms representing the addition of an extra electron or an extra hole can give rise to contributions that are larger than the first contribution to the canonical ensemble, one has to ask if the sum in the canonical ensemble is smaller. In the canonical ensemble, because of the restriction that the particle number is fixed, the lowest energy excitations must be pairs of particle excitations above the Fermi energy and hole excitations. It is not possible in the canonical ensemble to have excitations with only a single particle or with a single hole in the filled Fermi sea, since these would represent a change in the number of particles. Yet, single particle or hole excitations will always give low temperature contributions to the partition function that are larger than the particle hole pairs. In the calculations to follow this will manifest itself in a temperature dependence of β^{-1} for the single particle or hole excitations and a temperature dependence of β^{-2} for the particle hole pairs [Pines, 1989]. It is the fact that the canonical ensemble only allows low lying excitations made up of particle-hole pairs and the grand canonical ensemble contains single particle or hole excitations which have come from the reservoir that makes the essential difference between the two ensembles.

As will be shown in section 6.3, the contributions due to as many as 5 additional holes or electrons in the ground state with N particles give a sizeable fraction of the coefficient of $\pi^2/3$ which is characteristic of the degenerate free electron gas.

6.2 Canonical partition function

In this section we will outline the evaluation of the canonical partition function using the cumulant summation formula written out above. The first step is to begin with the standard formula for the partition function for N free electrons with single particle energies ε_{ks} for momentum k and spin s:

$$Q_N = \frac{1}{N!} \sum_{k_1,\ldots,k_N}{}' \exp[-\beta \sum_{i=1}^{N} \varepsilon_{k_i s_i}] \tag{6.14}$$

where the prime on the sum indicates that terms where any two particles have the same momentum and spin are excluded from the sum. In order to simplify the writing of the equations, the spin variables have been left off the summation variables in Eq.(6.14), but they should be considered to be included in the summation implicitly. Below, the inclusion of the spin variables will be explicitly included, where needed. At this stage the prime on the summation symbol is the only manifestation of the Pauli exclusion principle beyond the fact that the ground state is constructed using it.

Since we are interested in the low temperature properties of the electron gas partition function, we start with a ground state which is the filled Fermi sea: all states with momentum below the Fermi momentum $|\mathbf{k}_F|$ are occupied and all states with larger momentum are unoccupied. For later simplicity of notation we designate the set of occupied momenta by the set F. Also, we will use the convention that momentum variables representing states not in the Fermi sea will be represented by **p** and momentum variables representing states inside the Fermi sea will be represented by **q**.

Let us re-arrange the terms in Eq.(6.14) so they are collected together by the number of particle-hole excitations out of the Fermi Sea. Each set of terms is labeled by $t_n/n!$, where n is the number of particle-hole excitations. In such a re-arrangement the first term corresponds to no particles excited out of the Fermi Sea:

$$t_0 = \frac{1}{N!} \sum_{q_1,\ldots,q_N}{}' \exp[-\beta \sum_{i=1}^{N} \varepsilon_{q_i s_i}] \tag{6.15a}$$

There are exactly N! ways the q_i can be assigned the N specific values contained in F. For each of these N! assignments the argument of the exponential is E_0, and the value of t_0

becomes

$$t_0 = e^{-\beta E_0} \tag{6.15b}$$

The single particle-hole pair excitations contribute the term t_1 which will have a sum over (N-1) q's and one p,

$$t_1 = \frac{1}{N!} \sum_{q_1,\ldots,q_{N-1},p}{}' \exp[-\beta \sum_{i=1}^{N-1} \varepsilon_{q_i s_i}] \exp(-\beta\varepsilon_{ps}) \tag{6.16a}$$

Each term in this series can be represented much more simply by noting that it represents a single hole in the Fermi Sea. For each of these the argument of the first exponential in Eq.(6.16a) can be written as

$$\sum_{i=1}^{N-1} \varepsilon_{q_i s_i} = E_0 - \varepsilon_q$$

Remember that there are N! ways to distribute the N electrons in the system such that the same physical state is represented, therefore:

$$t_1 = \sum_{p,s,q,s'}{}' e^{-\beta E_0} \exp(-\beta\varepsilon_{ps}) \exp(+\beta\varepsilon_{qs'}) \tag{6.16b}$$

For simplification it is useful to introduce a diagrammatic representation for the sums in Eq.(6.16b). We represent the momentum (and spin) sums over the initially unoccupied particle states by (•) and the sum over hole momenta (and spins) by (o). Since the particle and hole sums are independent we will be able to write t_1 as

$$t_1 e^{\beta E_0} = (\bullet \circ) = (\bullet)(\circ) \tag{6.16c}$$

where we have factored out the common exponential factor between t_0 and t_1.

The two particle-hole contributions to the partition function can be derived in the same fashion as above. This begins by recognizing that each (N-2) particle Fermi Sea is best represented by the two holes q_1 and q_2, and that if the pair of holes (or particles) are interchanged, the system remains in the same state. Therefore it is necessary to devide the summation over all possible q_1 and q_2 by 2! in order to avoid over counting, the same argument is true for summing over all possible p_1 and p_2, so that

$$t_2 = \frac{1}{2!} \sum_{q_1,q_2,p_1,p_2}{}' e^{-\beta\Delta_1} e^{-\beta\Delta_2} e^{-\beta E_0} \tag{6.17a}$$

where $\Delta_i = (\varepsilon_{p_i} - \varepsilon_{q_i})$ and the prime on the sum implies the Pauli Exclusion where no two particles (or holes) can have the same momentum and spin. Using the diagrammatic notation we can write for t_2 the following:

$$2!\, t_2\, e^{\beta E_0} = \sum_{q_1,q_2,p_1,p_2}{}' e^{-\beta\Delta_1} e^{-\beta\Delta_2} = (\bullet \circ \bullet \circ)' \tag{6.17b}$$

Since the holes and particles do not have the same range of momenta, there is no Pauli exclusion principle between them, i.e.,

$$(\bullet \circ \bullet \circ)' = (\bullet \bullet)' (\circ \circ)'$$

By similar argument it can be shown that the general term can be written as

$$n!\, t_n\, e^{\beta E_0} = \sum_{q_1 \cdots q_n, p_1 \cdots p_n}{}' \exp(-\beta \sum_{i=1}^{n} \Delta_i) = (\bullet \circ \ldots \bullet \circ)' \tag{6.18}$$

where the number of $(\bullet \circ)$ pairs in the parentheses is n.

Using this symbolic notation it is found that the partition function for N free electrons can be written as

$$Q_N e^{\beta E_0} = 1 + (\bullet \circ) + \frac{1}{2!}\frac{(\bullet \circ \bullet \circ)'}{2!} + \frac{1}{3!}\frac{(\bullet \circ \bullet \circ \bullet \circ)'}{3!} + \ldots$$

$$+ \frac{1}{n!}\frac{(\bullet \circ \ldots \bullet \circ)'}{n!} + \ldots \qquad (6.19)$$

where the last term has n ($\bullet\ \circ$) pairs. This is now the series that we will attempt to sum using the cumulant summation formula from which we seek a formula for Q_N of the form

$$Q_N = e^{-\beta E_0} \exp[\Theta(T,N)] \qquad (6.20)$$

Each of the terms in Eq.(6.19) has a prime indicating that the summations must be carried out with the Pauli exclusion in effect. The cumulants will enable systematic treatment of Pauli exclusion. However, it is instructive and heuristically useful to derive an approximation that will give the dominant low temperature approximation. This approximation is to consider Θ to be equal to the first cumulant κ_1:

$$\Theta = (\bullet \circ)$$

Another way to think about this approximation is to neglect the primes on the diagrams and to factor each diagram into independent pairs of ($\bullet\ \circ$). Equivalently, keeping only the first cumulant ignores the Pauli exclusion principle except in so far as it was used to construct the Fermi sea.

The notation ($\bullet\ \circ$) can be quantified by combining Eq.(6.16b) and (6.16c),

$$(\bullet \circ) = \sum_{p,s} \exp(-\beta\varepsilon_{ps}) \sum_{q,s} \exp(+\beta\varepsilon_{qs}) \qquad (6.21a)$$

Assuming, for simplicity, a constant density of states 2ρ and a band from -D to D, then

$$(\bullet \circ) = N^2 (2\rho)^2 \int_0^D e^{-\beta\varepsilon} d\varepsilon \int_{-D}^0 e^{\beta\varepsilon} d\varepsilon \tag{6.21b}$$

So that at low temperatures, we have

$$(\bullet \circ) = \left(\frac{2\rho N}{\beta}\right)^2 \tag{6.21c}$$

Inserting Eq.(6.21c) into the heuristic approximation gives a heat capacity of

$$C = 12\, k_B\, (N \rho\, k_B\, T)^2 \tag{6.22}$$

where k_B is the Boltzmann constant.

These results (that the canonical partition function is not extensive, and the heat capacity is not linear in T) are not due to our neglect of the Pauli exclusion principal, as will be demonstrated below, but reflect the very limited energy fluctuations that are allowed in the canonical ensemble when the particle number is fixed. It is quite surprising that nowhere in the literature has this property of the canonical ensemble been noted before. In our discussion of the grand canonical partition function below, we will see that the fluctuations in the particle number are critical for recovering the linear heat capacity.

Before discussing the grand canonical ensemble, let us examine the first few corrections to this simple result for the canonical partition function and demonstrate the manner in which the Pauli exclusion principle can be included. The second order term in the sum t_2 is given by

$$t_2 = \frac{1}{2!}(\bullet\ \bullet)'(\circ\ \circ)' \qquad (6.23a)$$

In Appendix A it is shown that the Pauli exclusion principle summation restrictions in the sum represented by $(\bullet\ \bullet)'$ can be carried out by adding in and subtracting out the excluded terms. Using these results from Appendix A we see that

$$t_2 = \frac{1}{2}(16x^4 - 8x^3 + x^2) \qquad (6.23b)$$

where $x = N\rho/\beta$. Combining this with $t_1 = 4x^2$, we can calculate the second cumulant:

$$\kappa_2 = -\frac{1}{2}x^2(16x^2 + 8x - 1) \qquad (6.24)$$

Now the first few terms of the exponential argument can be written as:

$$\Theta = \frac{1}{4}x^2(17 - 8x - 16x^2) \qquad (6.25)$$

where Θ is clearly not extensive.

The higher order terms represent higher powers of the particle number N and temperature T. The fact that the canonical partition function is not extensive from this cumulant expansion calculation is rather surprising. Since Θ converges only for small values of x, our result may only reflect series expansion of an analytical function in the small x regime, whereas the same function should be extensive at large x (i.e., large N) limit. We need to determine the analytic continuation to large real x to verify that Θ is extensive in N and agrees with the grand canonical ensemble. In any case, the 'proof' of the equivalence between the canonical and grand canonical ensembles is not as trivial as indicated in standard textbooks. The rest of the chapter will focus on the experimentally more important grand canonical ensemble.

6.3 The grand partition function

The formula for the grand partition function requires the sum $\exp\{\beta[N'\mu - E_{N'}(\alpha)]\}$ for all possible numbers of particle numbers N' and all states α for each N'. When we want to compare with the evaluation for a system of N particles, we can rewrite the series by first summing all of the terms for N particles, then summing all of the states for (N+1) particles, (N-1) particles, (N±2) particles, etc. Symbolically, we can write the grand partition function as

$$\begin{aligned} Z \exp[-\beta\,(N\mu - E_0)] \;=\; & \ldots \\ & + (\circ\,\circ)'/2! + (\circ\,\circ\,\bullet\,\circ)'/3! + \ldots \\ & + (\circ) + (\circ\,\bullet\,\circ)'/2! + \ldots \\ & + 1 + (\bullet\,\circ) + (\bullet\,\circ\,\bullet\,\circ)'/(2!)^2 + \ldots \\ & + (\bullet) + (\bullet\,\bullet\,\circ)'/2! + \ldots \\ & + (\bullet\,\bullet)'/2! + (\bullet\,\bullet\,\bullet\,\circ)'/3! + \ldots \\ & + \ldots \end{aligned} \tag{6.26a}$$

Here the terms in the partition function are written in lines by the particle number in the system. The first line displayed is for N-2, the next lines are for N-1, N, N+1, N+2, etc.

For the purpose of applying the cumulant formula we need to regroup the terms by dominant powers of the number of particles, i.e., terms that are proportional to N, N^2, etc. The partition function now has the expression

$$
\begin{aligned}
&Z \exp[-\beta\,(N\mu - E_0)] \\
&= 1 + (\bullet) + (\circ) \\
&\quad + \frac{1}{2!}[(\bullet\,\bullet)' + (\circ\,\circ)' + 2(\bullet\,\circ)] \\
&\quad + \frac{1}{3!}[(\bullet\,\bullet\,\bullet)' + (\circ\,\circ\,\circ)' + 3(\bullet\,\circ\,\circ)' + 3(\bullet\,\bullet\,\circ)'] \\
&\quad + \frac{1}{4!}[(\bullet\,\bullet\,\bullet\,\bullet)' + (\circ\,\circ\,\circ\,\circ)' + 4(\bullet\,\circ\,\circ\,\circ)' + 4(\bullet\,\bullet\,\bullet\,\circ)' + 6(\bullet\,\bullet\,\circ\,\circ)'] \\
&\quad + \ldots \\
&\equiv 1 + \sum_{n=1}^{\infty} \frac{t_n}{n!} \qquad (6.26b)
\end{aligned}
$$

Note that only the 1 and the terms with equal numbers of particles and holes represent the contributions from the canonical ensemble. In Eq.(6.26b) there are only two terms explicitly shown excluding the initial 1. Most of the terms displayed in Eq.(6.26b) represents small fluctuations in particle number. To evaluate Z, various cumulants need to be calculated. Using the results from Appendix A and the definitions of t_n's in Eq.(6.26b), we have:

$$\kappa_1 = t_1 = (\bullet) + (\circ) = 4x \qquad (6.27a)$$

where $x = N\rho/\beta$. It should be noted that it is κ_1 that determines the major temperature dependence of the partition function. In this case the contributions to κ_1 represent fluctuations in the particle number by ±1. The first contribution from the N-particle states arises not in t_1, but in t_2 in the form of one particle-hole pair excitation ($\bullet\ \circ$). Using the results of Appendix A it is easy to show that $t_2 = 16x^2 - 2x$. Note that t_2 is of order N^2, thus guarantees the second cumulant to be extensive as required:

$$\kappa_2 \;=\; t_2 - t_1^2 \;=\; -2\,x \tag{6.27b}$$

In the same fashion, it is found that

$$t_3 \;=\; 64\,x^3 \;-\; 24\,x^2 \;+\; \frac{8}{3}\,x$$

$$\kappa_3 \;=\; \frac{8}{3}\,x \tag{6.27c}$$

$$t_4 \;=\; 256\,x^4 \;-\; 192\,x^3 \;+\; \frac{164}{3}\,x^2 \;-\; 6\,x$$

$$\kappa_4 \;=\; -6\,x \tag{6.27d}$$

The higher order terms begin to be significantly more complicated. We have evaluated t_5 and κ_5 using a computer based algebra manipulation program Mathematica [Wolfram, 1988]. The combination of all of the cumulants evaluated including t_5 yields

$$\Theta \;=\; 4\,x\,(\,1 - \frac{1}{2^2} + \frac{1}{3^2} - \frac{1}{4^2} + \frac{1}{5^2}\,) \tag{6.28}$$

which consists the first five terms of the series expansion of the correct result Θ = $4x(\pi^2/12)$, because the grand partition function can be derived from Eq.(6.26b) as

$$Z \;=\; \exp[-\beta\,(E_0 - N\mu)]\;\, e^{\Theta} \tag{6.29}$$

Note that the Θ approximated by the first five cumulants is within 1.96 percent of the exact result, which shows that the cumulant expansion calculation of the partition function is an efficient approximation scheme.

6.4 Summary

This research originated in an attempt to explore methods for many body calculations which dealt directly with the many particle states and did not start with the independent single particle approximation. The fact that the Grand Canonical Partition function can be approximated in this way indicates that this approach may have merit for more complex interacting systems. Indeed, calculations using this approach have been started.

The result that there is a difference between the canonical and grand canonical ensembles has been quite surprising. Since the difference seems to arise from the distinctly different terms that are allowed in the sums of the two ensembles, there seems no way to avoid the results of this study. This descrepancy raises a number of questions that merit further study.

The first question arises from the surprisingly strong role that extremely small fluctuations in particle number play in the low termperature properties of the free electron gas. Our traditional understanding has assumed that experimental measurements should be most closely described by the canonical ensemble for a fixed number of particles. Indeed, all comparisons of calculated heat capacities use the formula for $C_{<N>}$ derived from the grand canonical ensemble in which the chemical potential changes with temperature to constrain the average number of particles be be equal to N.

The fact that the canonical ensemble does not agree qualitatively with experiment suggests that heat capacity experiments should rather be compared with C_{μ}, where μ at T=0 is determined by the particle number. Using C_{μ} instead of $C_{<N>}$ for a free electron gas density of states would give rise to an increase in the theoretical estimate by a factor of 1.5. A cursory comparison of reported experimental heat capacities [Kittel, 1970] and band theory calculations for simple metals [Moruzzi, 1978] shows that for Li and other few electron systems the ratio of experimental to theoretical $C_{<N>}$ is greater than 1 and close to 1.5. For more complicated systems there is no correlation with this simple picture. Since no consideration has been made here of corrections due to the coulomb interaction, the lack of agreement is not unexpected.

Nevertheless, the role that particle number fluctuation plays in the thermodynamics of the free electron gas raises the question of validity for approximation schemes where it is implicitly assumed that the canonical ensemble most closely represents experimental measurements. These questions should be studied for other systems.

The application of these ideas to an interacting system, such as a Hubbard Hamiltonian, appears to be tractable, at least to the inclusion of the first few κ_n. The procedure would select a basis set of many-particle states $|\psi>$ which may be close to eigenvectors of the Hamiltonian. Approximations will be constructed for the resolvents of the Hamiltonian H with these states and terms t_n will be evaluated by using contour integrals of the type:

$$Z = \int dz <\psi| (z - H)^{-1} |\psi> e^{-\beta z}$$

By collecting terms representing the same number of excitations above an approximate ground state in much the same way as in Eq.(6.26b), it is possible to approximate the first few cumulants κ_n. This study will not be discussed here.

Chapter 7

Conclusion

With many approximation schemes and numerical methods developed for solving strongly-correlated systems, the study of many-body interactions remains a very difficult and challenging problem, and its solution reveals amazing and important insights about electromagnetic properties of materials which can not be easily achieved from single-electron based calculations. Many physicists have made enormous efforts in order to have a better understanding of these many-electron interacting systems and their properties. The research works described in this dissertation, which are intended to make contributions to the effort in various ways, have been fruitful.

We have focused our study on two important many-electron models: the Anderson model and the Hubbard model. Among these two model Hamiltonians, many systems can be well represented, and some other interesting models can be derived in various parameter limits. Either of the two Hamiltonians can also appear in many forms when used for modelling specific physical systems, including the Anderson single impurity model and lattice model, and the single-band (standard) and multi-band (extended) Hubbard models. These specific Hamiltonians have been studied using various methods and approximation schemes with moderate success. However, there does not exist a single method which yields accurate solutions consistently for all model Hamiltonians. That is the reason for our looking into many-electron partition functions in order to find a systematic approximation for any many-particle interacting system. As described in Chapter 6, this attempt produced rather surprising results even for a simple free-electron system. The findings from each and every one of these research projects are helpful, in one way or another, for our better understanding of properties of many-electron systems.

The magnetic susceptibility calculation for YbN using the Anderson model Hamiltonian yielded very good agreement between theory and experiment, yet the reason for the success of the ZZF approximation is not yet clear, mainly because it is not understood why NCA violates the Fermi-liquid relations. If that issue can be resolved, there is a great potential of applying ZZF approximation to the Anderson lattice model as well, based on the so-called extended non-crossing approximation (XNCA) [Kim, 1991], where the intersite interaction is incorporated via self-consistent modification of the conduction electron propagator. It will supply us a way of treating systems which do not have strong hybridization between localized and conducting bands without great computational effort.

The variational calculations of one- and two-dimensional Anderson lattice models generated rather accurate ground state energies, but the corresponding wavefunctions are not well approximated for reasons discussed in Chapter 3, where some suggestions on how to improve the results are also discussed. We have applied this variational scheme to Kondo, Anderson single-impurity and Anderson lattice models. It is easy to see that, with the increase of the degrees of freedom in localized states, the approximation gets worse because the basis used in the calculations becomes a smaller part of the space spanned by all possible many-particle Bloch states; also the orthogonalization of basis states gets more tedious. While it is possible to do some of the derivations with a computer, however, it is hard to justify the amount of work required for computer programming because it is difficult to apply the variational scheme to other model Hamiltonians unless the conducting states play an important role.

Many interesting results have been derived from the projection-operator based mean-field (MF) calculations of the two-dimensional single-band and multi-band Hubbard models. The formalism has been verified by comparing with other MF theories and quantum Monte Carlo simulation results, and the computational effort required is much less than other calculations like the slave-boson MF theory. Therefore it is straightforward to apply this projection-operator MF formalism to get approximate results of static properties for systems such as high-T_C superconductors. It should also be interesting to compare the normal state density of states with experimental results. However, as shown in Chapter 5, this formalism has its valid parameter range. Among others, it does not always yield an antiferromagnetic ground state for certain parameters while QMC does. Without the life-time effect, the discussion about Fermi surface is not convincing (even though systematic improvement over the Hubbard I approximation is seen), and dynamic properties cannot be calculated from this MF formalism. Nevertheless, with many energy and interaction parameters incorporated in the theory, it is convenient to obtain an estimate of certain physical quantities using this calculation.

Despite the significance of very interesting results obtained from the study of the many-particle partition function of the free-electron gas system, our original intention of the research was to find a systematic approach to partition functions of many-body interacting systems. By following the cumulant expansion steps shown in Chapter 6, approximation of partition functions to any order can be derived in principle for any given Hamiltonian. Using the information from low-lying state wavefunctions extracted from the exact-diagonalization of the one-dimensional Hubbard model Hamiltonian presented in Chapter 4, progress is being made in trying to construct the many-electron partition function for the Hubbard model in large U limit. Also, initial attempts at approximating the partition function of the single-impurity Anderson model shows promising results, and the first few terms in the cumulant expansion can be derived without much effort.

By combining single-electron band theory and many-body theory, the electromagnetic properties of materials can be more thoroughly understood than by relying on band theory only. As incredibly complex as many-body problems seem to be, directly solving a Hamiltonian which describes a many-electron interacting system is, in many cases, the most logical and convenient approach. The solution may not be easily and accurately obtained, yet much progress has been made, and much more can be achieved. The difficulty of the study of many-electron systems makes any such achievement a great joy.

Bibliography

[Abramowitz, 1970] M. Abramowitz and I. A. Stegun, "Handbook of Mathematical Functions", Dover Publications, NY, 1970.

[Anderson, 1961] P. W. Anderson, Phys. Rev. **124**, 41 (1961).

[Andrei, 1983] N. Andrei, K. Furuya and J. H. Lowenstein, Rev. Mod. Phys. **55**, 331(1983).

[Bickers, 1985] N. E. Bickers, D. L. Cox and J. W. Wilkins, Phys. Rev. Lett. **54**, 230 (1985).

[Bickers, 1987] N. E. Bickers, D. L. Cox and J. W. Wilkins, Phys. Rev. B **36**, 2036 (1987).

[Blankenbecler, 1987] R. Blankenbecler, J. R. Fulco, W. Gill and D. J. Scalapino, Phys. Rev. Lett. **58**, 411 (1987).

[Bowen, 1988] S. P. Bowen and J. D. Mancini, J. Appl. Phys. **63**, 3402 (1988).

[Bowen, 1991] S. P. Bowen, Yu Zhou and J. D. Mancini, Phys. Rev. B, accepted for publication.

[Brandow, 1979] B. H. Brandow, Int. J. Quantum Chem. Symp. **13**, 423 (1979) and references therein.

[Brandow, 1986] B. H. Brandow, Phys. Rev. B **33**, 215 (1986) and references therein.

[Brout, 1959] R. Brout, Phys. Rev. **115**, 824 (1959).

[Callaway, 1987a]	J. Callaway, D. P. Chen and Y. Zhang, Phys. Rev. B **35**, 3705 (1987).
[Callaway, 1987b]	J. Callaway, D. P. Chen and Y. Zhang, Phys. Rev. B **36**, 2084 (1987).
[Chen, 1988]	D. P. Chen and J. Callaway, Phys. Rev. B **38**, 11869 (1988).
[Coleman, 1984]	P. Coleman, Phys. Rev. B **29**, 3035 (1984).
[Coleman, 1985]	P. Coleman, J. Magn. Magn. Mater **47-48**, 323 (1985).
[Coppersmith, 1989]	S. N. Coppersmith and C. C. Yu, Phys. Rev. B **39**, 11464 (1989).
[Cyrot, 1972]	M. Cyrot, J. Phys. (Paris) **33**, 125 (1972).
[Czyzcholl, 1982]	G. Czyzcholl and H. J. Leter, Z. Phys. **B48**, 67 (1982).
[Czyzcholl, 1985]	G. Czyzcholl, Phys. Rev. **B31**, 2867 (1985).
[Dagotto, 1989]	E. Dagotto, A. Moreo and T. Barnes, Phys. Rev. B **40**, 6721 (1989).
[Degiorgi, 1990]	L. Degiorgi, W. Bacsa and P. Wachter, Phys. Rev. B **42**, 530 (1990).
[Donni]	A. Donni, unpublished.
[Dopf, 1990]	G. Dopf, A. Muramatsu and W. Hanke, Phys. Rev. B **41**, 9264 (1990).
[Duncan, 1985]	A. Duncan and R. Roskies, Phys. Rev. D **31**, 364 (1985).
[Emery, 1987]	V. Emery, Phys. Rev. Lett. **58**, 2794 (1987).
[Falicov, 1981]	Valence Fluctuations in Solid, edited by L. M. Falicov, W. Hanke and M. B. Maple (North-Holland, Amsterdam, 1981).
[Fazekas, 1987]	P. Fazekas, J. Magn. Magn. Mater. **63-64**, 545 (1987).
[Fedro, 1982]	A. J. Fedro and S. K. Sinha, Valence Instabilities, ed. P. Wachter and H. Boppart (North-Holland, Amsterdam, 1982), p 371.

[Fedro, 1987] A. J. Fedro and B. D. Dunlap, Jpn. J. Appl. Phys., **26** Supplement **26-3**, 463, (1987).

[Fedro, 1991] A. J. Fedro, Yu Zhou, T. C. Leung and B. N. Harmon, "High Temperature Superconductivity: Physical Properties, Microscopics and Mechanism", Eds. J. Ashkenazi, et.al, Plenum Press (New York), 1991.

[Fermi, 1926] E. Fermi, Z. Phys. **36**, 902 (1926).

[Geipel, 1988] G. Geipel and W. Nolting, Phys. Rev. B **38**, 2608 (1988).

[Goryachev, 1982] E. G. Goryachev, E. V. Kuzmin and S. G. Ovchinnikov, J. Phys. C **15**, 1481 (1982).

[Gunnarsson, 1983] O. Gunnarsson and K. Schonhammer, Phys. Rev. B **28**, 4315 (1983).

[Hewson, 1985] A. C. Hewson and J. W. Rasul, J. Phys. C **16**, 6799 (1985).

[Hirsch, 1982] J. E. Hirsch, D. J. Scalapino, R. L. Sugar and R. Blankenbecler, Phys. Rev. B **26**, 5033 (1982).

[Hirsch, 1983] J. E. Hirsch and D. J. Scalapino, Phys. Rev. B **27**, 7169 (1983).

[Hirsch, 1984a] J. E. Hirsch and D. J. Scalapino, Phys. Rev. B **29**, 5554 (1984).

[Hirsch, 1984b] J. E. Hirsch, Phys. Rev. Lett, **53**, 2327 (1984).

[Hirsch, 1985] J. E. Hirsch, Phys. Rev. B **31**, 4403 (1985).

[Huang, 1963] K. Huang, "Statistical Mechanics", John Wiley and Sons, New York, 1963.

[Hubbard, 1963] J. Hubbard, Proc. Roy.Soc. A **276**, 238 (1963).

[Hybertsen, 1989] M. S. Hybertsen, M. Schluter and N. E. Christensen, Phys. Rev. B **39**, 9028 (1989).

[Jayaprakash, 1989] C. Jayaprakash, H. R. Krishnamurthy and S. Sarker, Phys. Rev. B **40**, 2610 (1989).

[Julian, 1977a] R. Julian, J. Fields and S. Doniach, Phys. Rev. B **16**, 4489 (1977).

[Julian, 1977b] R. Julian, J. Fields and S. Doniach, Phys. Rev. Lett. **38**, 1500 (1977).

[Julian, 1982a] R. Julian and R. M. Martin, J. Appl. Phys. **53**, 2137 (1982).

[Julian, 1982b] R. Julian and R. M. Martin, Phys. Rev. B **26**, 6173 (1982).

[Julian, 1982c] R. Julian and R. M. Martin, Sol. Sta. Comm. **41**, 967 (1982).

[Kim, 1991] C. Kim, Y. Kuramoto and T. Kasuya, preprint.

[Kittel, 1970] C. Kittel, "Introduction to Solid State Physics", J. Wiley and Sons, New York, 1970.

[Korn, 1968] G. A. Korn and T. M. Korn, "Mathematical Handbook for Scientists and Engineers", McGraw Hill, 1968.

[Kotliar, 1986] G. Kotliar and A. E. Ruckenstein, Phys. Rev. Lett. **57**, 1362 (1986).

[Kotliar, 1988] G. Kotliar Phys. Rev. B **37**, 3664 (1988).

[Kubo, 1962] R. Kubo, J. Phys. Soc. Jpn. **17**, 1100 (1962).

[Kuramoto, 1985] Y. Kuramoto and E. Muller-Hartmann, J. Magn. Magn. Mater. **52**, 122 (1985).

[Kuramoto, 1989] Y. Kuramoto, Physica B **156&157**, 789 (1989).

[Kurata, 1980] Y. Kurata, J. Phys. **F10**, 893 (1980).

[Langreth, 1966] David C. Langreth, Phys. Rev. **150**, 516 (1966).

[Lee, 1988] K.-J.-B. Lee and P. Schlottmann, Phys. Rev. B **38**, 11566 (1988).

[Lieb, 1968] E. H. Lieb and F. Y. Wu, Phys. Rev. Lett. **20**, 1445 (1968).

[Lilly, 1990] L. Lilly, A. Muramatsu and W. Hanke, Phys. Rev. Lett. **65**, (1990).

[Lin, 1988] H. Q. Lin, J. E. Hirsch and D. J. Scalapino, Phys. Rev. B **37**, (1988).

[Malik, 1991] S. K. Malik and D. T. Adroja, Phys. Rev. B **43**, 6295 (1991).

[Mancini, 1983] J. D. Mancini and D. C. Mattis, Phys. Rev. B **28**, 6061 (1983).

[Mancini, 1984] J. D. Mancini and D. C. Mattis, Phys. Rev. B **29**, 6988 (1984).

[Mancini, 1985] J. D. Mancini and D. C. Mattis, Phys. Rev. B **31**, 7440 (1985).

[Mancini, 1990] J. D. Mancini, S. P. Bowen and Yu Zhou, Phys. Rev. **B41**, 6061 (1990).

[Mattis, 1985] D. C. Mattis, "The Theory of Magnetism II", Springer Verlag, 1985.

[Mayer, 1940] J. E. Mayer and M. G. Mayer, "Statistical Mechanics", J. Wiley and Sons, 1940, Chapter 13.

[Mazumdar, 1979] S. Mazumdar and Z. G. Soos, Synth. Met. **1**, 77 (1979).

[McMahan, 1988] A. K.McMahan, R. M. Martin and S. Satpathy, Phys. Rev. B **38**, 6650 (1988).

[Misra, 1987] P. K. Misra, D. G. Kanhere and J. Callaway, Phys. Rev. B **35**, 5013 (1987).

[Monnier, 1986] R. Monnier, L. Degiorgi and D. D. Koelling, Phys. Rev. Lett. **56**, 2744 (1986).

[Monnier, 1990] R. Monnier, L. Degiorgi and B. Delley, Phys. Rev. B **41**, 573 (1990).

[Moreo, 1990] A. Moreo, D. J. Scalapino, R. L. Sugar, S. R. White and N. E. Bickers, Phys. Rev. B **41**, 2313 (1990).

[Moruzzi, 1978] V. C. Moruzzi, J. F. Janak and A. R. Williams, "Calculated Electronic Properties of Metals", Pergamon Press, New York, 1978]

[Muller-Hartmann, 1984] E. Muller-Hartmann, Z. Phys. B **57**, 281 (1984).

[Nolting, 1989] W. Nolting and W. Borgiel, Phys. Rev. B **39**, 6962 (1989).

[Oguchi, 1987] A. Oguchi, Prog. Theor. Phys. **77**, 278 (1987).

[Ott, 1982] H. R. Ott, F. Hulliger and H. Rudigier, in "Valence Instabilities" eds. P. Wachter and H. Boppart, North Holland (Amsterdam, 1982) p.511.

[Oyamada, 1988] A. Oyamada, S. Takagi, T. Kasuya, K. Sugiyama and M. Date, J. Phys. Soc. Japan **57**, 3557 (1988).

[Parks, 1977] Valanced Instabilities and Related Narrow-Band Phenomena, edited by R. D. Parks (Plenum, New York, 1977).

[Pines,1989] David Pines and Philippe Nozieres, "The Theory of Quantum Liquids," Addison-Wesley, Redwood City, 1989, p. 63.

[Popielewicz, 1976] A. Popielewicz, Phys. Status Solidi B **74**, 383 (1976).

[Rasul, 1989] J. W. Rasul and P. Schlottmann, Phys. Rev. B **39**, 3065 (1989).

[Read, 1984a] N. Read and D. M. Newns, Sol. Sta. Comm. **52**, 993 (1984).

[Read, 1984b] N. Read, D. M. Newns and S. Doniach, Phys. Rev. **B30**, 384 (1984).

[Rice, 1987] T. M. Rice and K. Ueda, Phys. Rev. B **34**, 6420 (1987).

[Ruckenstein, 1987] A. E. Ruckenstein, P. J. Hirschfeld and J. Appel, Phy. Rev. B **36**, 375 (1987).

[Ruckenstein, 1988] A. E. Ruckenstein and S. Schmitt-Rink, Phys. Rev. B **38**, 7188 (1988).

[Scalettar] R. T. Scalettar, D. J. Scalapino, R. L. Sugar and S. R. White, Preprint.

[Shiba, 1972] H. Shiba, Prog. Theor. Phys. **48**, 2171 (1972).

[Shiba, 1975] H. Shiba, Prog. Theor. Phys. **54**, 967 (1975).

[Soos, 1984] Z. G. Soos and S. Ramasesha, Phys. Rev. B **29**, 5410 (1984).

[Stewart, 1984] G. R. Stewart, Rev. Mod. Phys. **56**, 755 (1984).

[Stutius, 1969] W. Stutius, Phys. Kondens. Materie **10**, 152 (1969).

[Tsvelick, 1982] A. M. Tsvelick and P. B. Wiegmann, J. Phys. C **15**, 1707 (1982)

[Tsvelick, 1983] A. M. Tsvelick and P. B. Wiegmann, Adv. Phys. **32**, 453 (1983)

[Varma, 1985a] C. M. Varma, Comments Solid State Phys. **11**, 221 (1985).

[Varma, 1985b] C. M. Varma, J. Magn. Magn. Mater. **47-48**, 606 (1985).

[Varma, 1987] C. M. Varma, S. Schmitt-Rink and E. Abrahams, Solid State Comm. **62**, 681 (1987).

[White, 1989] S. R. White, D. J. Scalapino, R. L. Sugar, E. Y. Loh, J. E. Gubernatis and R. T. Scalettar, Phys. Rev. B **40**, 506 (1989).

[Wojciechowski, 1988] R. J. Wojciechowski and L. Kowalewski, Physica B **153**, 24 (1988).

[Wolfram, 1988] Stephan Wolfram, "Mathematica", Addison Wesley, 1988.

[Yamada, 1983] K. Yamada and K. Yosida, J. Magn. Magn. Mater. **31-34**, 461 (1983).

[Yamamoto, 1956] T. Yamamoto and H. Matsuda, Prog. Theor. Phys. **16**, 269 (1956).

[Yoshioka, 1989] D. Yoshioka, J. Phys. Soc. Jpn. **58**, 1516 (1989).

[Yushankhai, 1991] V. Yu. Yushankhai, N.M. Plakida and P. Kalinay, Physica C **174**, 401 (1991).

[Yvon,1969]	J. Yvon, "Correlations and Entropy in Classical Statistical Mechanics", Pergamon Press, New York, 1969.
[Zevin, 1988]	V. Zevin, G. Zwicknagl and P. Fulde, Phys. Rev. Lett **60**, 2331 (1988).
[Zhang, 1984]	F. C. Zhang and T. K. Lee, Phys. Rev. B **30**, 1556, (1984).
[Zhang, 1988]	Y. Zhang and J. Callaway, Phys. Rev. B **38**,641 (1988).
[Zhang, 1990]	W. Zhang, M. Avignon and K. H. Bennemann, Phys. Rev. B **42**, 10192 (1990).
[Zhou, 1991a]	Yu Zhou, S. P. Bowen, D. D. Koelling and R. Monnier, Phys. Rev. B **43**, 11071 (1991).
[Zhou, 1991b]	Yu Zhou, A. J. Fedro, S. P. Bowen, D. D. Koelling, T. C. Leung, B. N. Harmon and S. K. Sinha, Phys. Rev. B **44**, 10291 (1991).
[Zhou, 1991c]	Yu Zhou, A. J. Fedro, T. C. Leung, B. N. Harmon and S. K. Sinha, Phys. Rev. B, to be published.
[Zhou, 1991d]	Yu Zhou, S. P. Bowen and J. D. Mancini, Phys. Lett. A **155**, 290 (1991).
[Zhou, 1991e]	Yu Zhou, S. P. Bowen and J. D. Mancini, Phys. Rev. B **44**, 5482 (1991).
[Zwicknagl, 1990]	G. Zwicknagl, V. Zevin and P. Fulde, Z. Phys. B **79**, 365 (1990).

Appendix A

Energy Sums in Partition Functions

In this appendix the details of the energy sums needed in the calculation of free-electron gas partition function in Chapter 6 is listed.

The sum of the exponential of the excited electron states is given by

$$(\bullet) \;=\; \sum_{p,s} \exp[\,-\beta\,(\,\varepsilon_{ps} - \mu\,)] \tag{A.1}$$

For simplicity in this paper we will assume that the density of states per spin for the electrons is constant over a band width of 2D with value ρ. At low temperatures the sum in Eq.(A.1) is $(\bullet) = 2x$ where

$$x \;=\; N\rho/\beta$$

and we have neglected exponentially small terms. The sum over the hole states yields the same result:

$$(\circ) \;=\; \sum_{q,s} \exp[\,\beta\,(\,\varepsilon_{qs} - \mu\,)] \;=\; 2x \tag{A.2}$$

The first example of the effect of the Pauli exclusion principle arises in the two particle (two hole) sums. The two particle sum (• •)' contains both momentum and spins sums and that restriction is that no two electrons can be in the same state (**p**,s),

$$(\bullet\ \bullet)' = \sum_{\mathbf{p}_1,s_1,\mathbf{p}_2,s_2}{}' \exp[-\beta(\varepsilon_{\mathbf{p}_1 s_1}-\mu)]\exp[-\beta(\varepsilon_{\mathbf{p}_2 s_2}-\mu)] \tag{A.3}$$

If $s_1 \neq s_2$, then the momentum sums are restricted and the evaluation reduces to $4x^2$. If the two spins are equal then the prime in the summation reminds us that the two momenta cannot be equal. For later use it is helpful to define the sums without the spins using square brackets:

$$[\bullet\ \bullet]' = \sum_{\mathbf{p}_1,\mathbf{p}_2}{}' \exp[-\beta(\varepsilon_{\mathbf{p}_1}-\mu)]\exp[-\beta(\varepsilon_{\mathbf{p}_2}-\mu)] \tag{A.4}$$

The summation restriction can be eliminated by adding and subtracting out the terms with both momenta equal and having no restriction on the momentum sums. This is most easily written with a delta function.

$$[\bullet\ \bullet]' = \sum_{\mathbf{p}_1,\mathbf{p}_2} \exp[-\beta(\varepsilon_{\mathbf{p}_1}-\mu)]\exp[-\beta(\varepsilon_{\mathbf{p}_2}-\mu)](1-\delta_{\mathbf{p}_1,\mathbf{p}_2}) \tag{A.5}$$

In this equation there are no restrictions on the sums and we may write this equation symbollically as

$$[\bullet\ \bullet]' = [\bullet]^2 - [\bullet - \bullet] \tag{A.6}$$

where the second term represents a single momentum sum of all terms with both momenta equal. It is straightforward to show that [•] = x and that

$$[\bullet - \bullet] = \frac{x}{2}$$

With these rules we can evaluate Eq.(A.3), taking into account the factor of two for the spin values.

$$(\bullet\,\bullet)' \;=\; 2\,[\,\bullet\,\bullet\,]' + 2\,[\,\bullet\,\bullet\,] \;=\; 2\,(\,[\,\bullet\,]^2 - [\,\bullet - \bullet\,]\,) + 2\,[\,\bullet\,]^2 \tag{A.7}$$

So we have that $(\bullet\,\bullet)' = 4x^2 - x$ which is the same value as for $(\circ\,\circ)'$.

For the evaluation of the Grand Canonical Ensemble it is necessary to evaluate more complicated diagrams. The first one of these is $(\bullet\,\bullet\,\bullet)'$, which will involve three spin sums and three momentum sums. If we consider the 8 different spin terms, we find that there are two with all spins the same and 6 with two spins the same. This means that we can write this three particle term in terms of the square brackets which contain only momentum sums,

$$(\,\bullet\,\bullet\,\bullet\,)' \;=\; 2\,[\,\bullet\,\bullet\,\bullet\,]' + 6\,[\,\bullet\,]\,[\,\bullet\,\bullet\,]'$$

The momentum restrictions in the three electron brac-ket can be removed by three delta function factors multiplying the momentum sums,

$$(\,1 - \delta_{p_1,p_2}\,)\,(\,1 - \delta_{p_2,p_3}\,)\,(\,1 - \delta_{p_1,p_3}\,)$$

Working out the sums and the delta functions yields,

$$[\,\bullet\,\bullet\,\bullet\,]' \;=\; [\,\bullet\,]^3 - 3\,[\,\bullet\,]\,[\,\bullet - \bullet\,] + 2\,[\,\bullet - \bullet - \bullet\,]$$

Combining this result with Eq.(A.7), we get

$$(\,\bullet\,\bullet\,\bullet\,)' \;=\; 8x^3 - 6x^2 + \frac{4x}{3} \tag{A.8}$$

Again, $(\circ\ \circ\ \circ)' = (\bullet\ \bullet\ \bullet)'$.

The four particle sum can be worked out in a similar fashion. The four spin sums give two terms with all spins equal, 8 terms with three spins the same, and 6 terms with 2 spins the same. This leads to the following equation:

$$(\bullet\ \bullet\ \bullet\ \bullet)' = 2\,[\bullet\ \bullet\ \bullet\ \bullet]' + 8\,[\bullet]\,[\bullet\ \bullet\ \bullet]' + 6\,[\bullet\ \bullet]'\,[\bullet\ \bullet]'$$

The Pauli exclusion summation restrictions can be lifted by including delta function factors and a lengthy graphical analysis leads to the following:

$$\begin{aligned}[\bullet\ \bullet\ \bullet\ \bullet]' = {} & [\bullet]^4 - 6\,[\bullet]^2\,[\bullet - \bullet] + 8\,[\bullet]\,[\bullet - \bullet - \bullet] \\ & + 3\,[\bullet - \bullet]^2 - 6\,[\bullet - \bullet - \bullet - \bullet]\end{aligned}$$

Substitutions from the above yield

$$(\bullet\ \bullet\ \bullet\ \bullet)' = 16\,x^4 - 24\,x^3 + \frac{41}{3}\,x^2 - 6\,x \tag{A.9}$$

Higher order contributions can be worked out quite easily using something like Mathematica. We have worked out the fifth order diagrams relatively easily.

Vita

Yu Zhou was born March 8, 1967 in Manzhouli, China. He obtained a B.S. degree in the physics department of Nankai University in Tianjin, China, in 1985. He went to Blacksburg, Virginia, in the fall of 1985 to pursue his advanced degree in condensed matter physics in the physics department of Virginia Polytechnic Institute and State University. In February of 1989, he followed his advisor, Dr. Samuel Bowen, to Argonne National Laboratory, and joined the Materials Science Division as a Laboratory-Graduate-Student under the supervising of Dr. Dale Koelling. After obtaining his PhD in December 1991, he will begin to work as a postdoctoral appointee at University of Zurich, Switzerland.